Elliptical (E) galaxies

M87 (Malin color scheme)

E1


M87 (SDSS color scheme)
E1


nglo-Australian Observatory

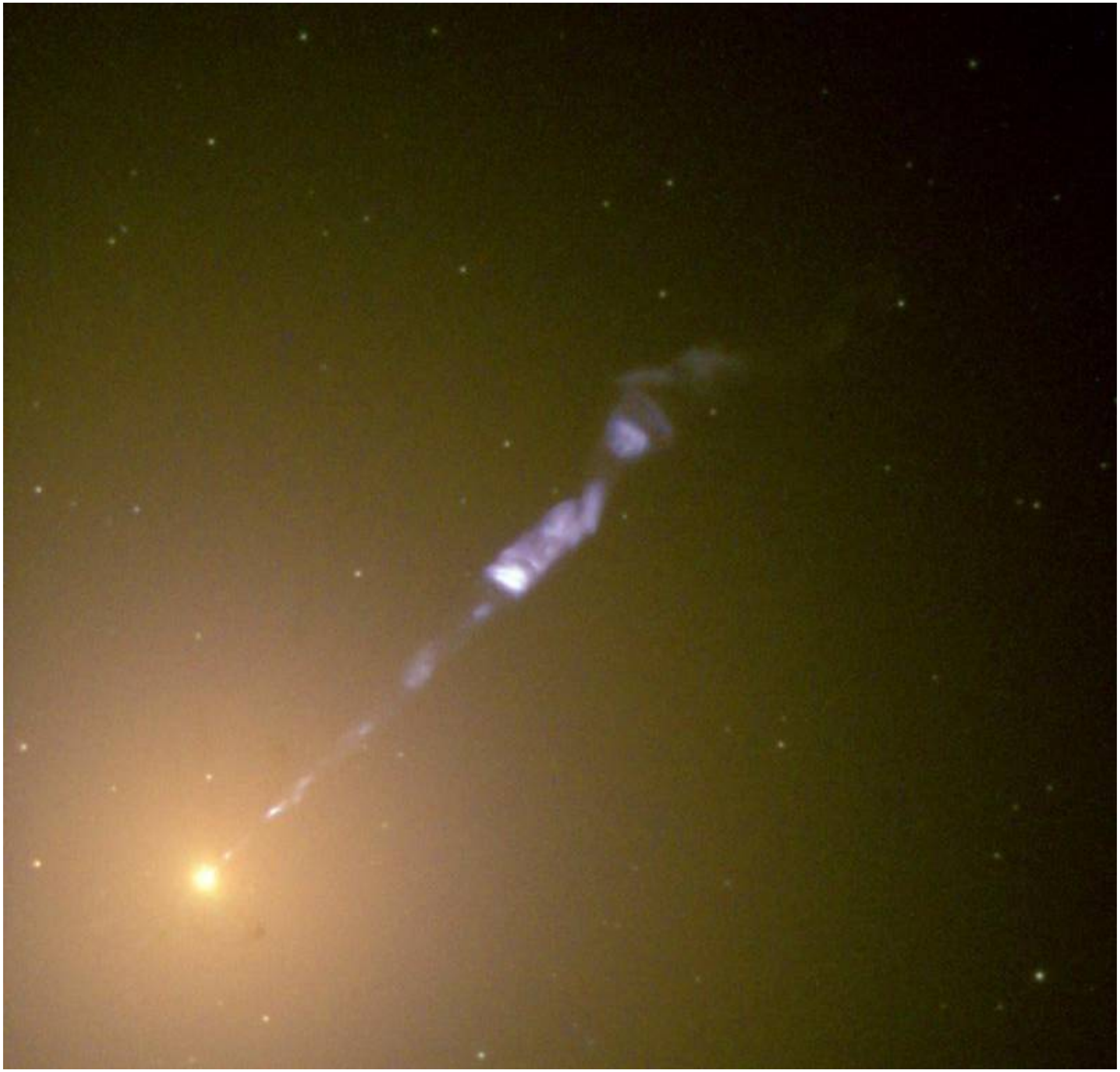

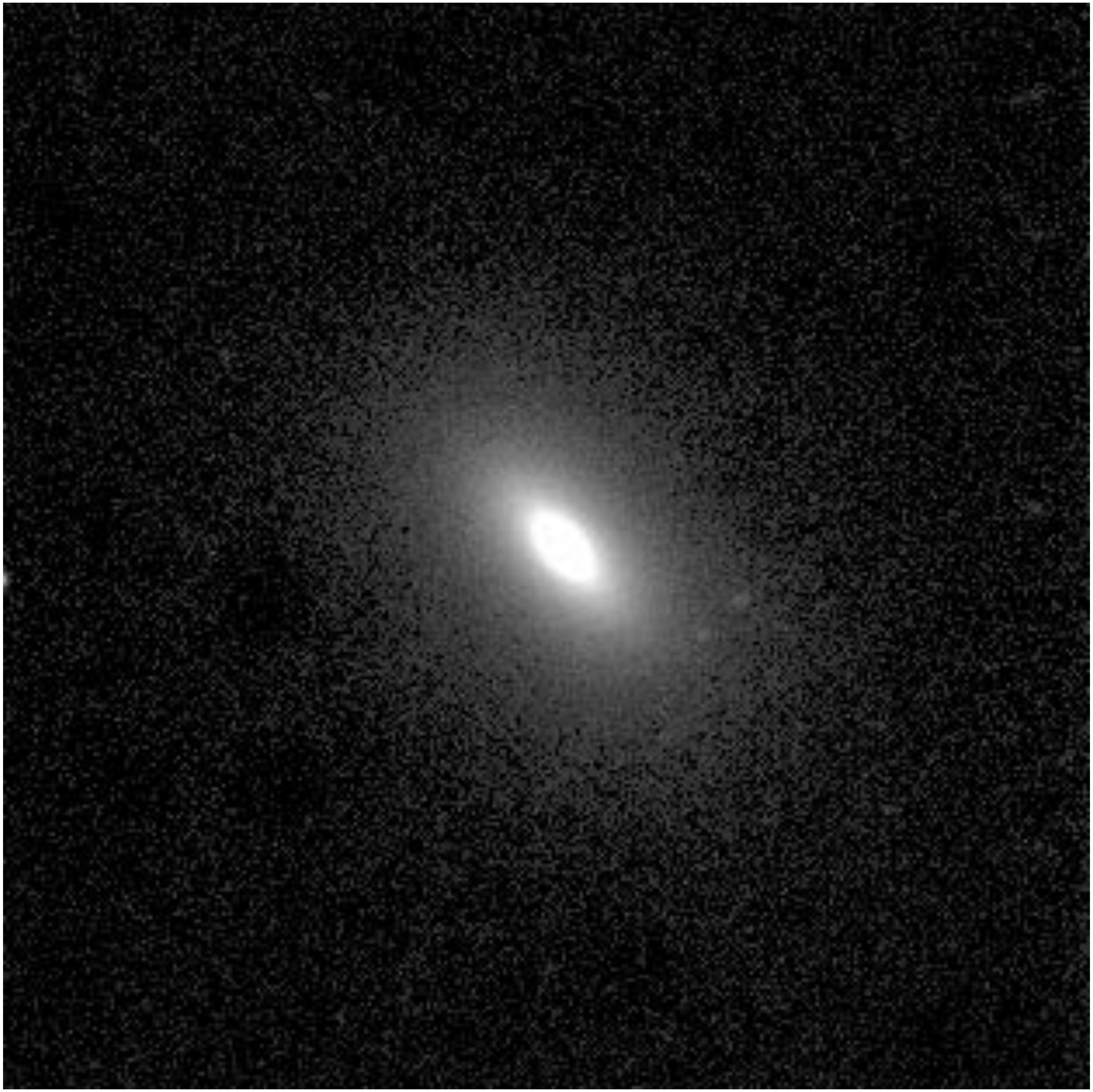

NGC 3377

E6

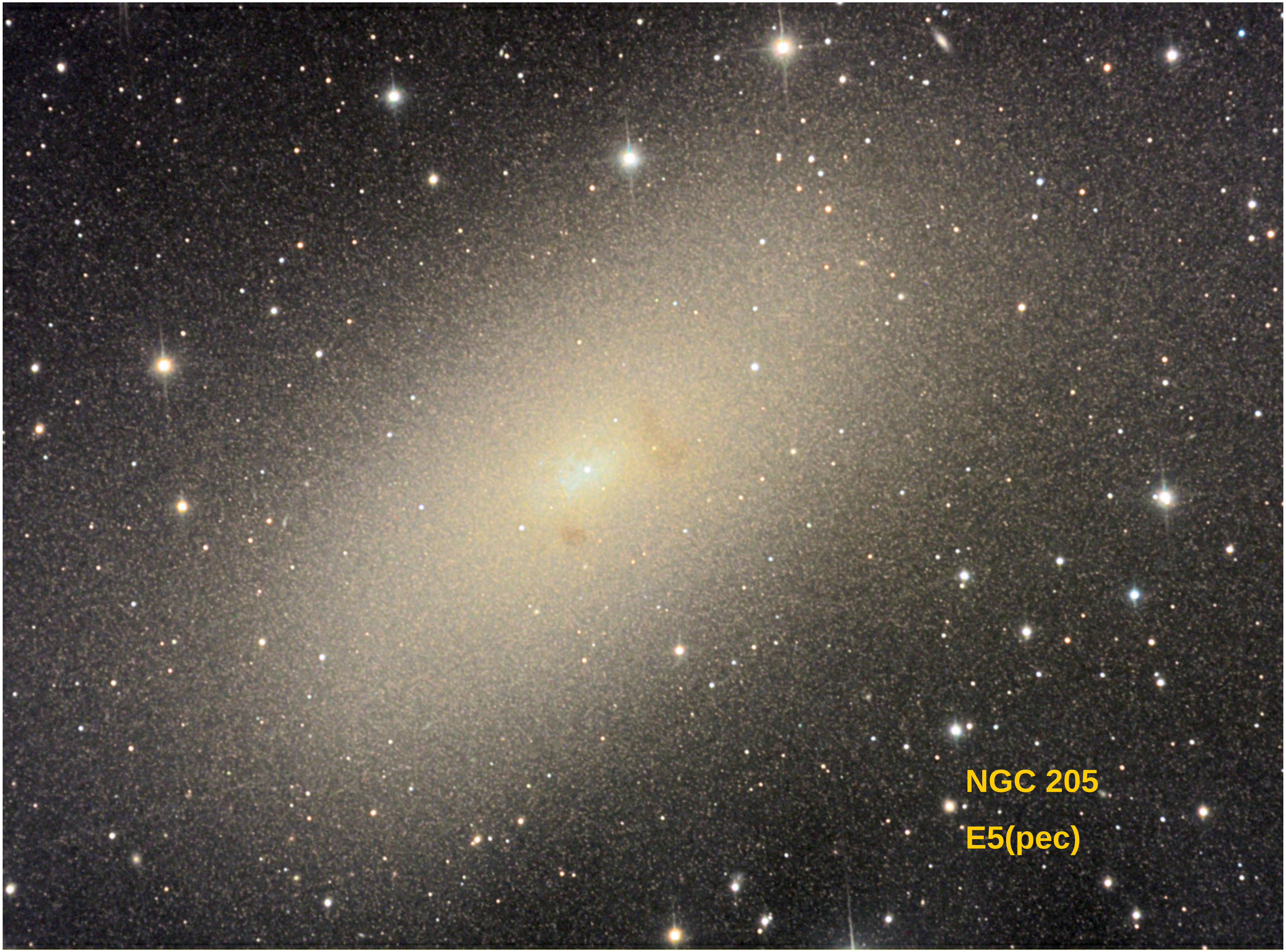
NGC 205
E5(pec)

NGC 147

E5

NGC 185

E3

M32

E2

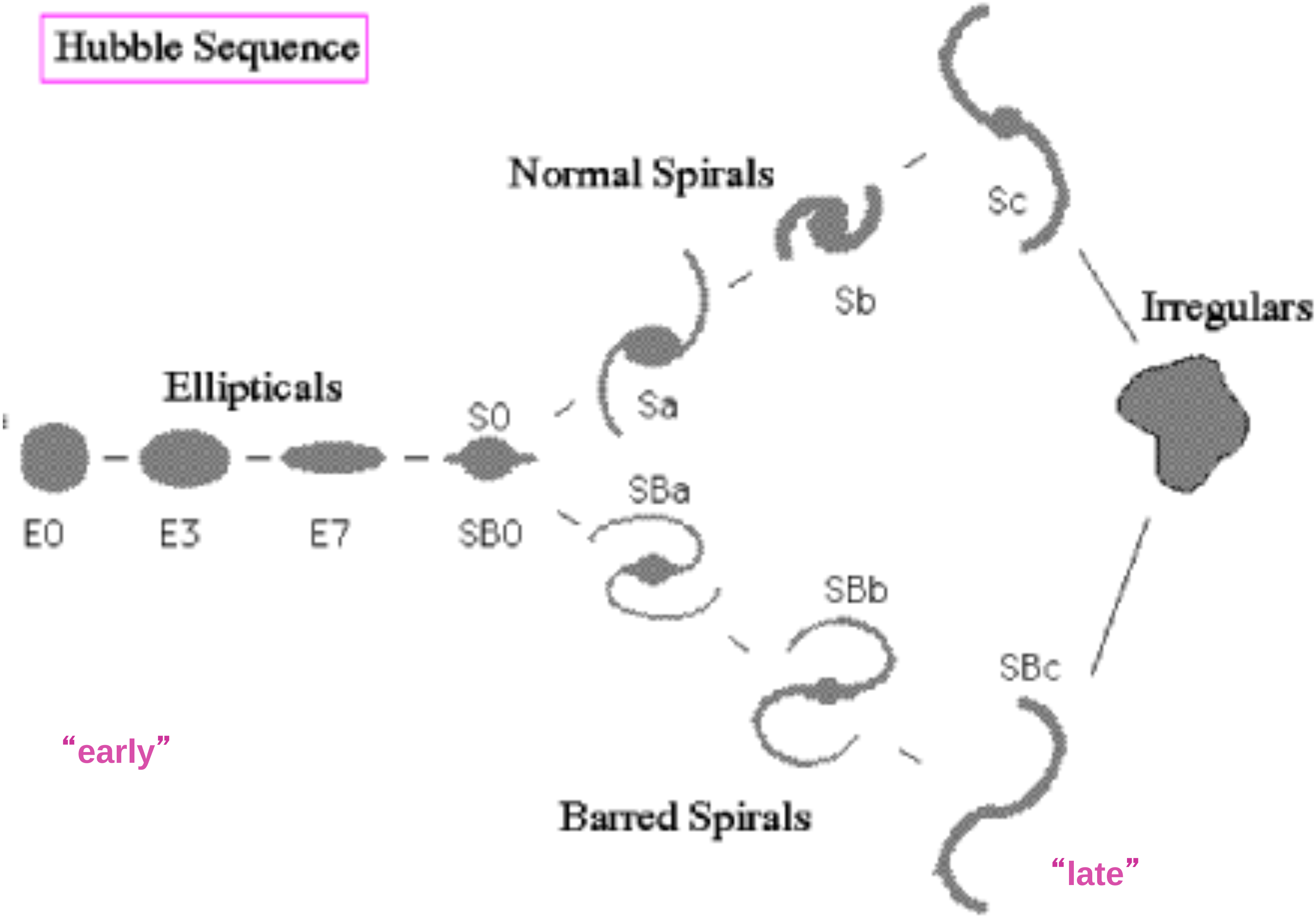
Hubble Sequence
Normal Spirals
Sc
Sb
Sa
Irregulars
Ellipticals
S0
E0
E3
E7
SB0
SBa
SBb
SBc
Barred Spirals
“early”
“late”

Sa galaxies


M104
Sa or SA(s)a
© Anglo-Australian Observatory


M104
Sa or SA(s)a

Sb galaxies

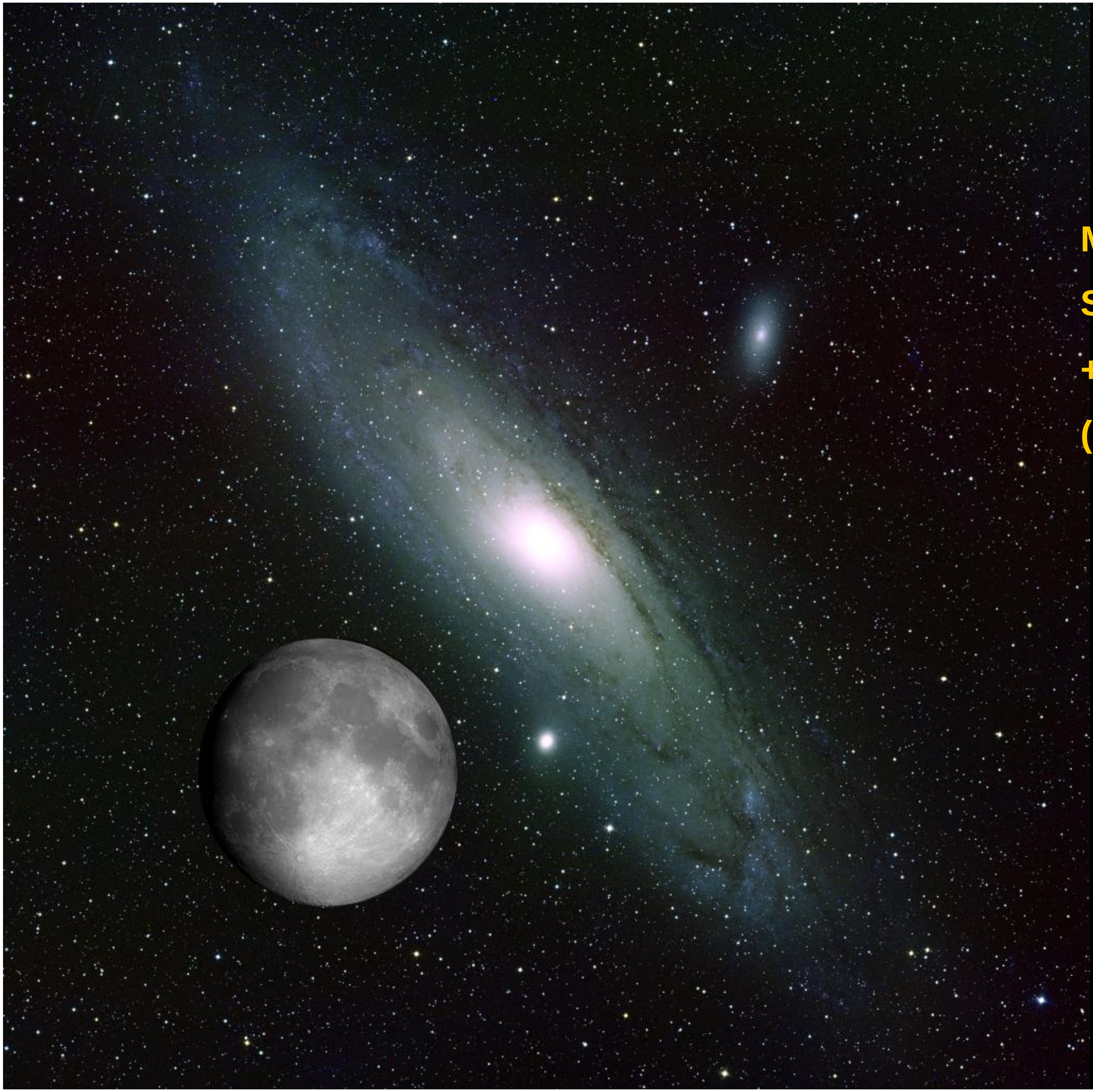

M31

Sb or SAb

+ NGC 205 + M32

(+ Moon, for scale)

45 Minute Exposure

30 Minute Exposure

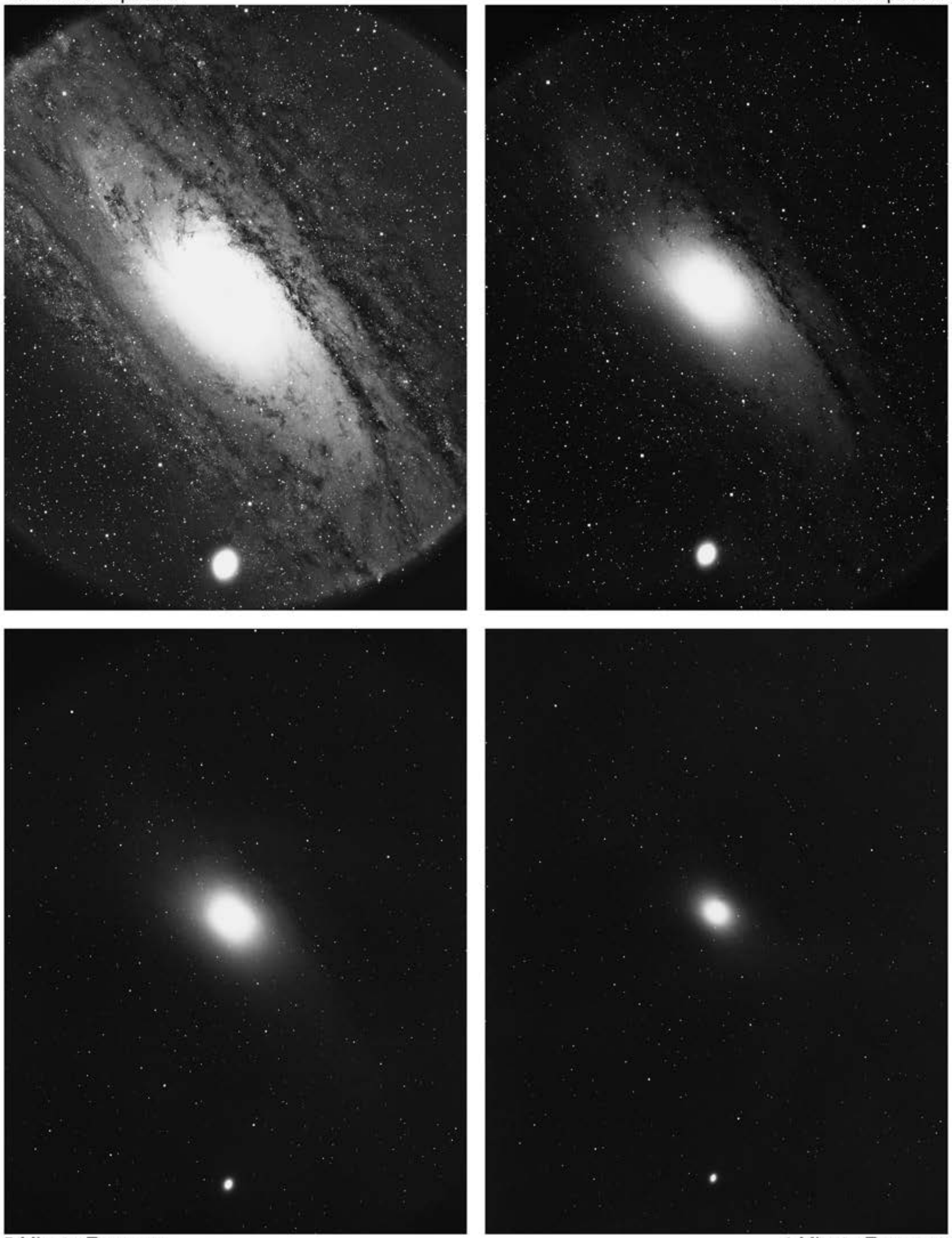

5 Minute Exposure

1 Minute Exposure

M31 and M32

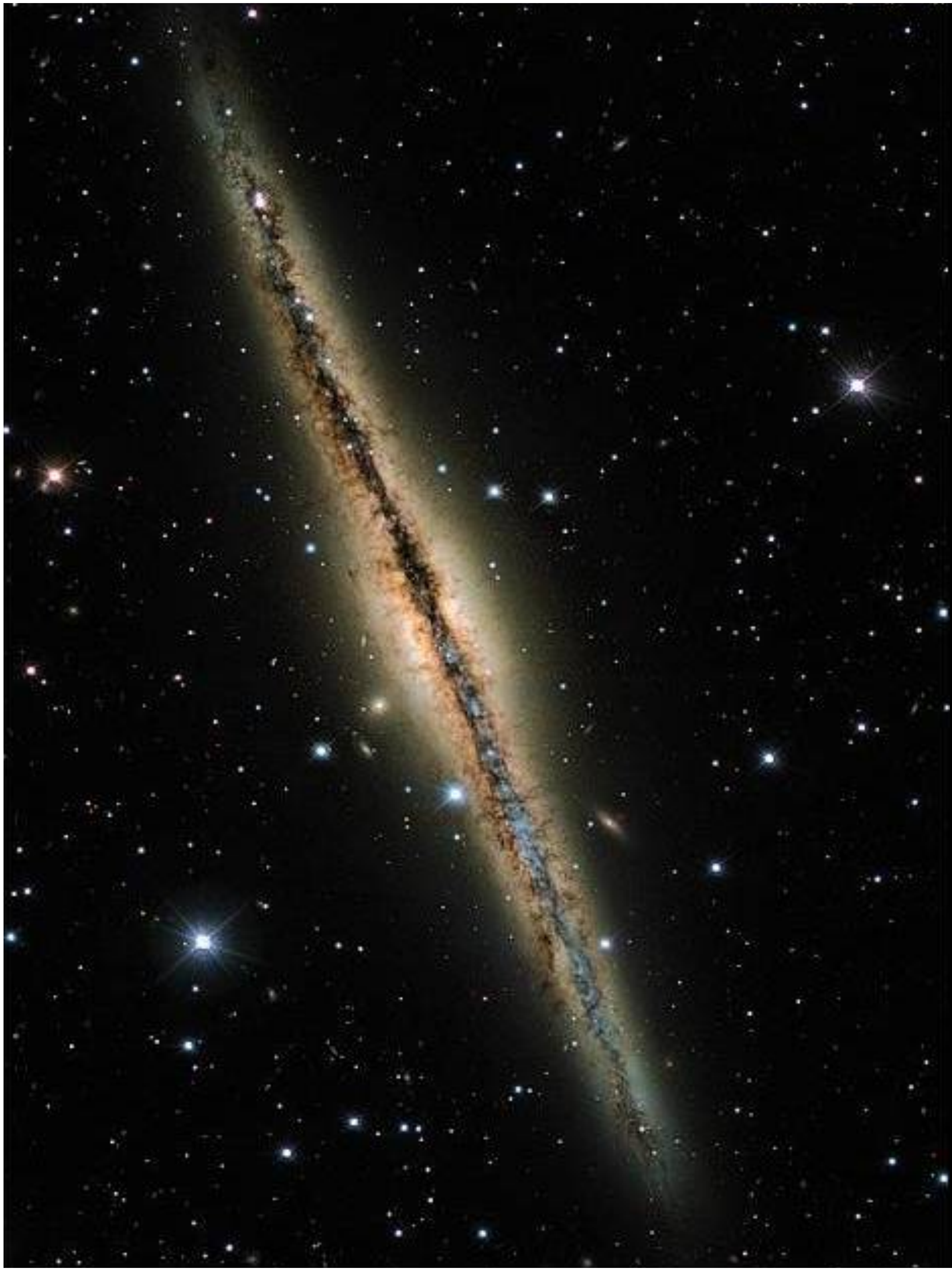

NGC 891

Sb SA(s)b?

NGC 1365

SBb or SB(s)b

Arm class 12 (grand design)

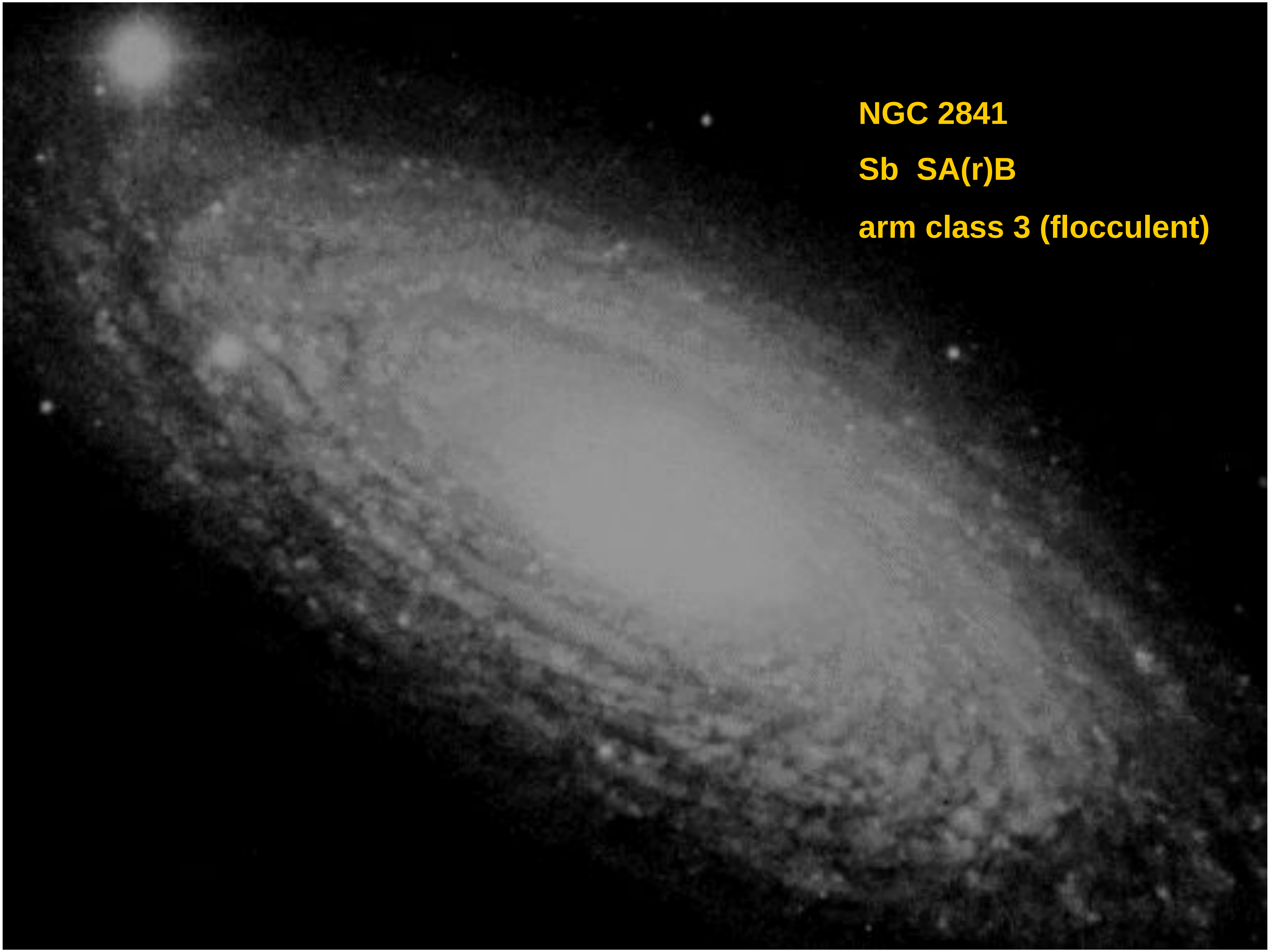
NGC 2841
Sb SA(r)B
arm class 3 (flocculent)

Sbc galaxies

M51

Sbc SAbc

arm class 12 (grand design)

NGC 5195

SB0(pec)

Lupton color scheme

M100

Sbc SAB(s)bc

arm class 12 (grand design)

NGC 1566

Sbc   SAB(rs)bc

arm class 12 (grand design)

NGC 1300

SBbc SB(s)bc

arm class 12 (grand design)

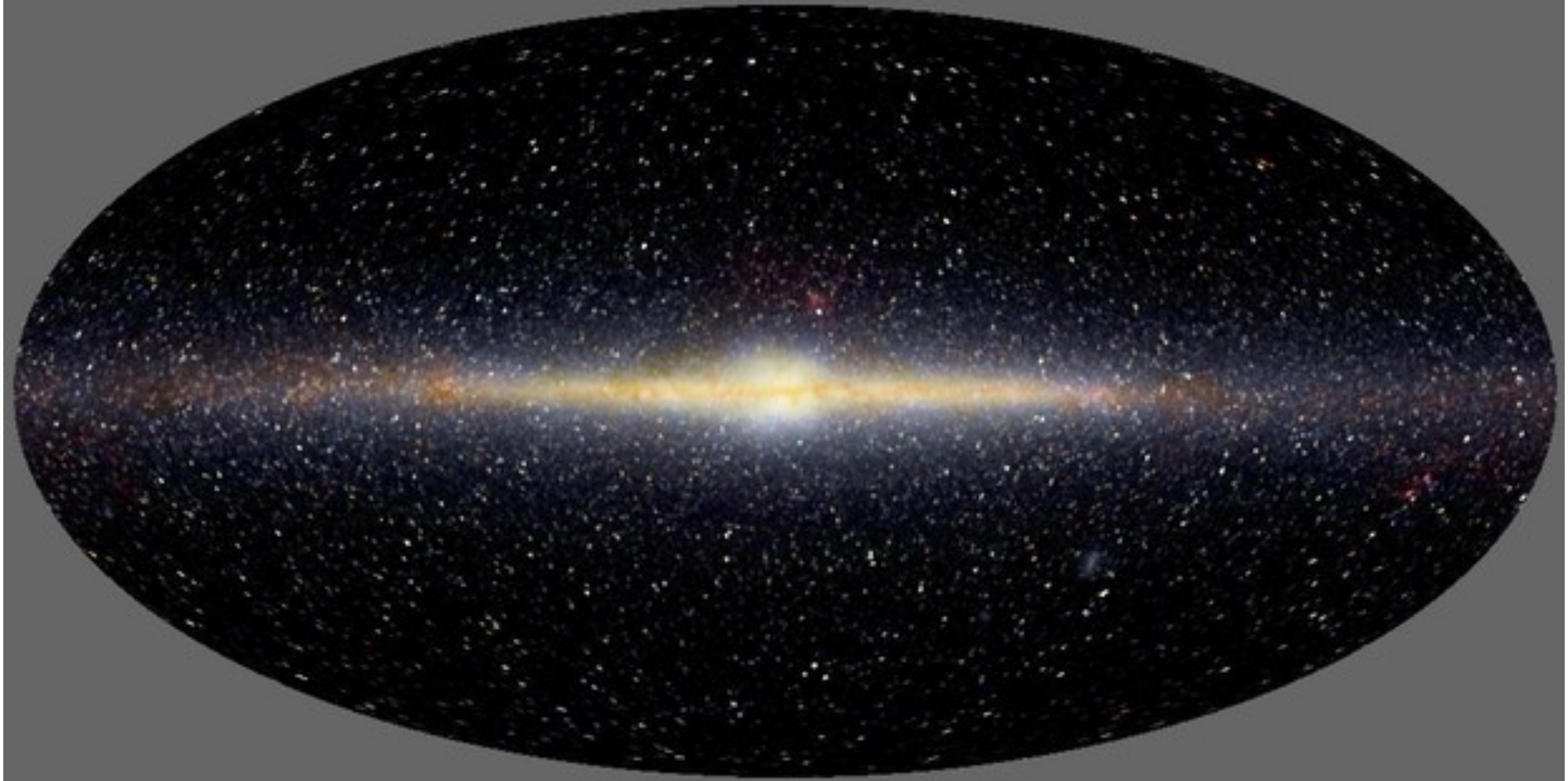

Milky Way   SBbc

2MASSShowcase

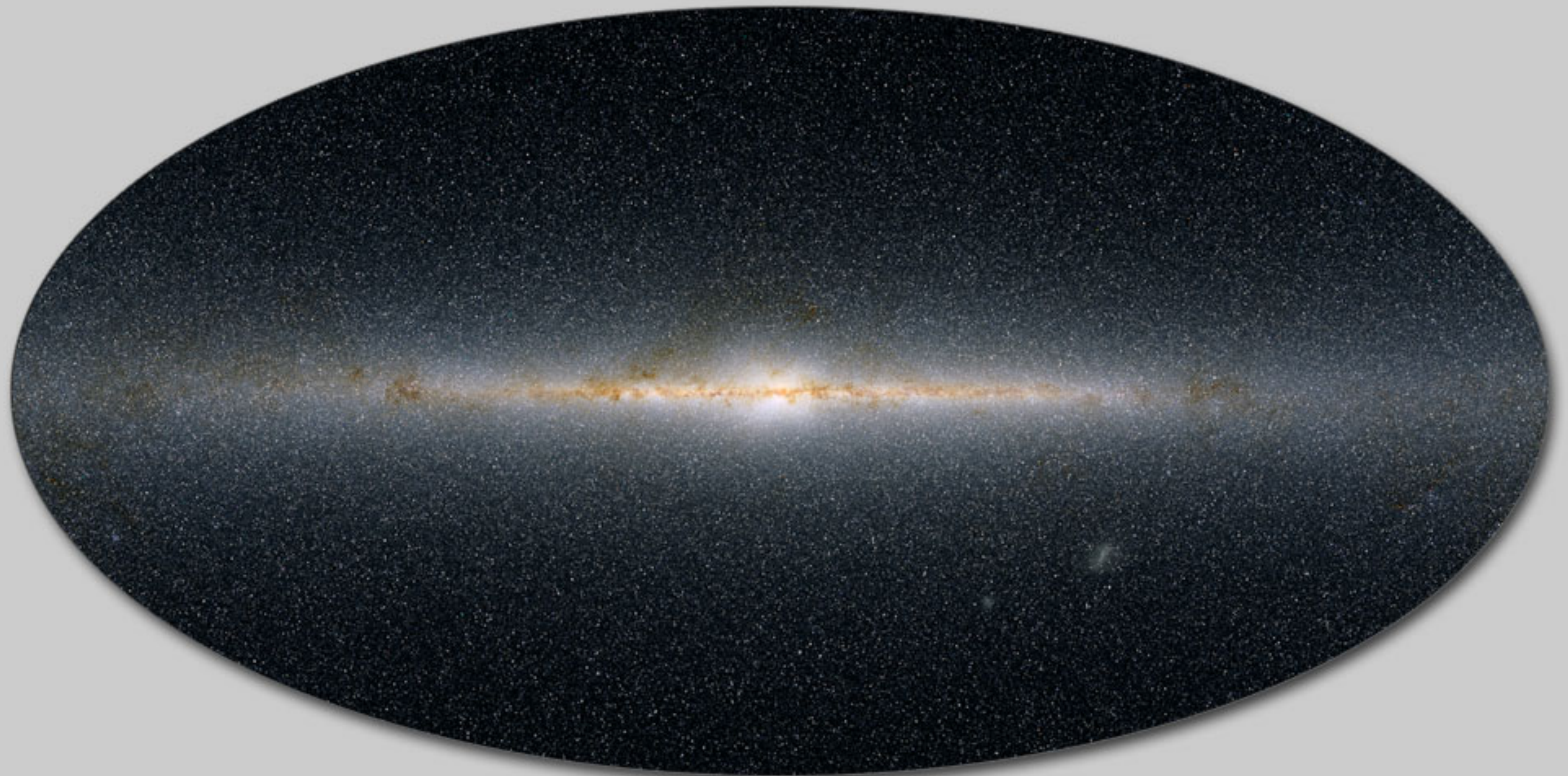

The Infrared Milky Way This map of the infrared sky includes the light of a half billion stars

Two Micron All Sky Survey Image Mosaic: Infrared Processing and Analysis Center/Caltech & University of Massachusetts

Sc galaxies

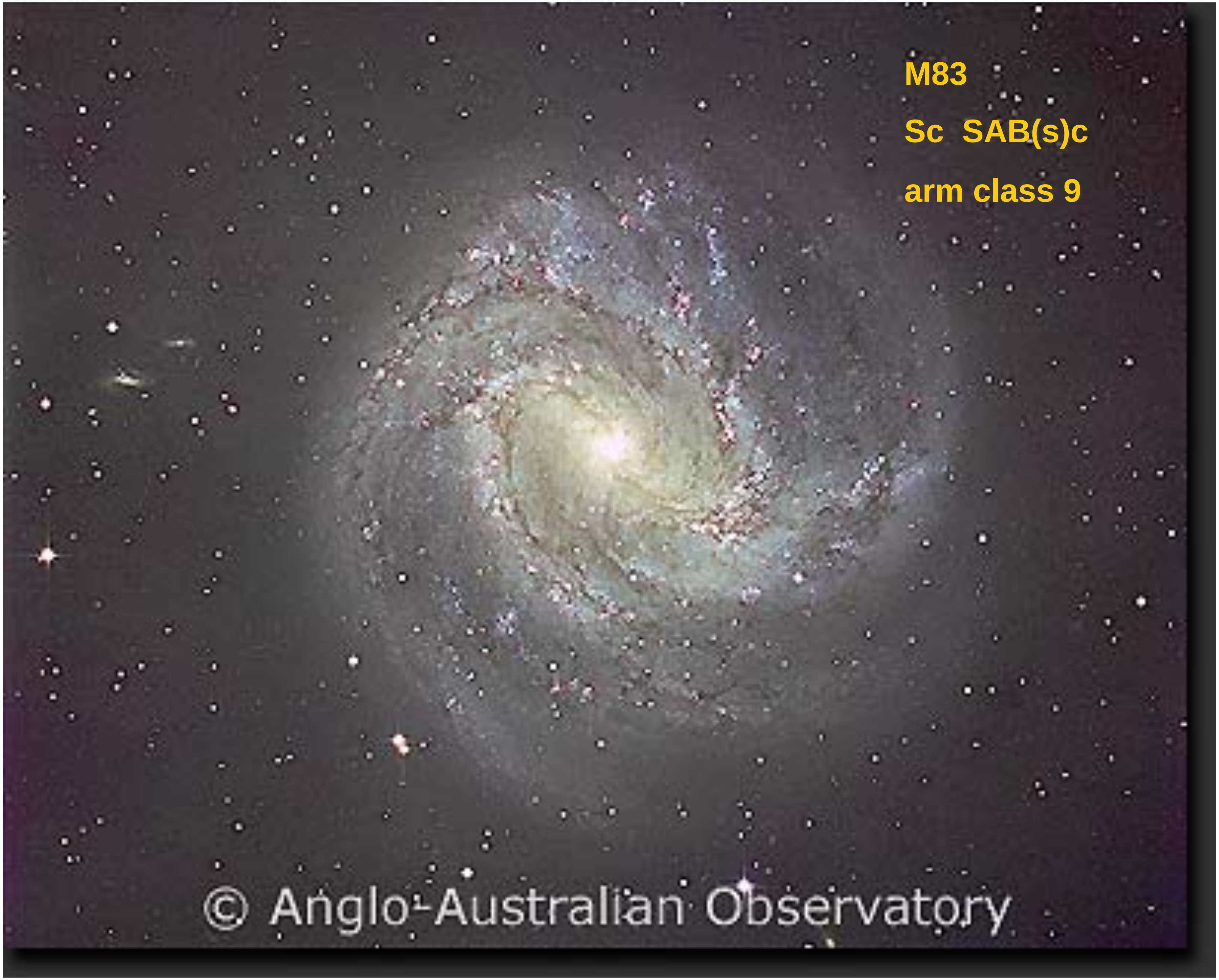
M83
Sc SAB(s)c
arm class 9
© Anglo-Australian Observatory


NGC 2997
Sc SA(s)c
arm class 9
©Anglo-Australian Observatory

NGC 5907

Sc SA(s)c

Scd galaxies


M101
Scd SAB(rs)cd
arm class 9


M101
Scd SAB(rs)cd
arm class 9

M33

Scd SA(s)cd

arm class 5

Sd galaxies

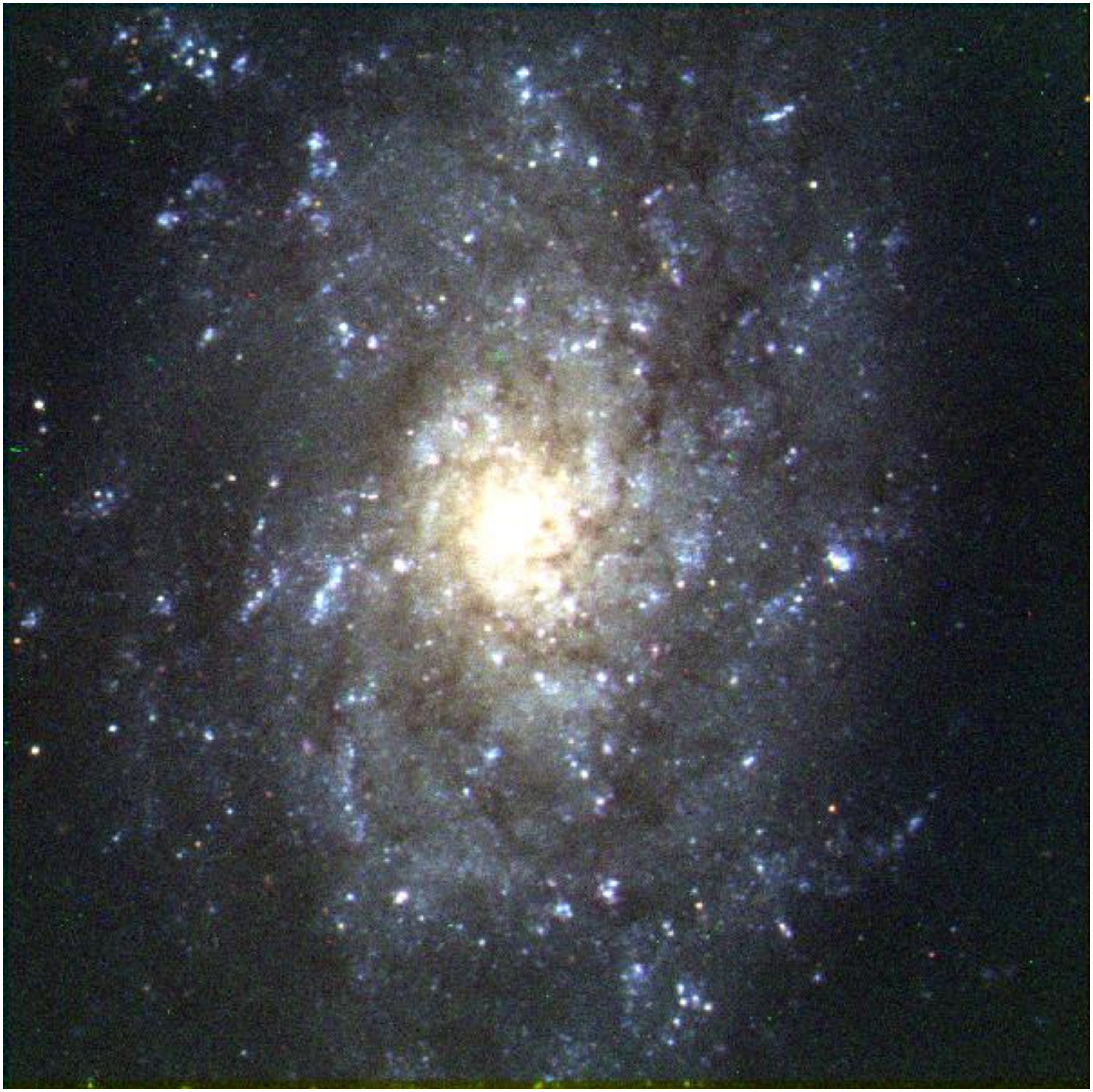

NGC 7793

Sc SA(s)d

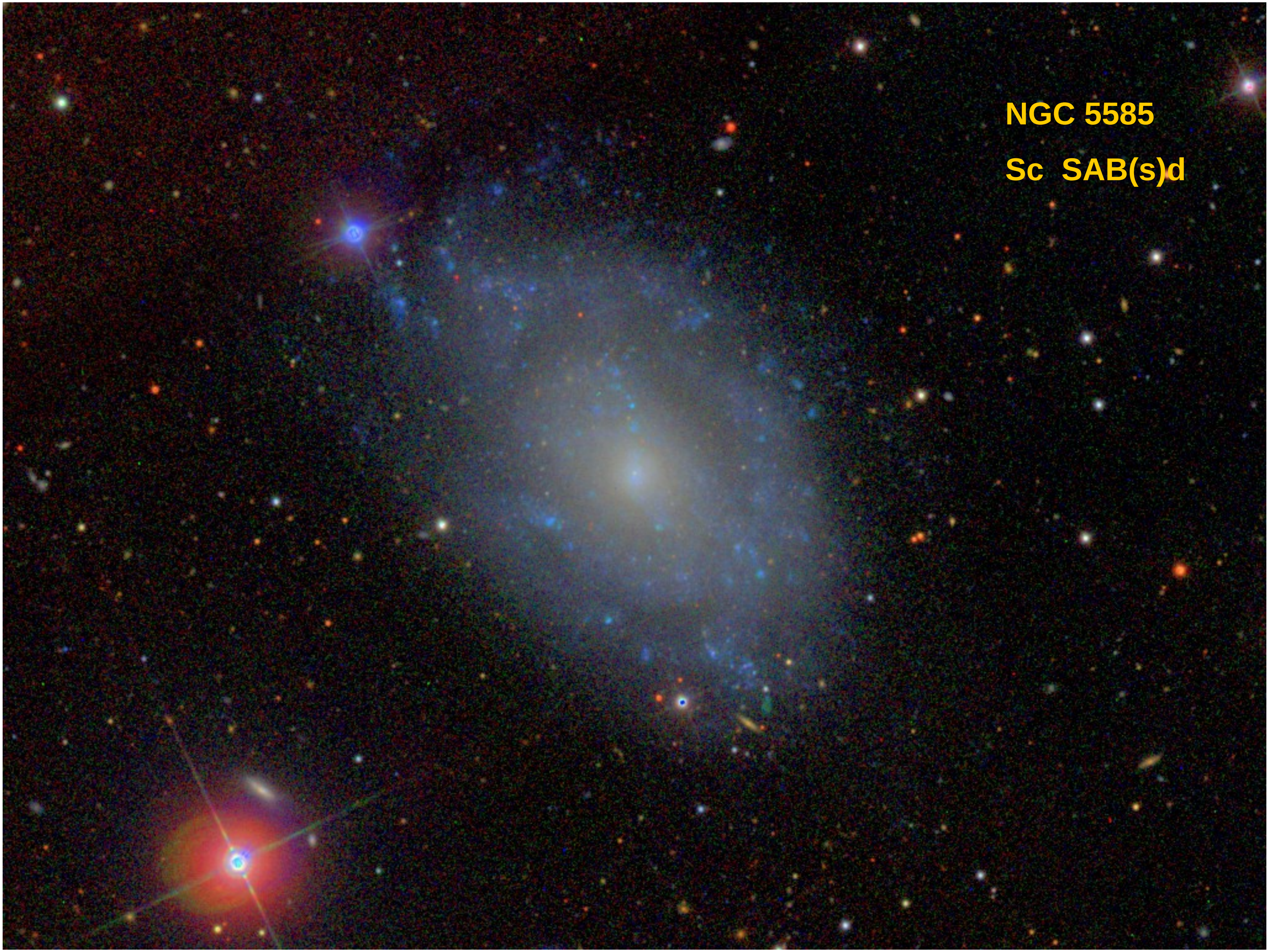
NGC 5585
Sc SAB(s)d

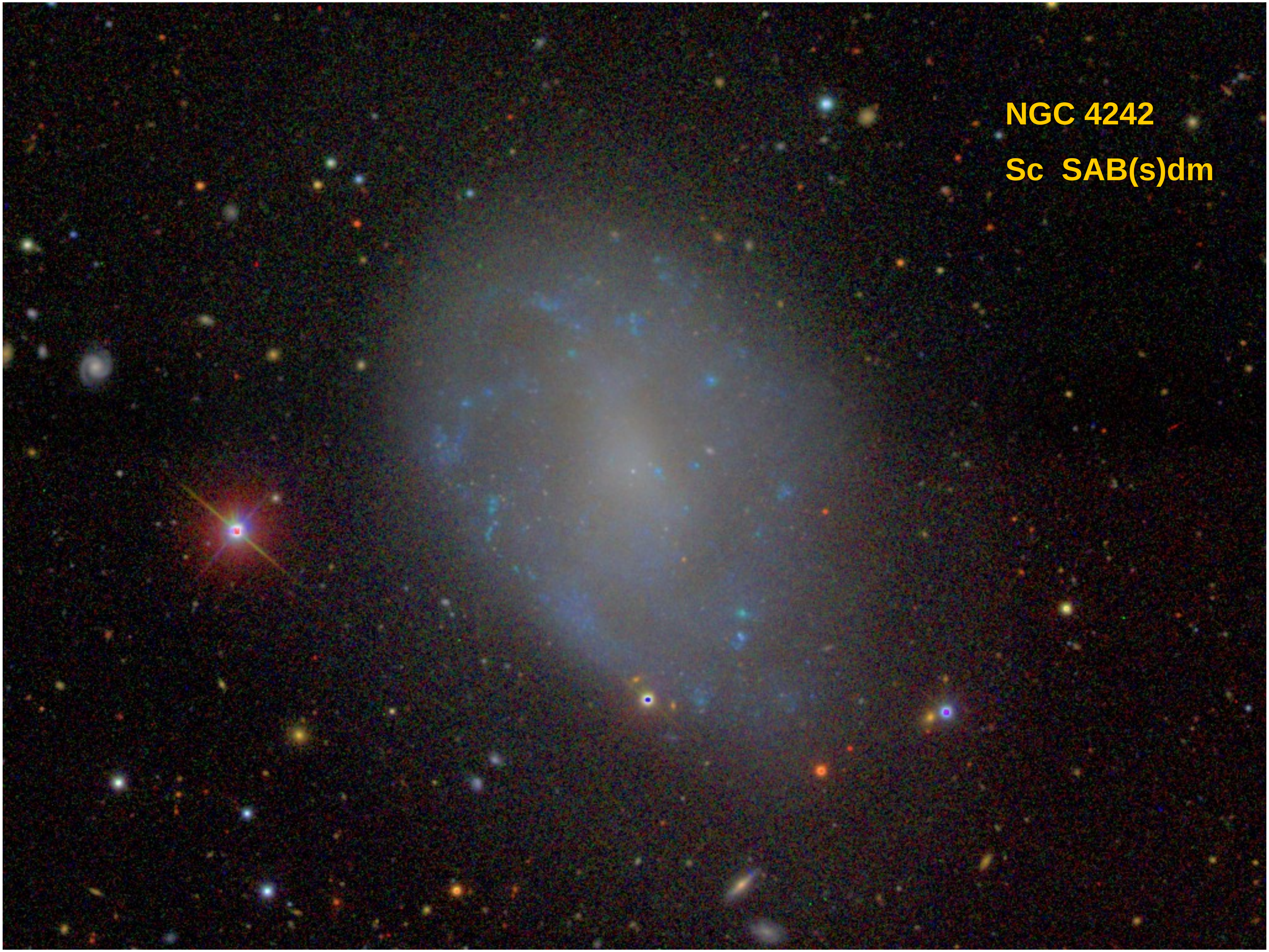
NGC 4242
Sc SAB(s)dm

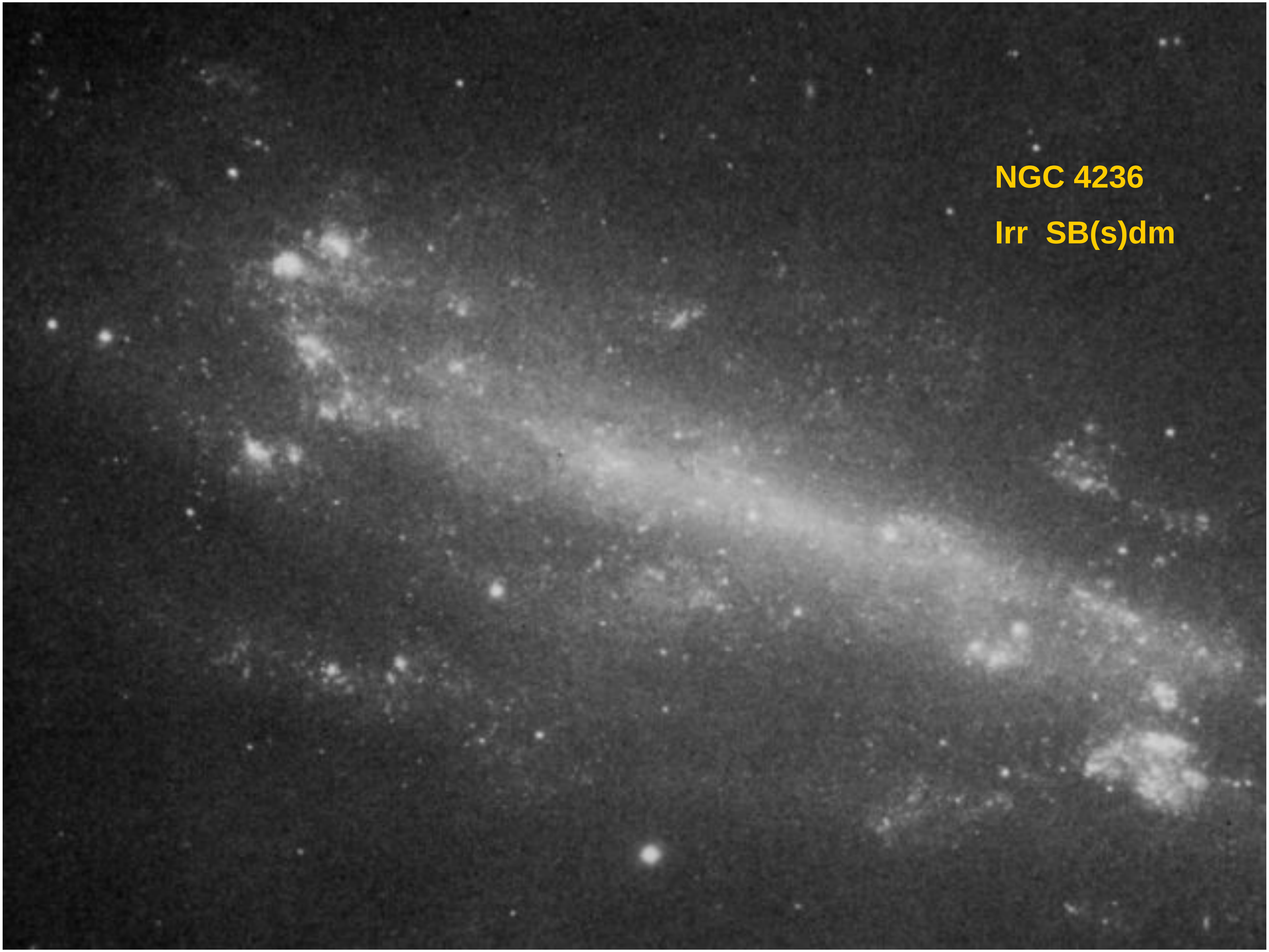
NGC 4236
Irr SB(s)dm

Lenticular (S0) galaxies

NGC 4382

S0   SA(s)0

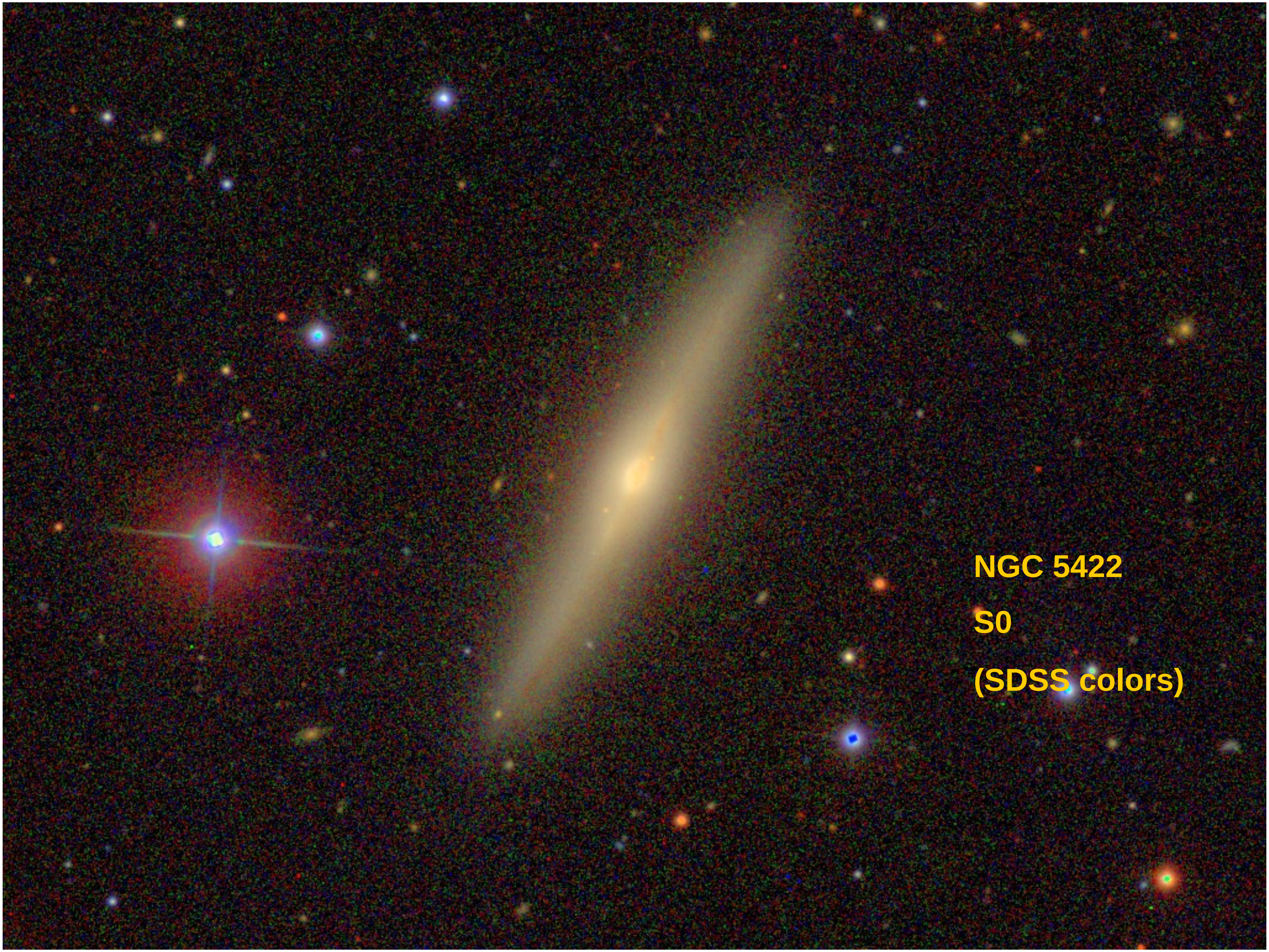
NGC 5422
S0
(SDSS colors)

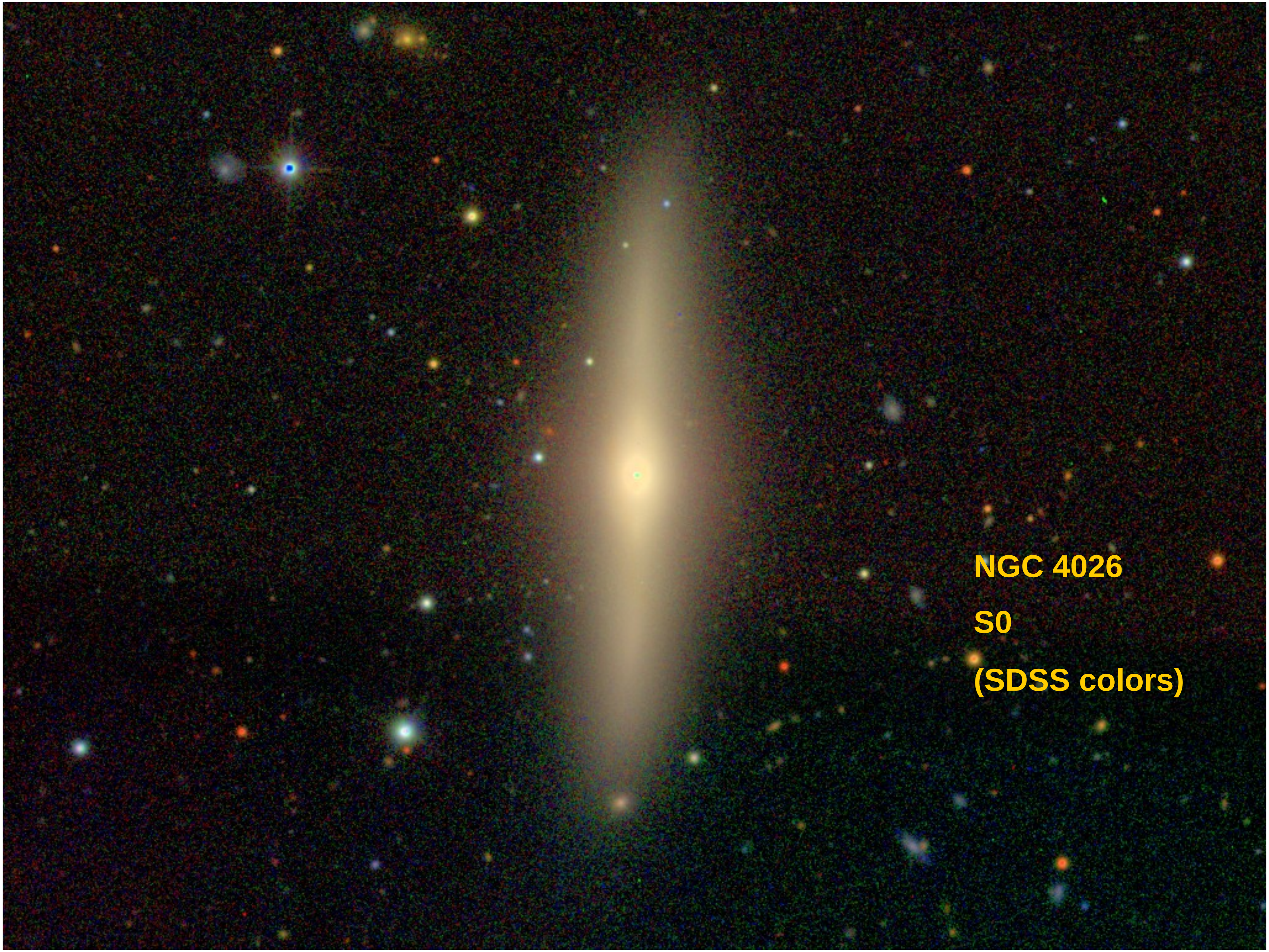
NGC 4026
S0
(SDSS colors)

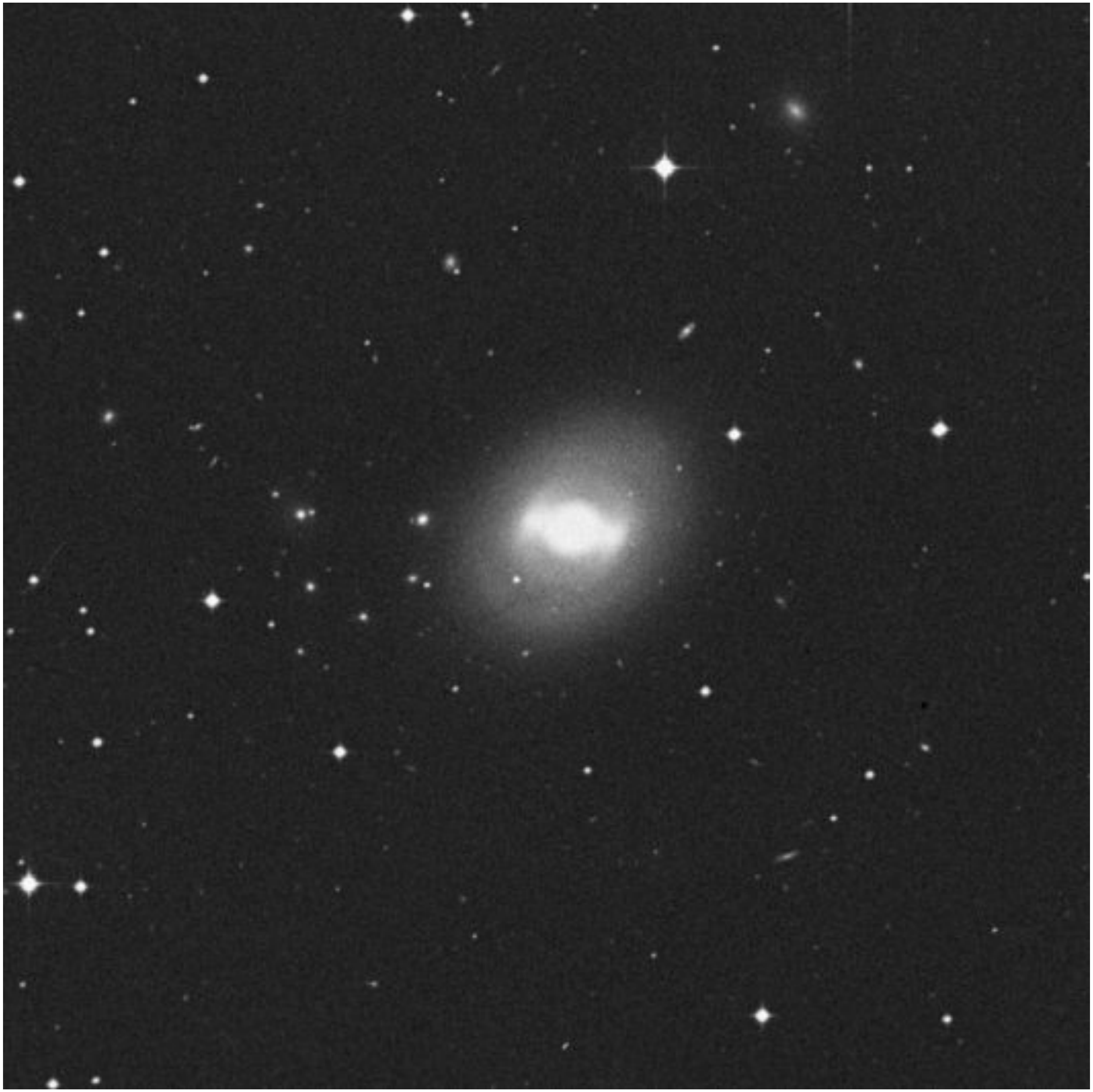

NGC 936

SB0 or SB(rs)0

Dwarf spheroidal (dSph) galaxies


Leo I
dSph or E
© Anglo-Australian Observatory

Fornax

dSph

cD galaxies (luminous red galaxies, brightest cluster galaxies)


Coma cluster with 2 (or maybe 1) cD galaxies

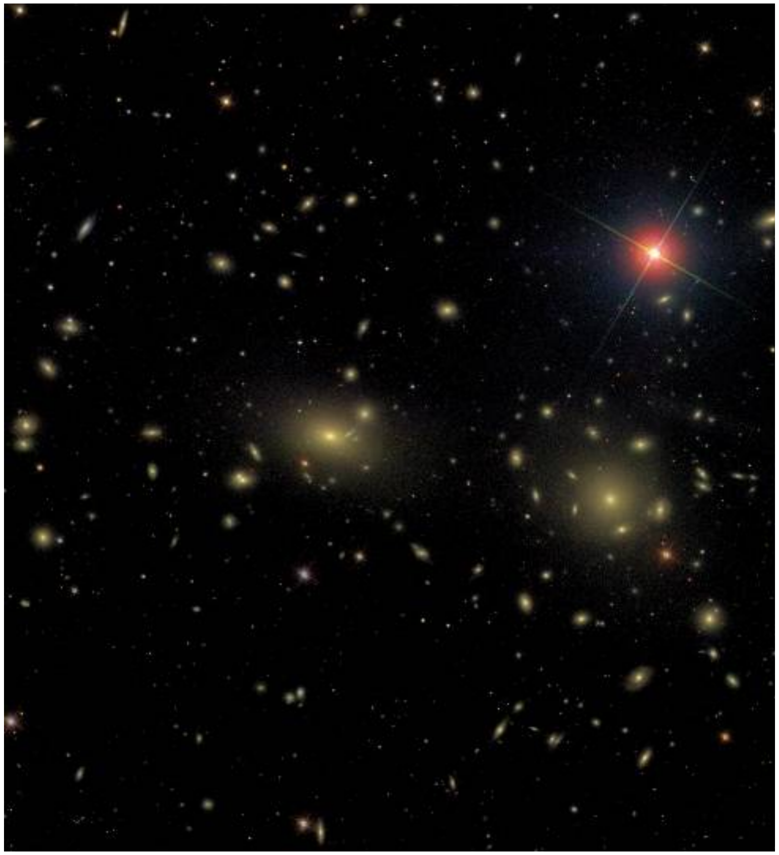

NOAO colors

SDSS colors

Irregular galaxies

Magellanic clouds


Large Magellanic Cloud
Irr SB(s)m
© Anglo-Australian Obs./Royal Obs. Edinburgh


Small Magellanic Cloud
Irr SB(s)m
© Anglo-Australian Obs./Royal Obs. Edinburgh

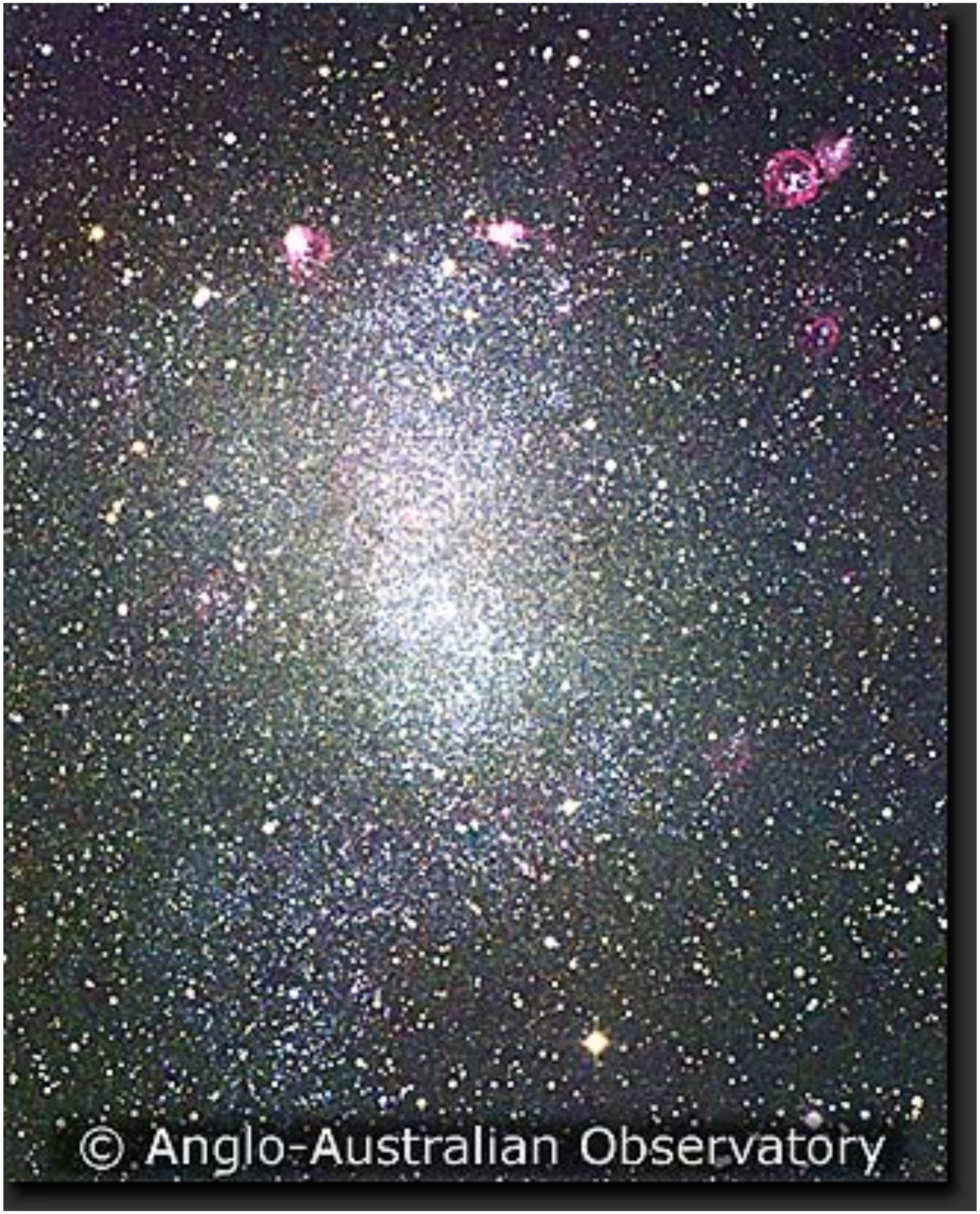

NGC 6822

Irr   IB(s)m


IC 5152
Irr IA(s)m
© Anglo-Australian Observatory

not galaxies

Omega Centauri - globular cluster (maybe)

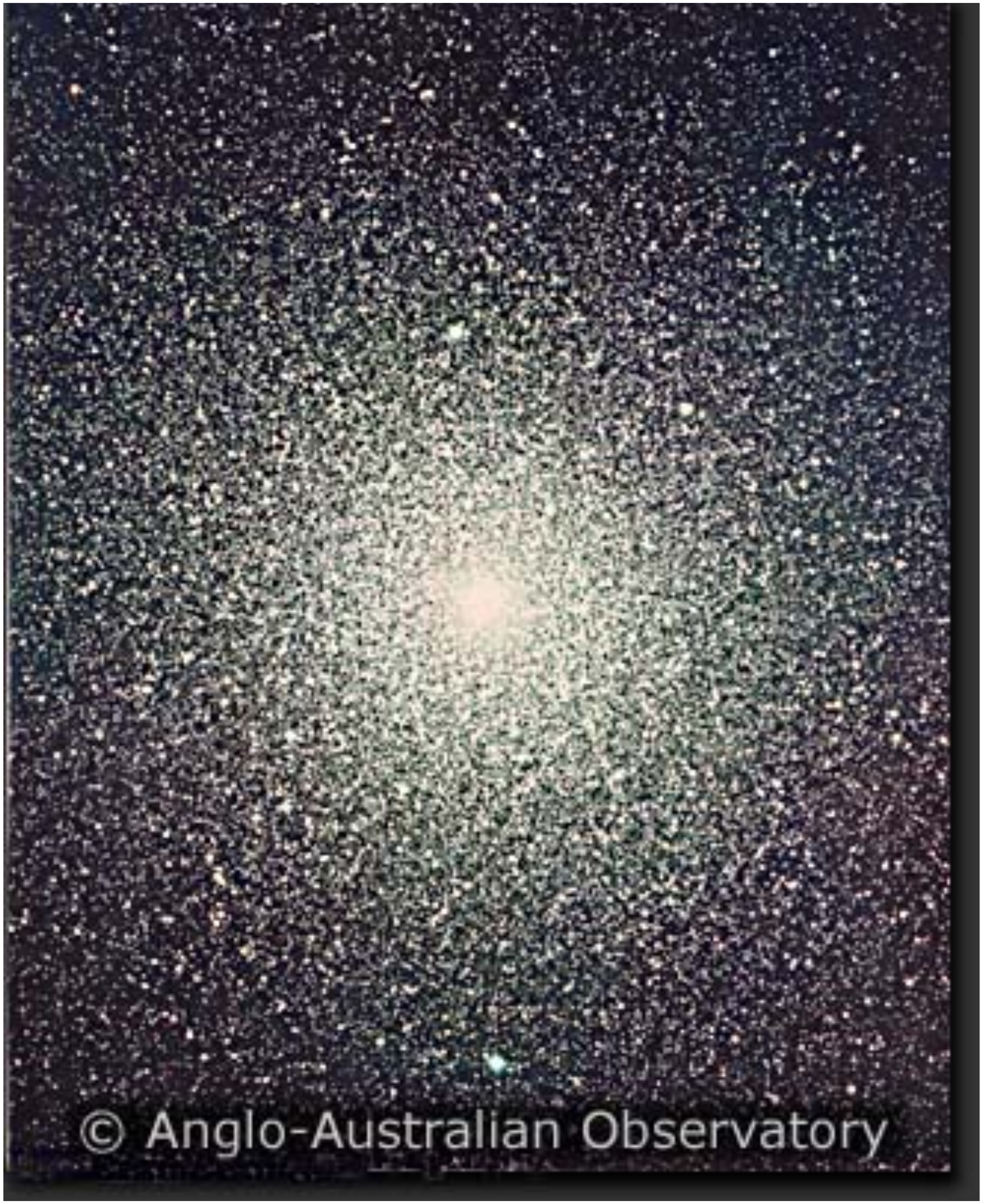

47 Tucanae

globular cluster

Peculiar galaxies

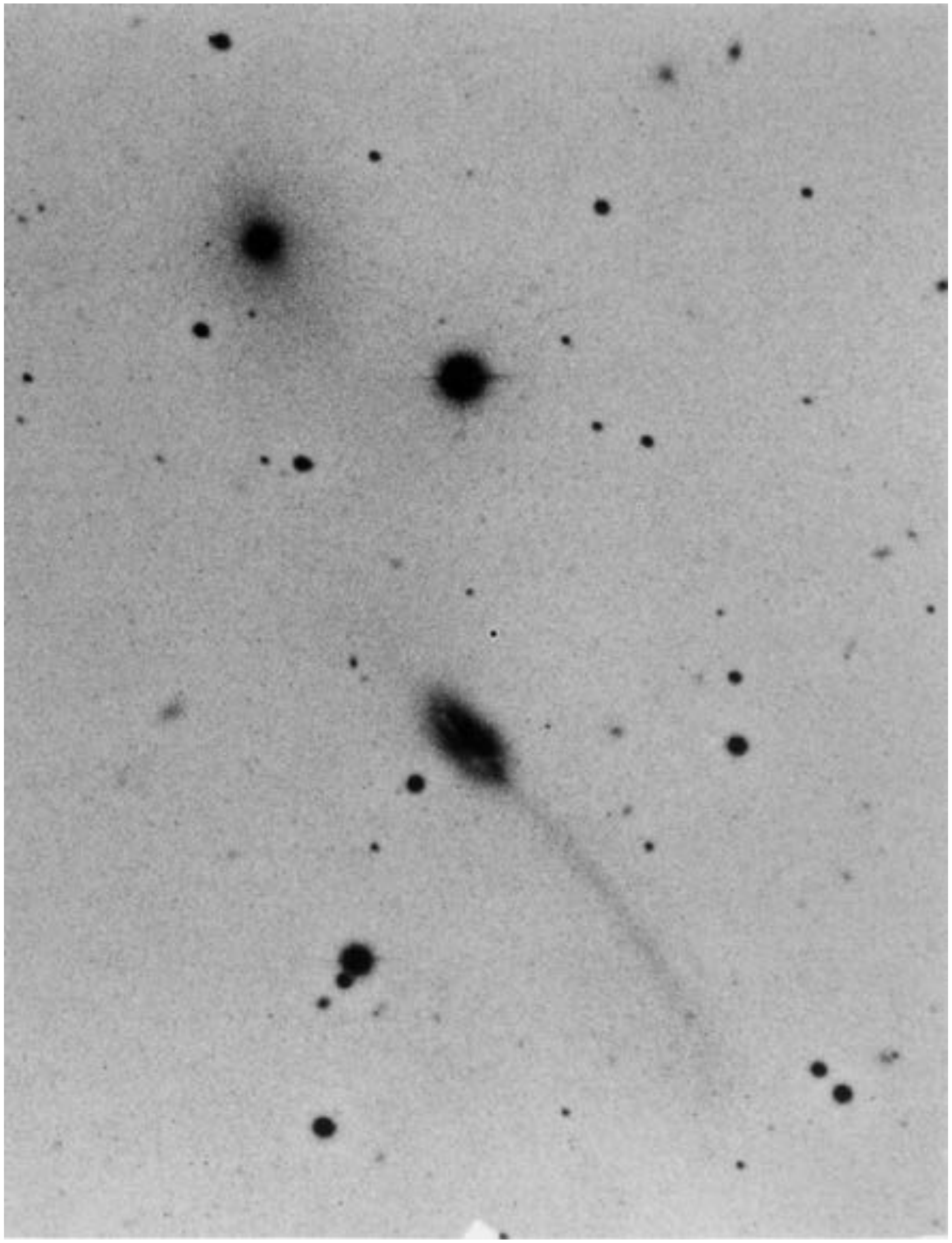
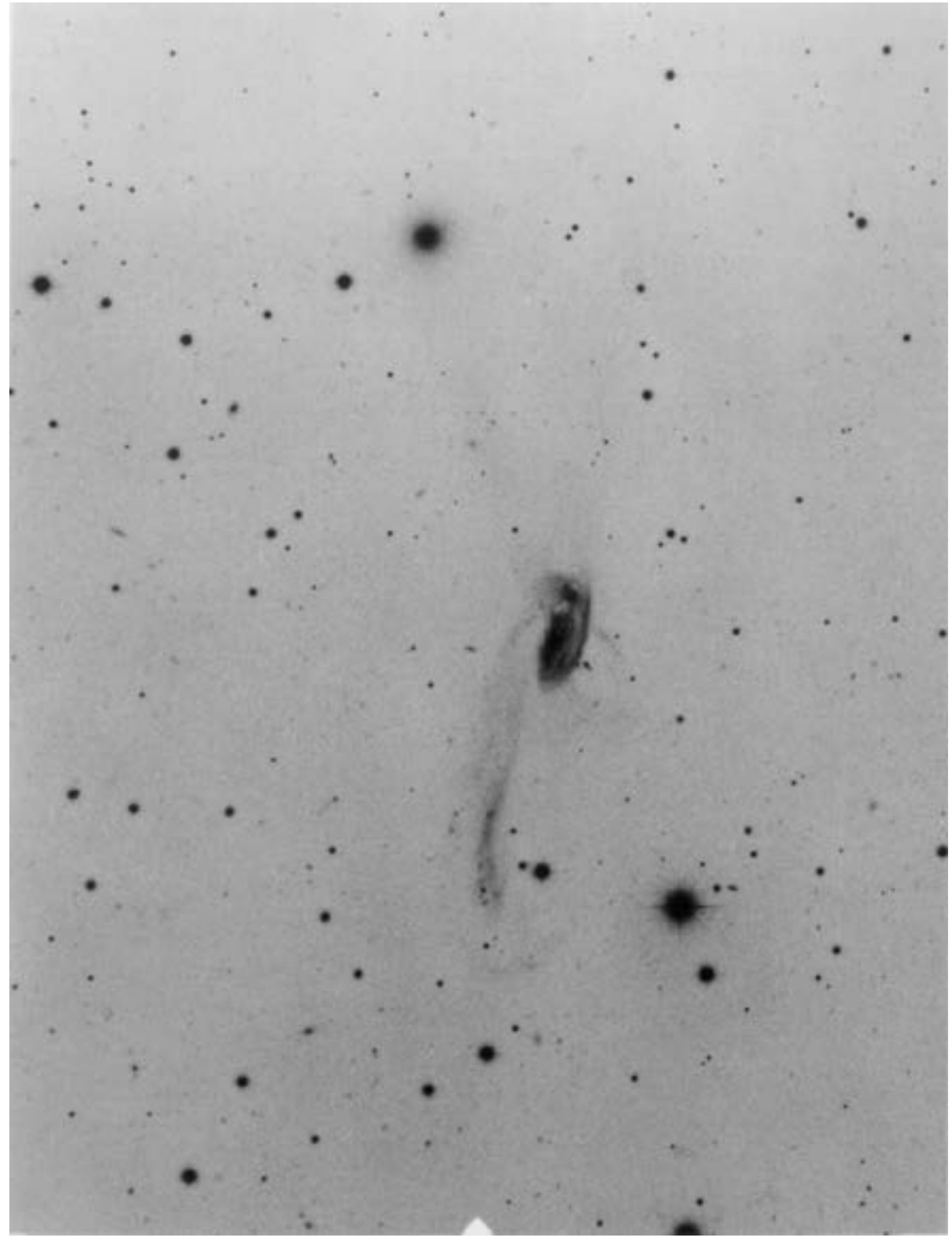

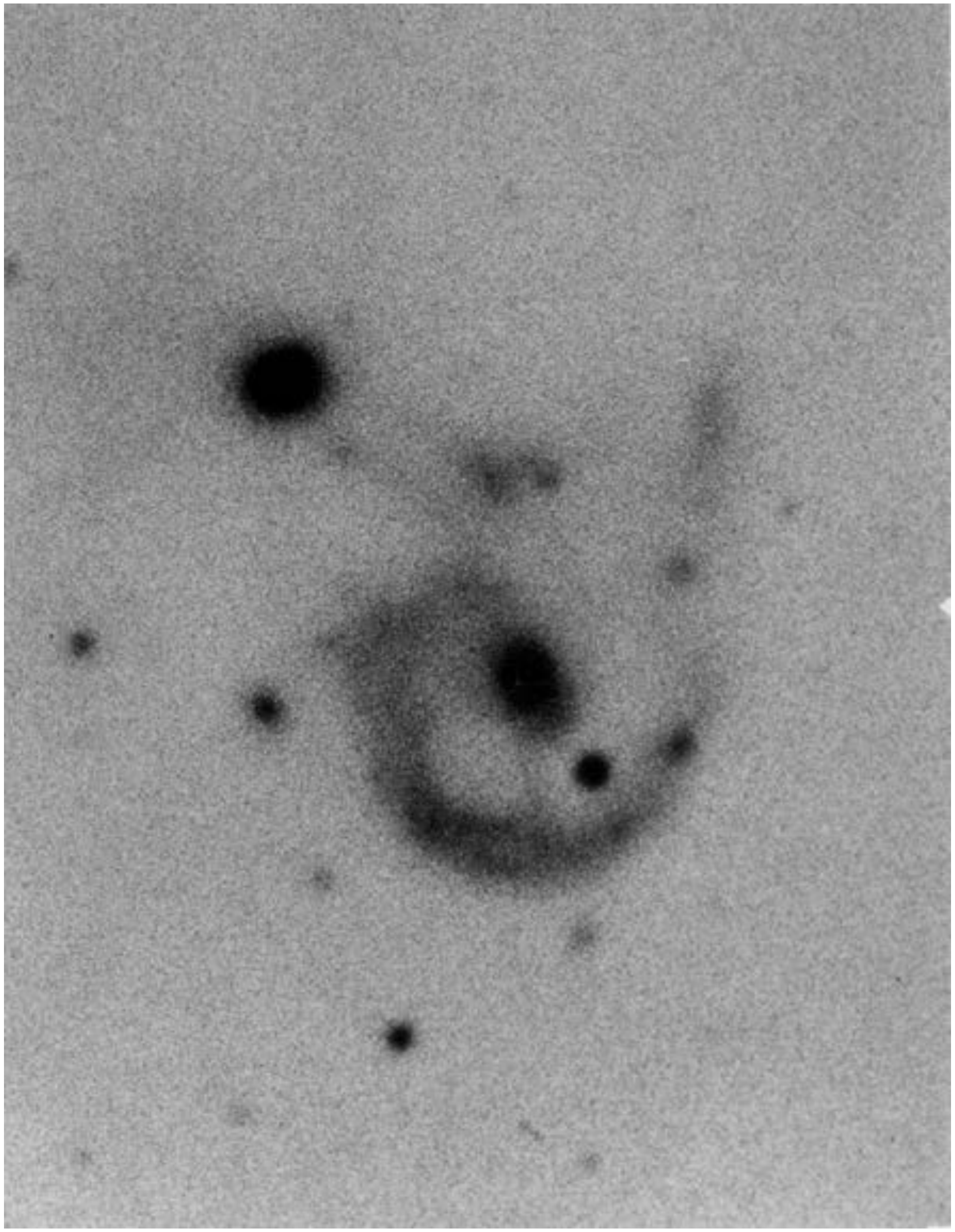
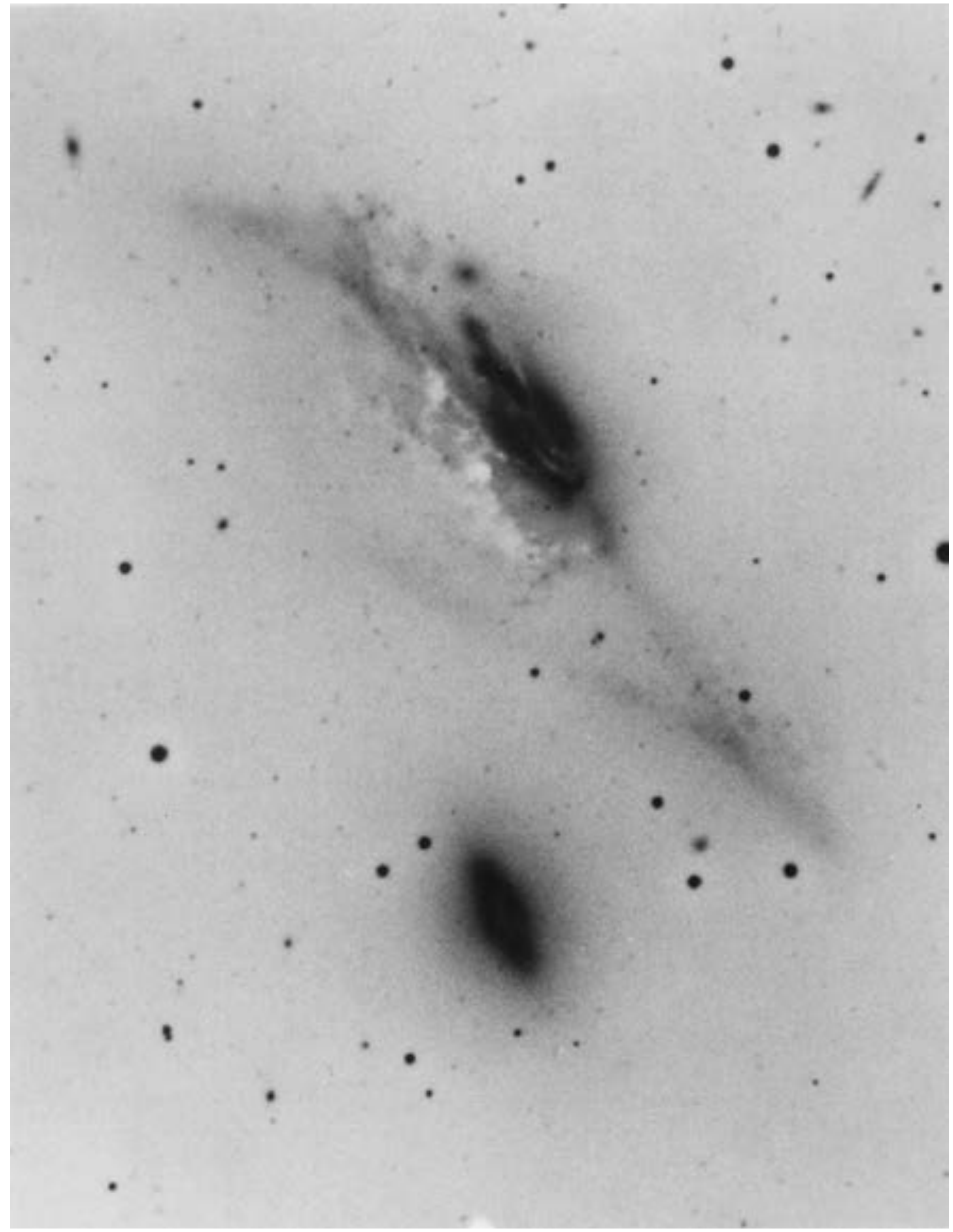

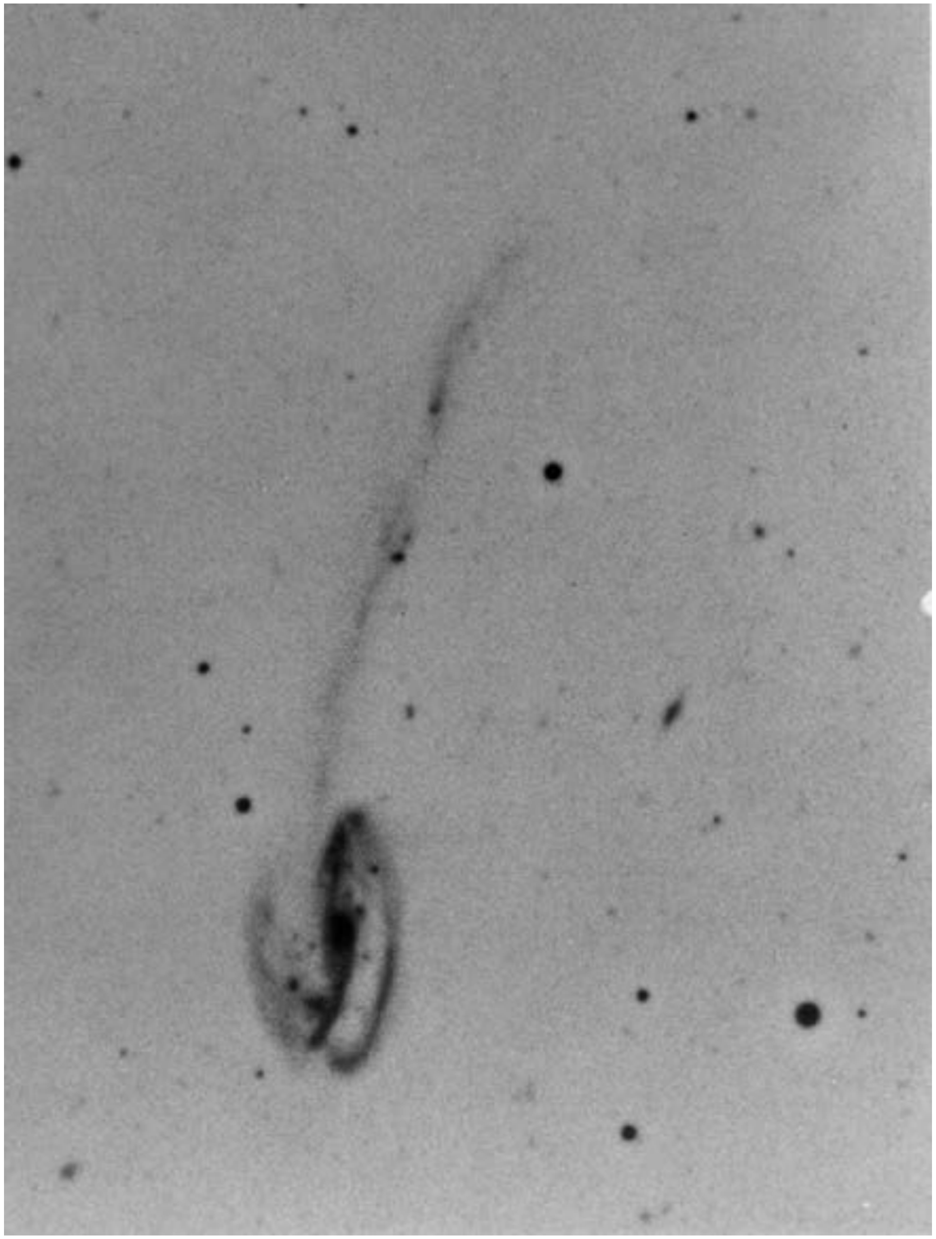
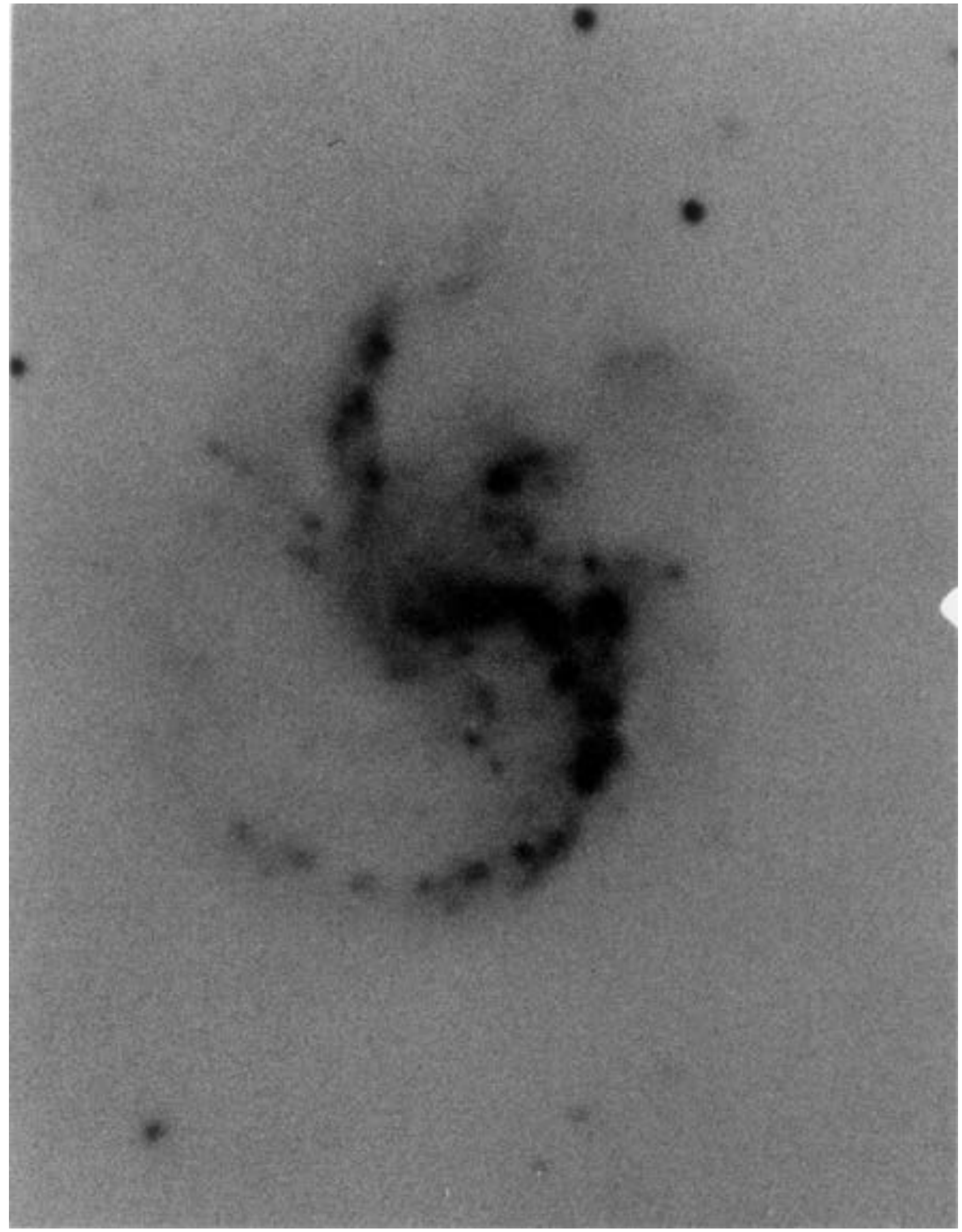

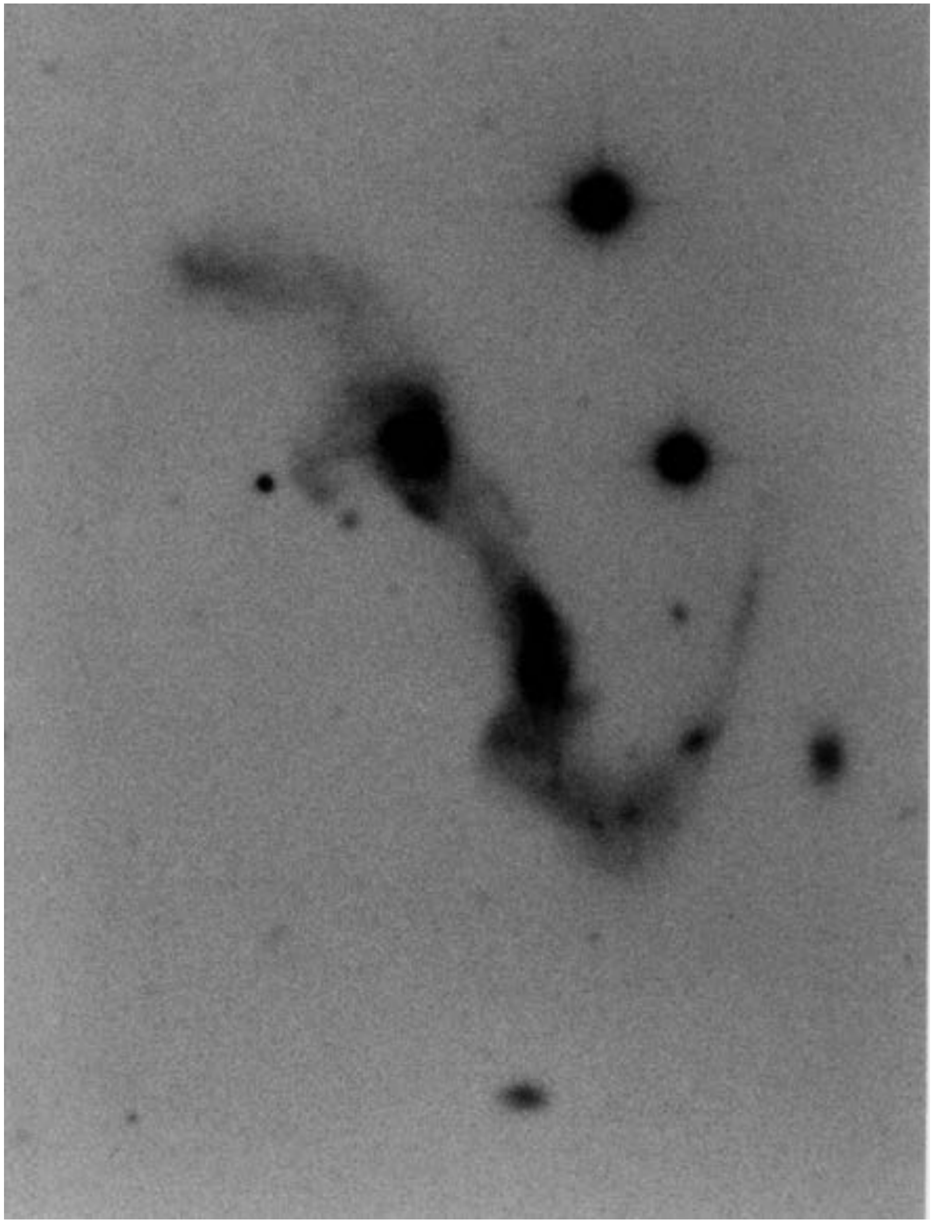

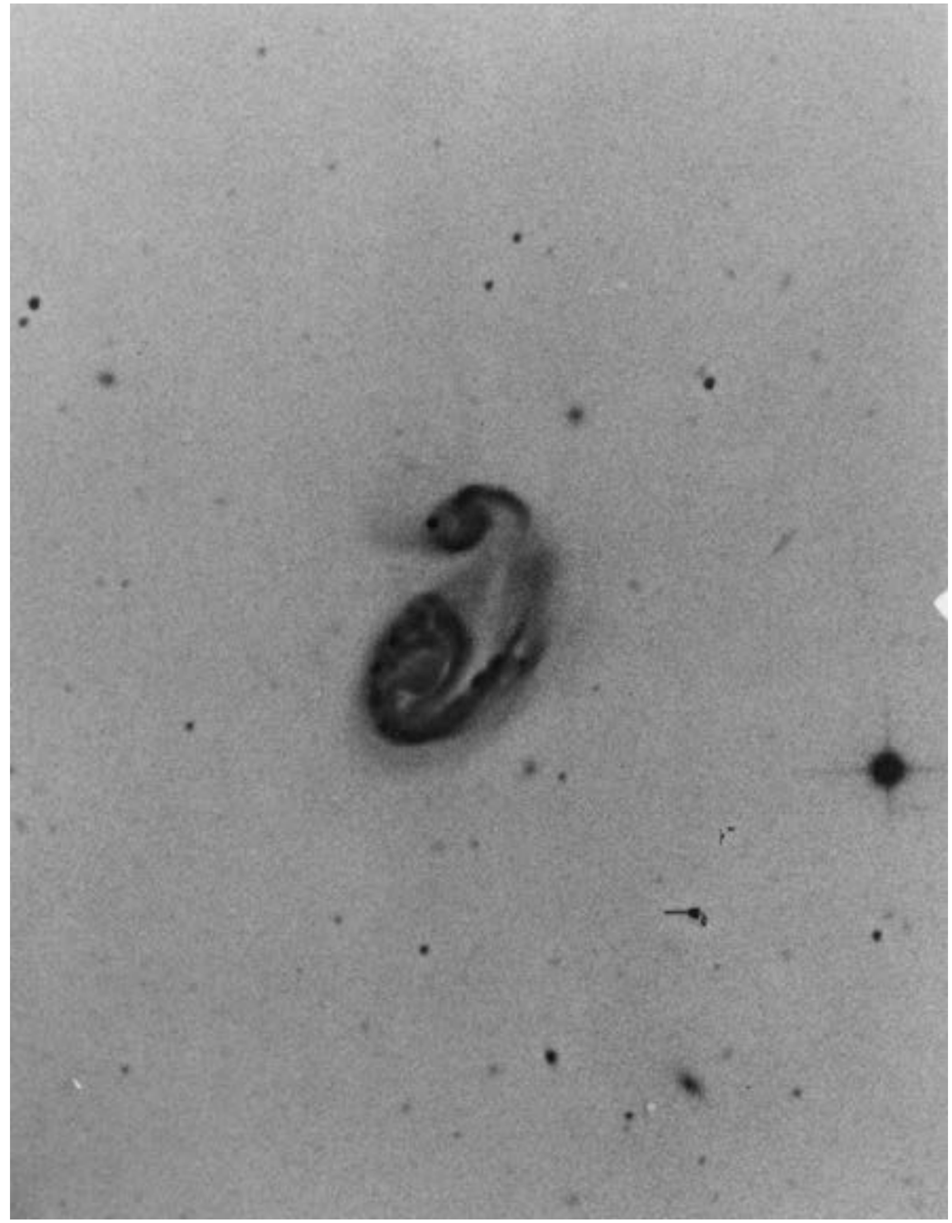

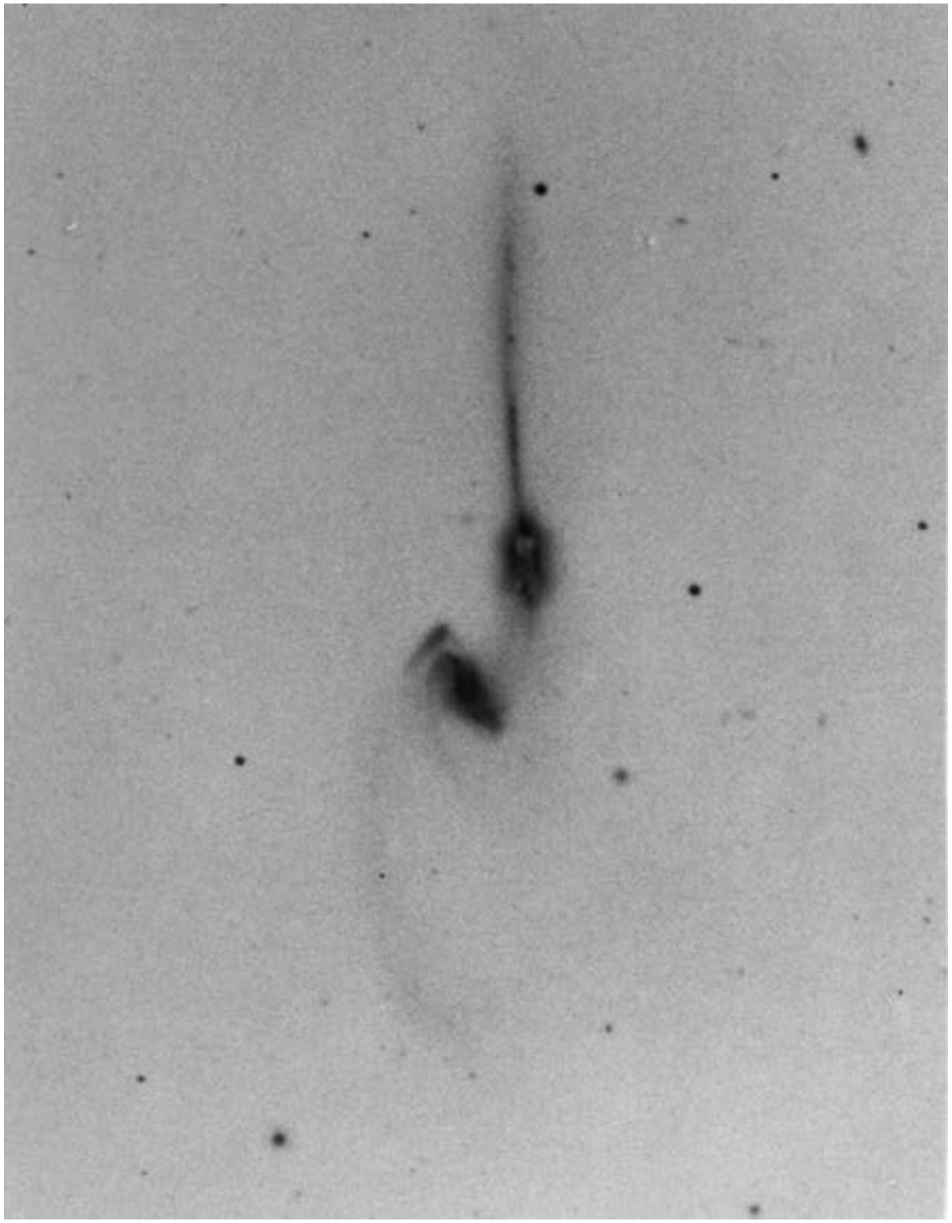

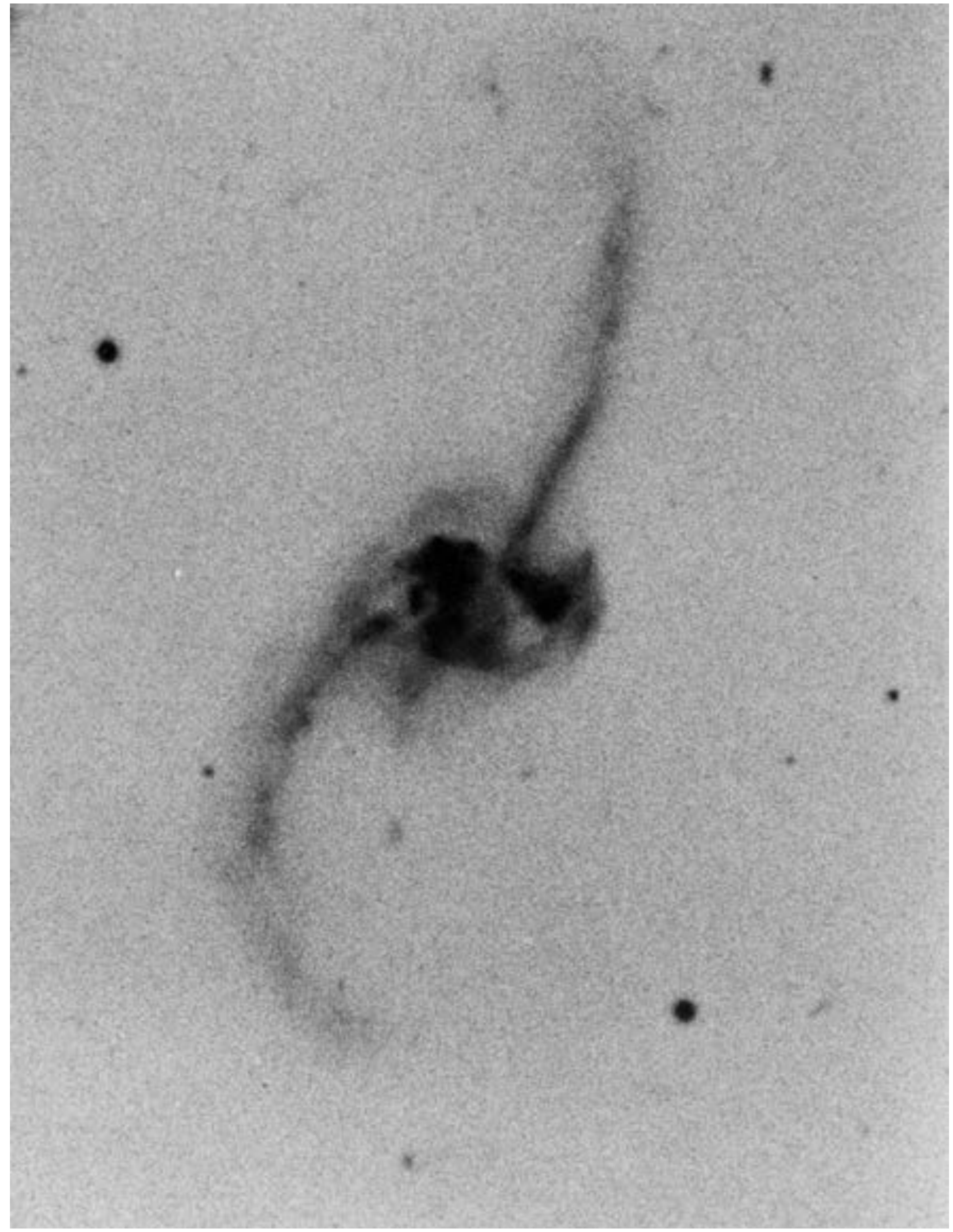

The Mice

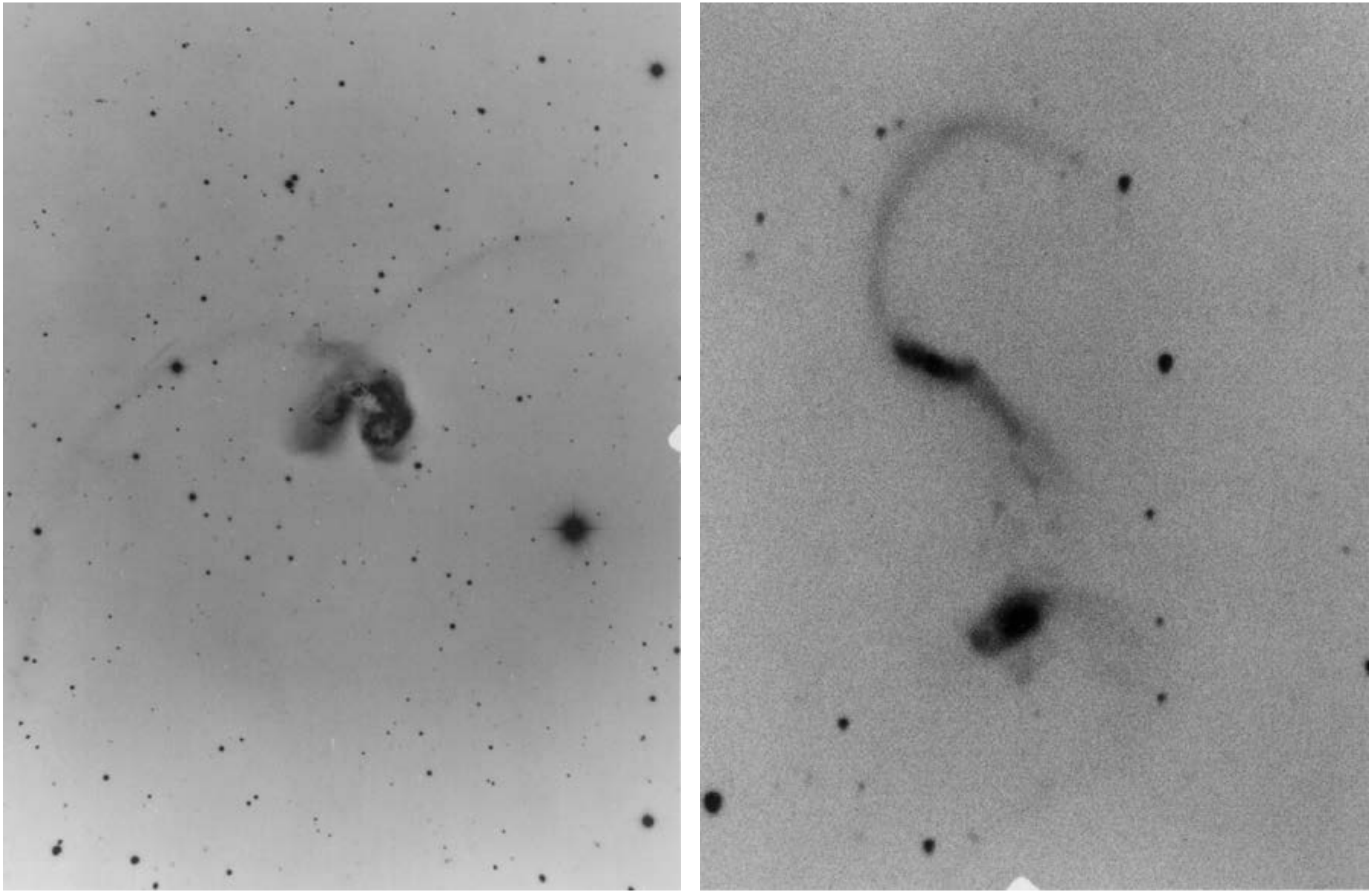

The Antennae

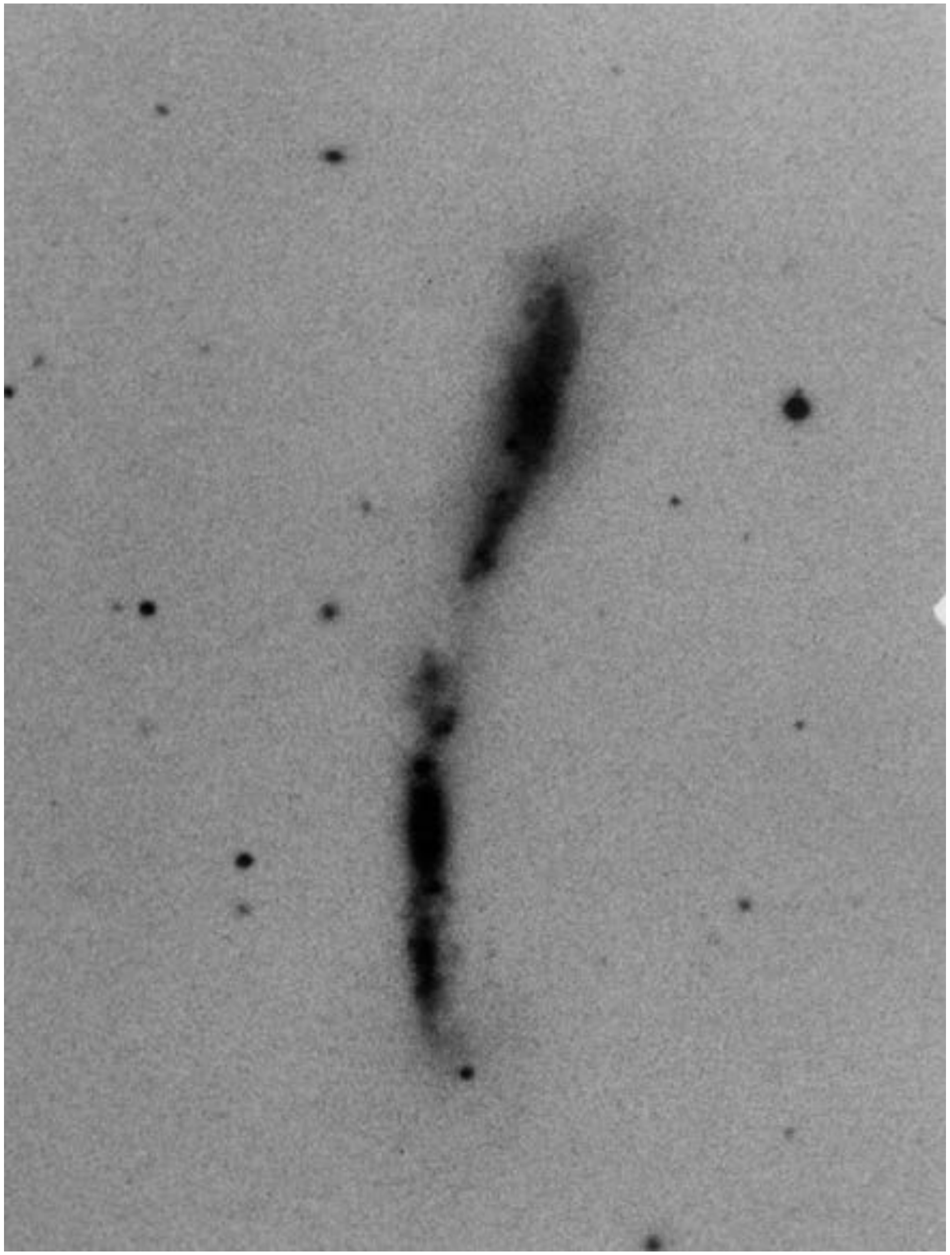
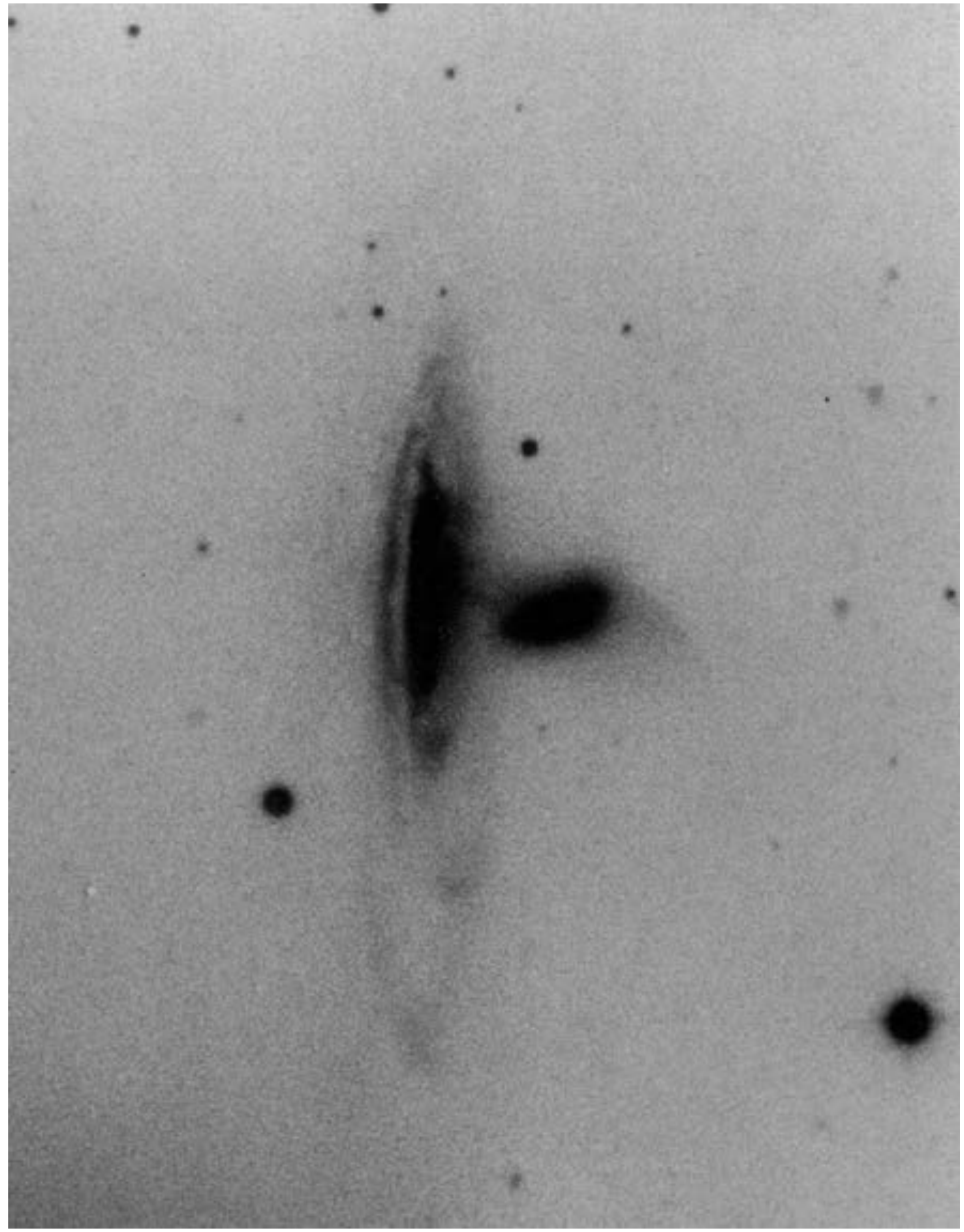

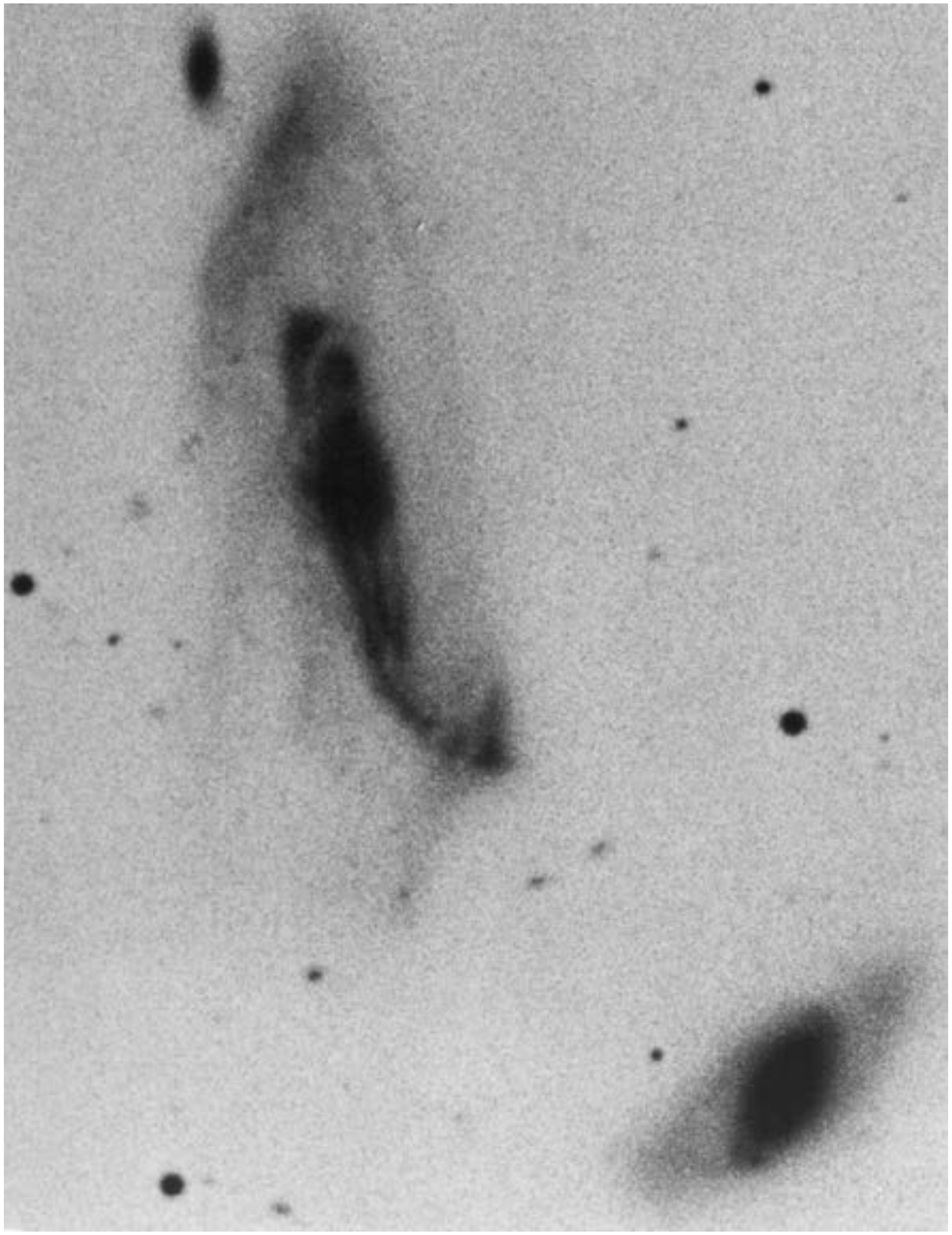
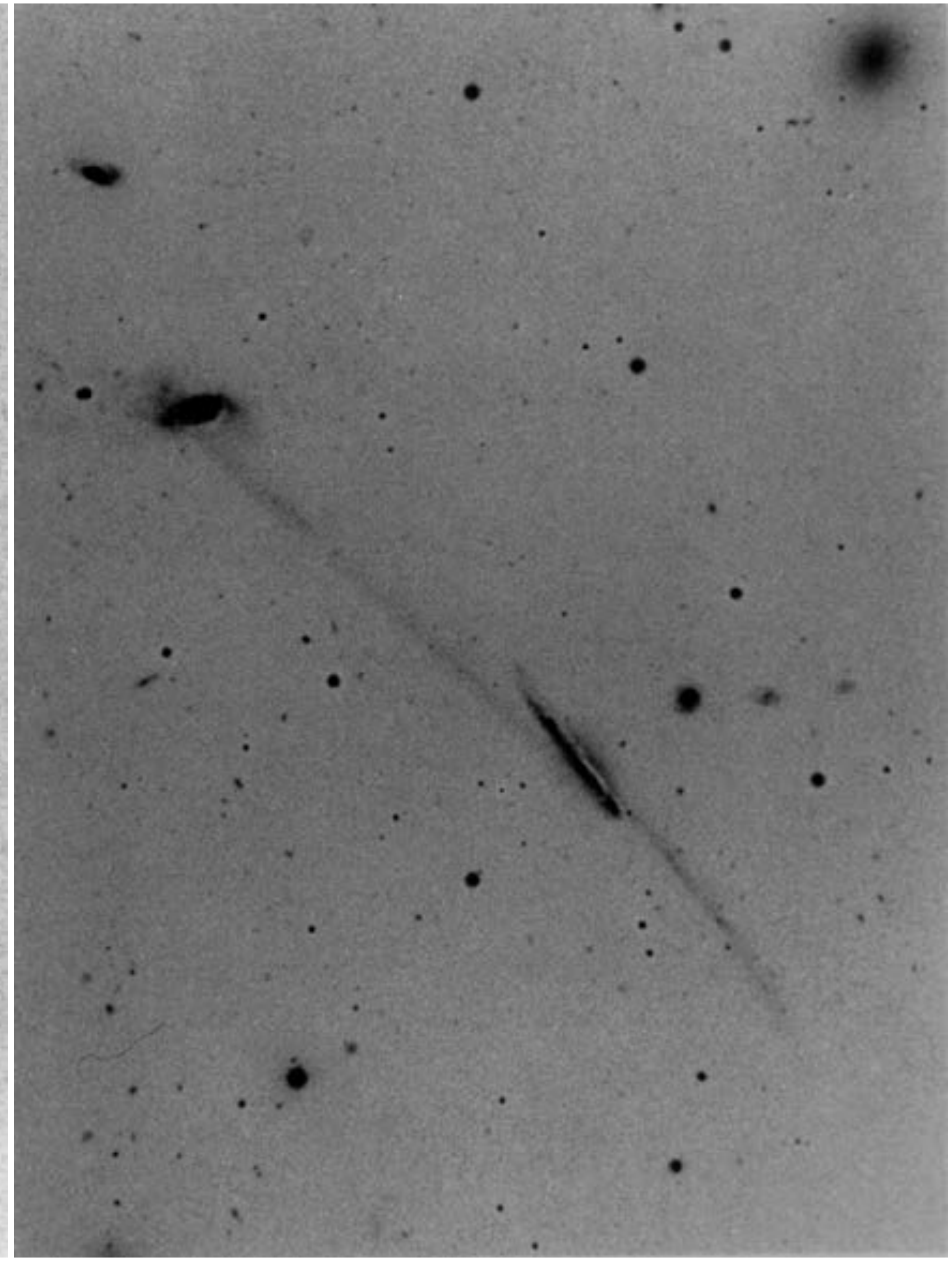

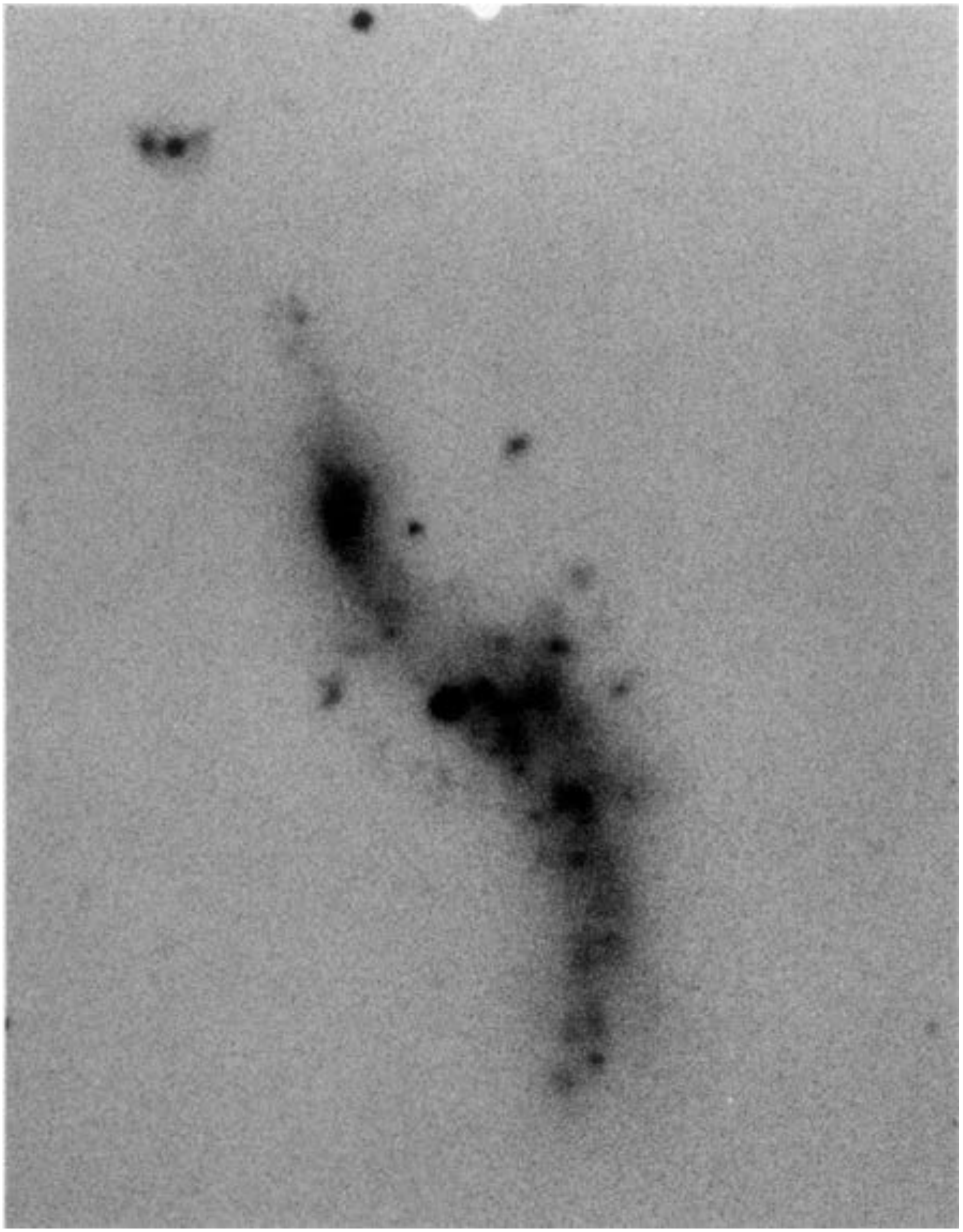

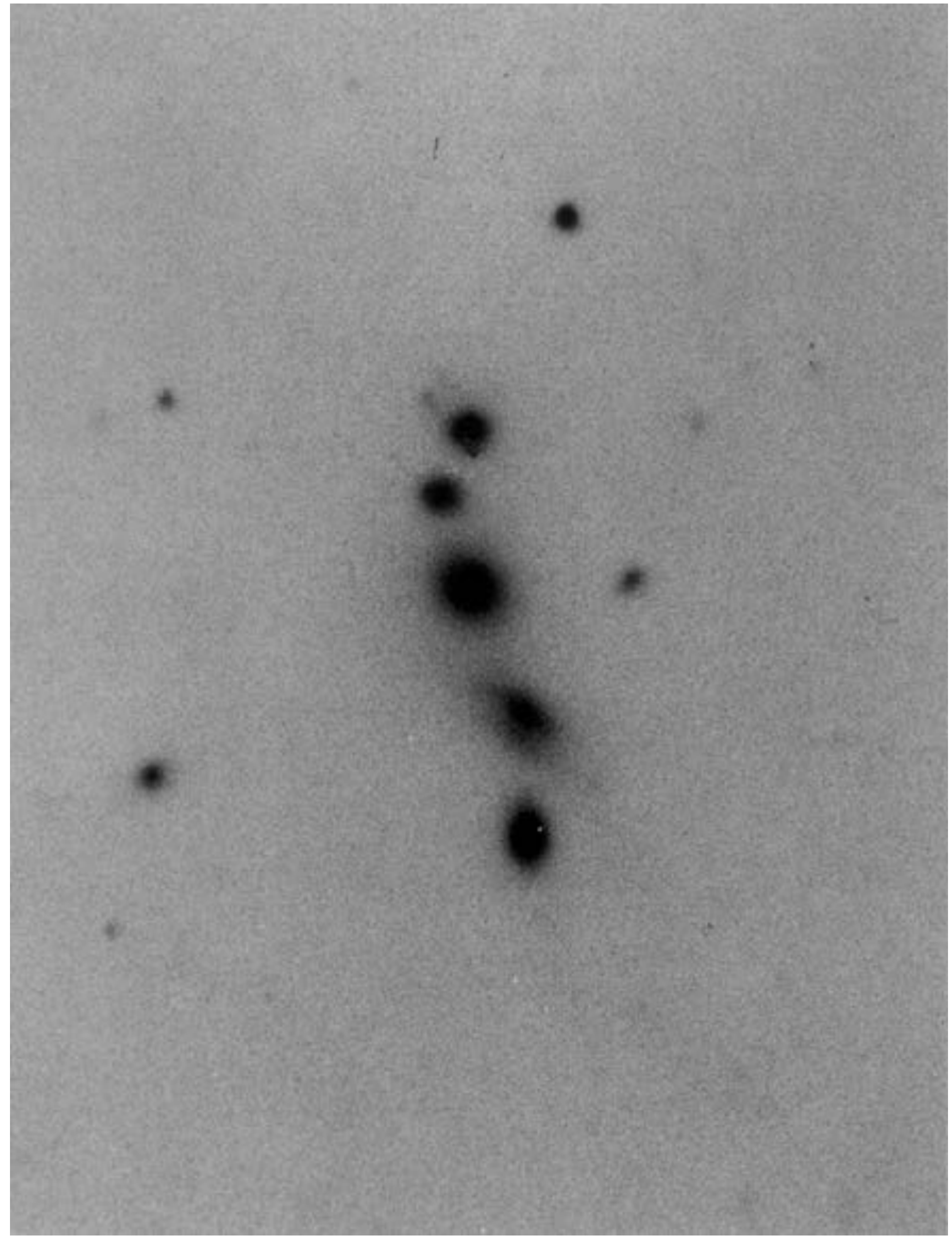

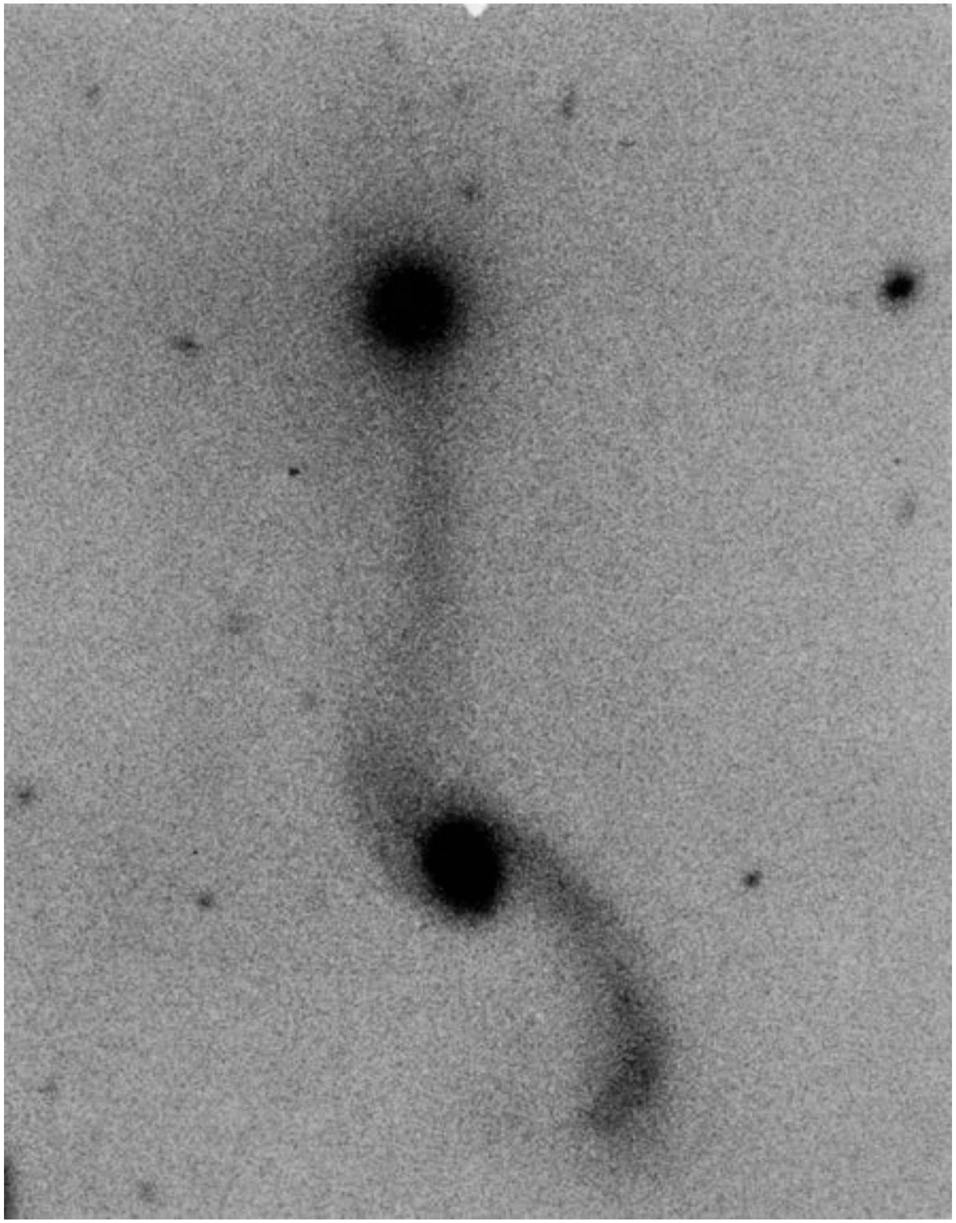

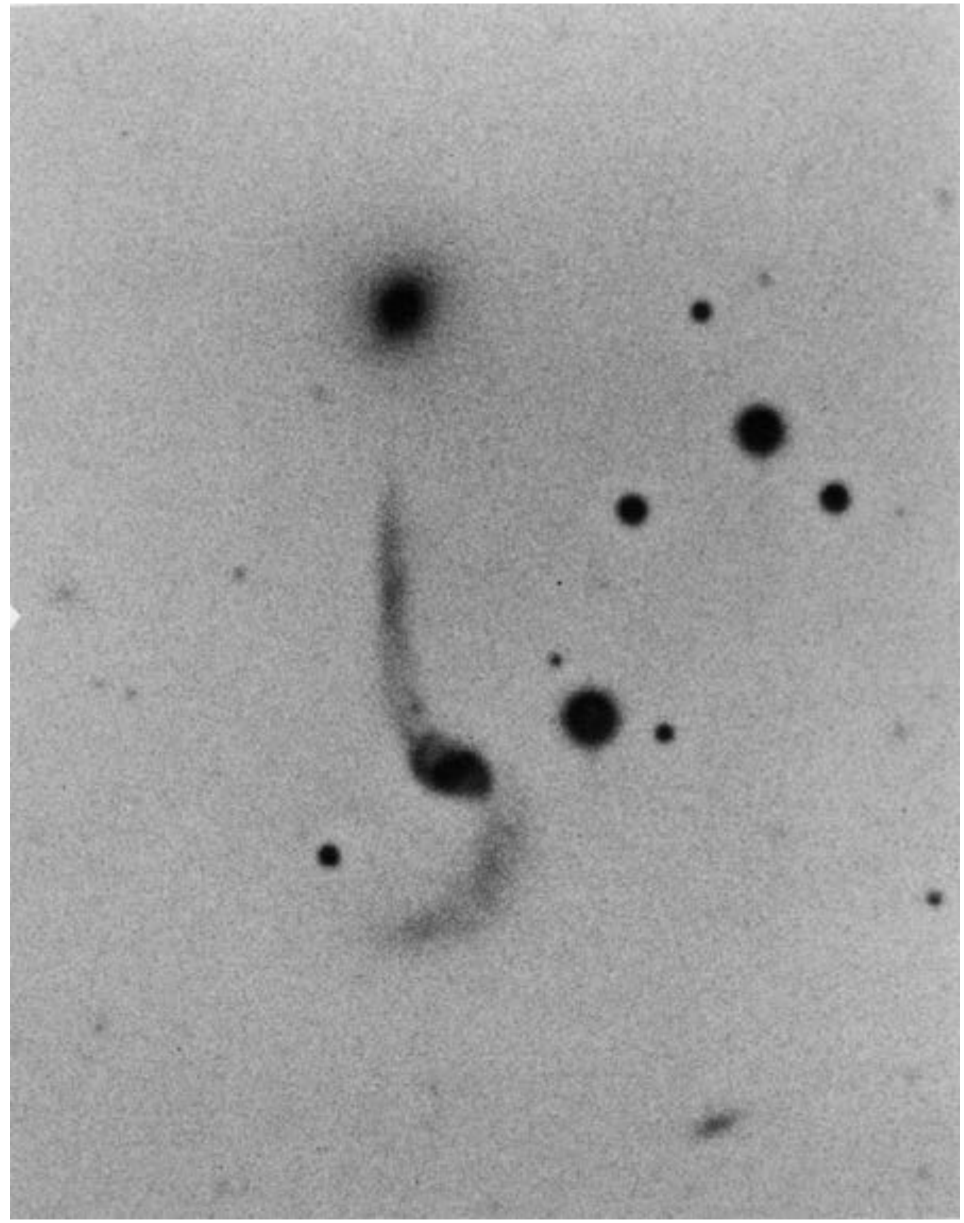

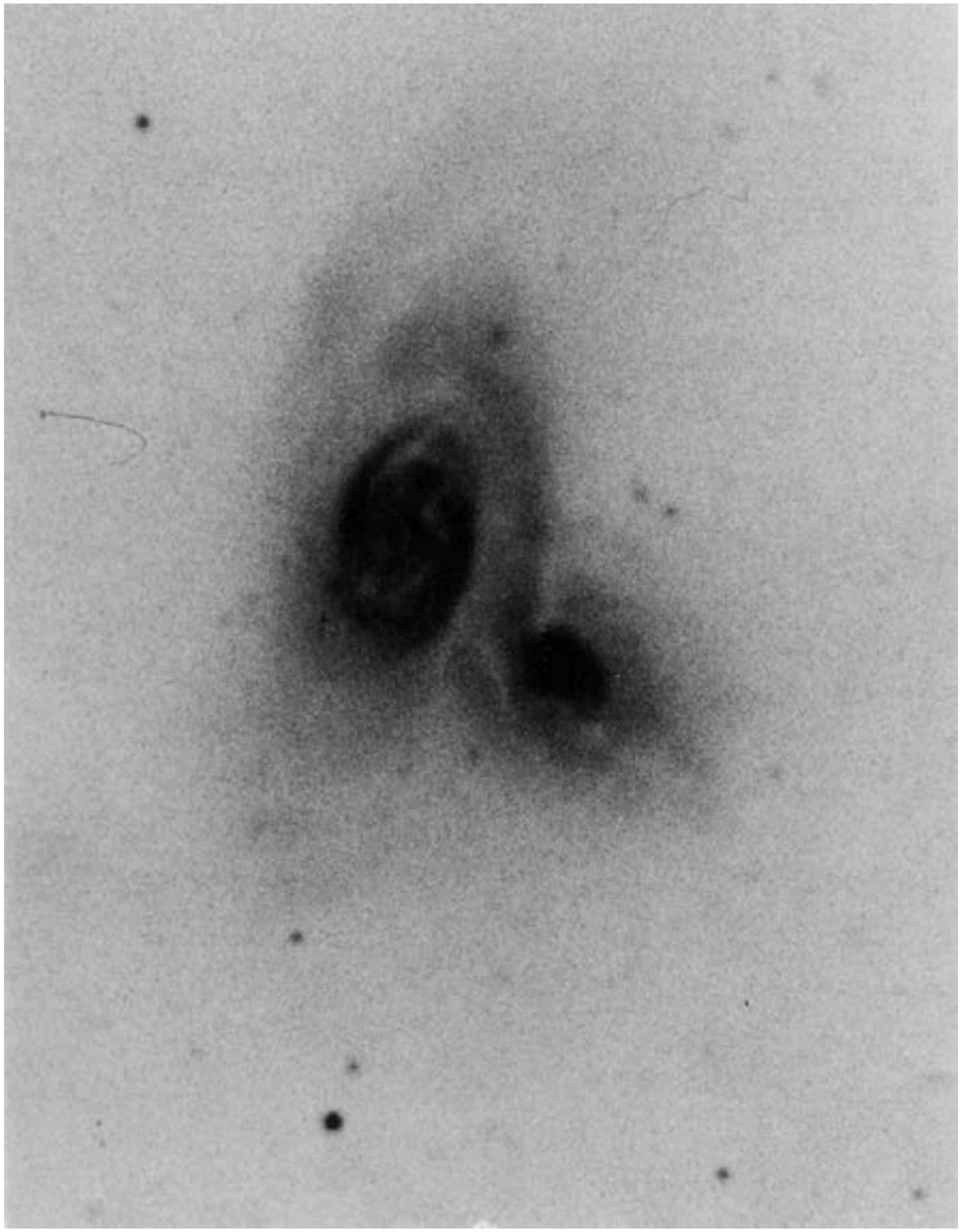

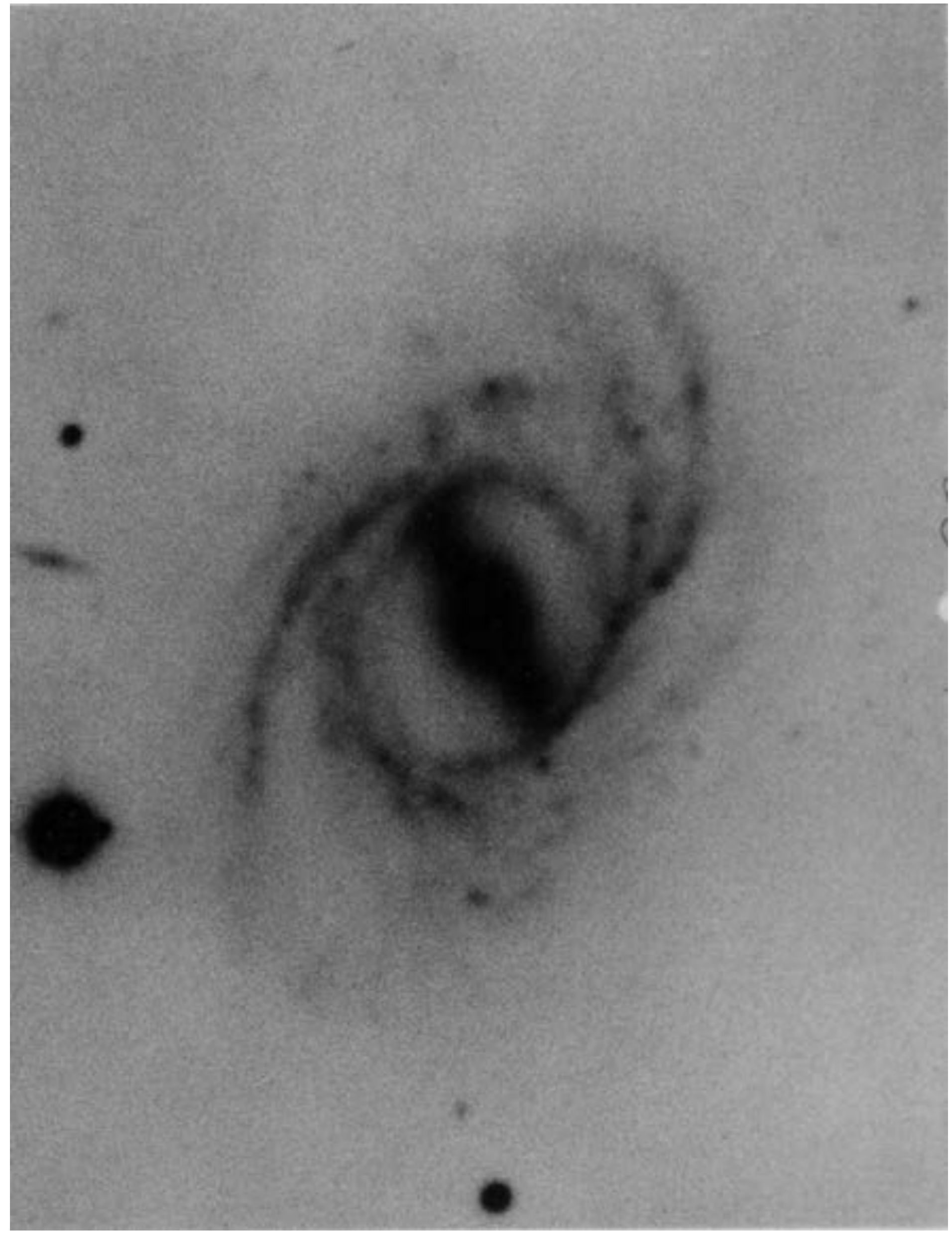

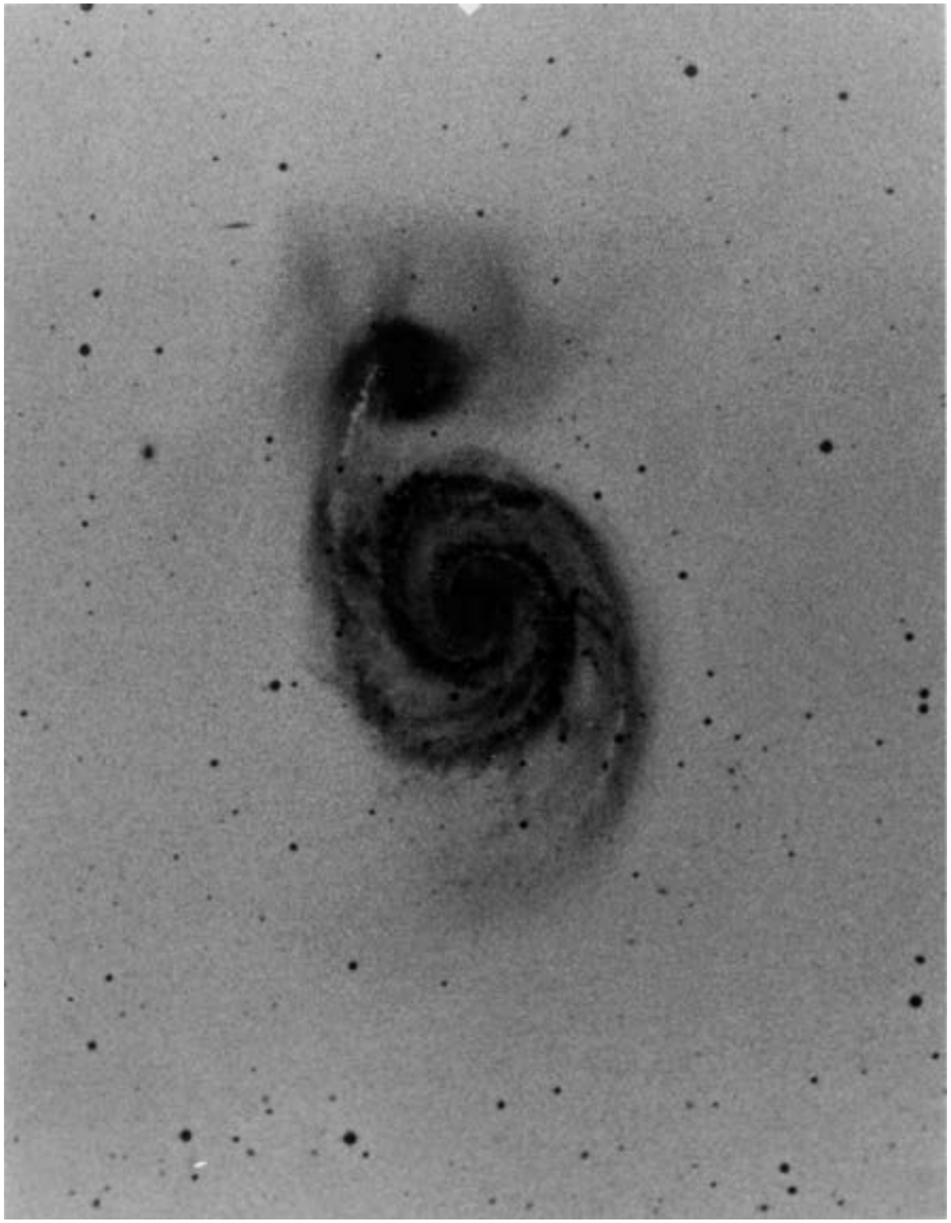

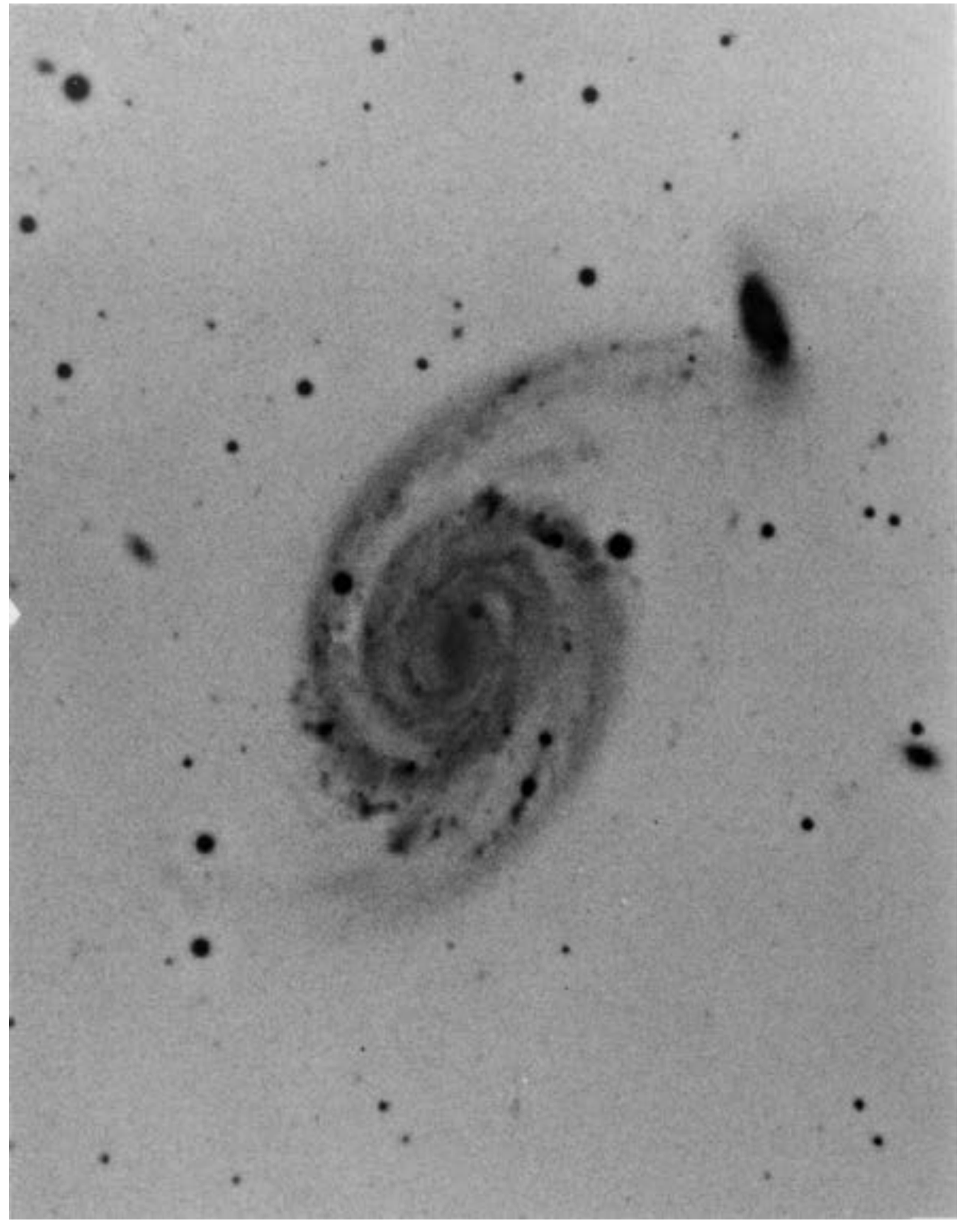

M51

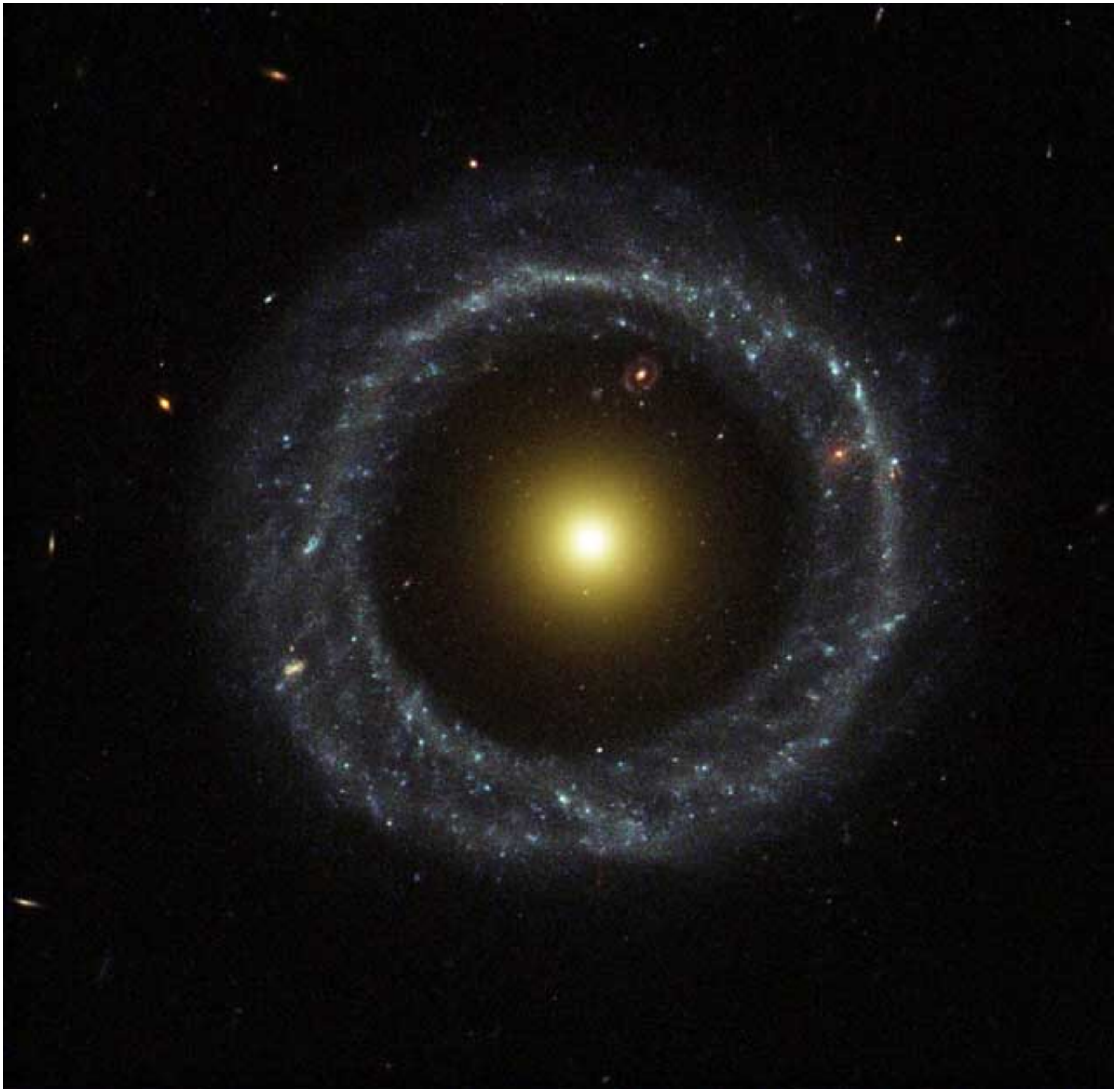

Hoag's object

Cartwheel galaxy

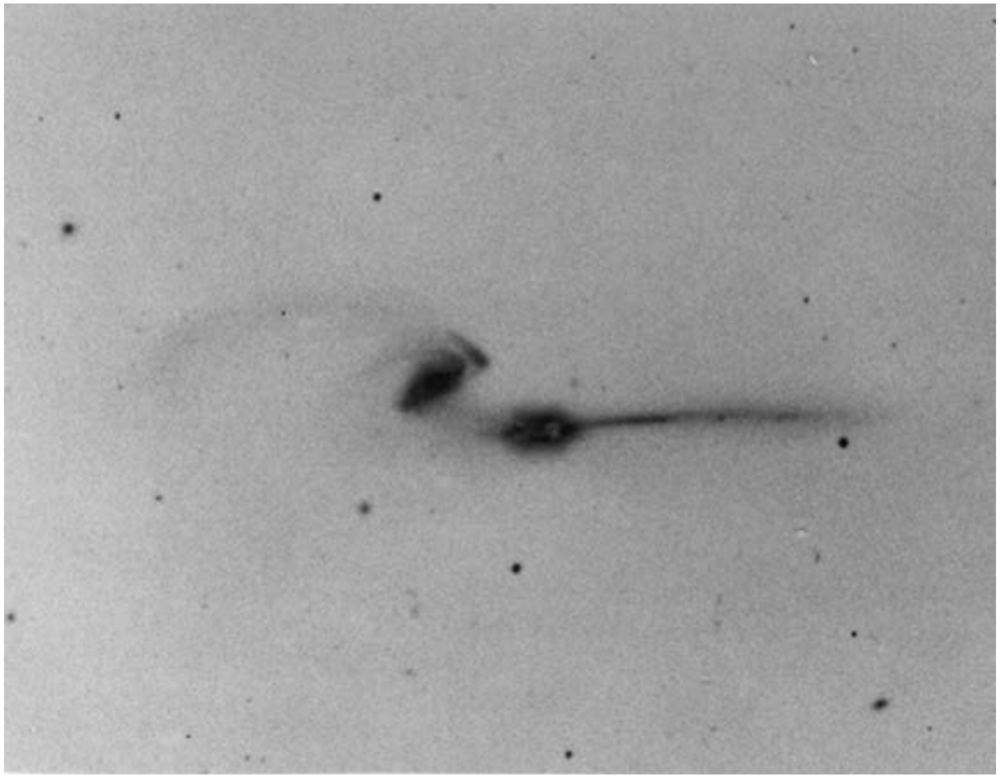

The Mice

model from Toomre & Toomre (1972)

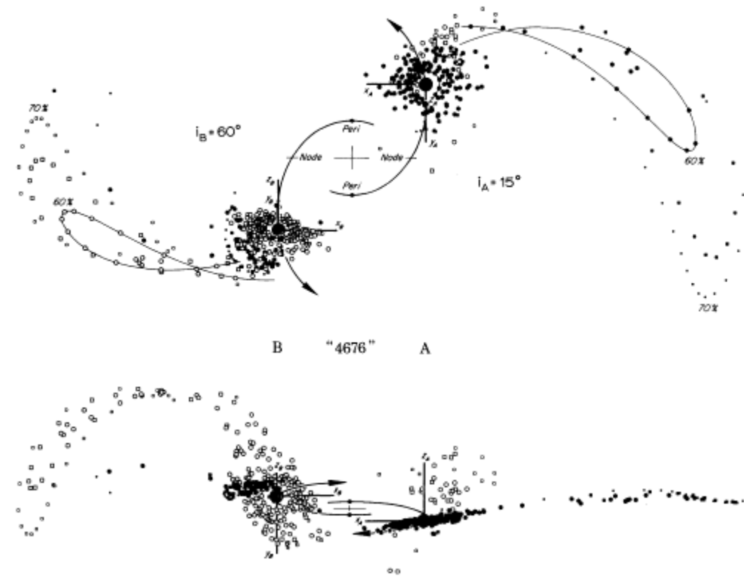

FIG. 22.—Model of NGC 4676. In this reconstruction, two equal disks of radius $0.7R_{min}$ experienced an $e = 0.6$ elliptic encounter, having begun flat and circular at the time $t = -16.4$ of the last apocenter. As viewed from either disk, the adopted node-to-peri angles $\omega_A = \omega_B = -90°$ were identical, but the inclinations differed considerably: $i_A = 15°$, $i_B = 60°$. The resulting composite object at $t = 6.086$ (cf. fig. 18) is shown projected onto the orbit plane in the upper diagram. It is viewed nearly edge-on to the same—from $\lambda_A = 180°$, $\beta_A = 85°$ or $\lambda_B = 0°$, $\beta_B = 160°$—in the lower diagram meant to simulate our actual view of that pair of galaxies. The filled and open symbols distinguish particles originally from disks A and B, respectively.

rather than elaborate, we chose the masses and loadings to be identical, did the same with the simple $\omega_A = \omega_B = -90°$, picked the round values $i_A = 15°$, $i_B = 60°$, chose the viewing longitude to be simply along the line of pericenters, and retained both the eccentricity and the 135° viewing time already used in figure 18. Thus the B object in figure 22 is virtually an “off-the-shelf” item. It differs from its predecessor in figure 18 only in the coding of certain of its particles, the display of its not-too-offensive accretion cloud above mass A, and a 45° more advanced longitude and 10° different latitude of viewing.

One almost incidental advantage of the present model is that, like the real tail A, ours looks slightly concave downward—or toward the west. More important is its agreement with the rough sense of the velocities measured in hulk B by the Burbidges: although our remnant B lacks the oval outline of the real object, its excess Doppler speeds are likewise positive and negative in the “north” and “south,” respectively. (Moreover, the fact that our remnant B happens to be viewed only 20° from face-on cautions that the actual rotation in 4676B could well be twice the observed ± 200 km s^{-1}, and hence also about twice the nominal speeds of our retained test particles. Thus

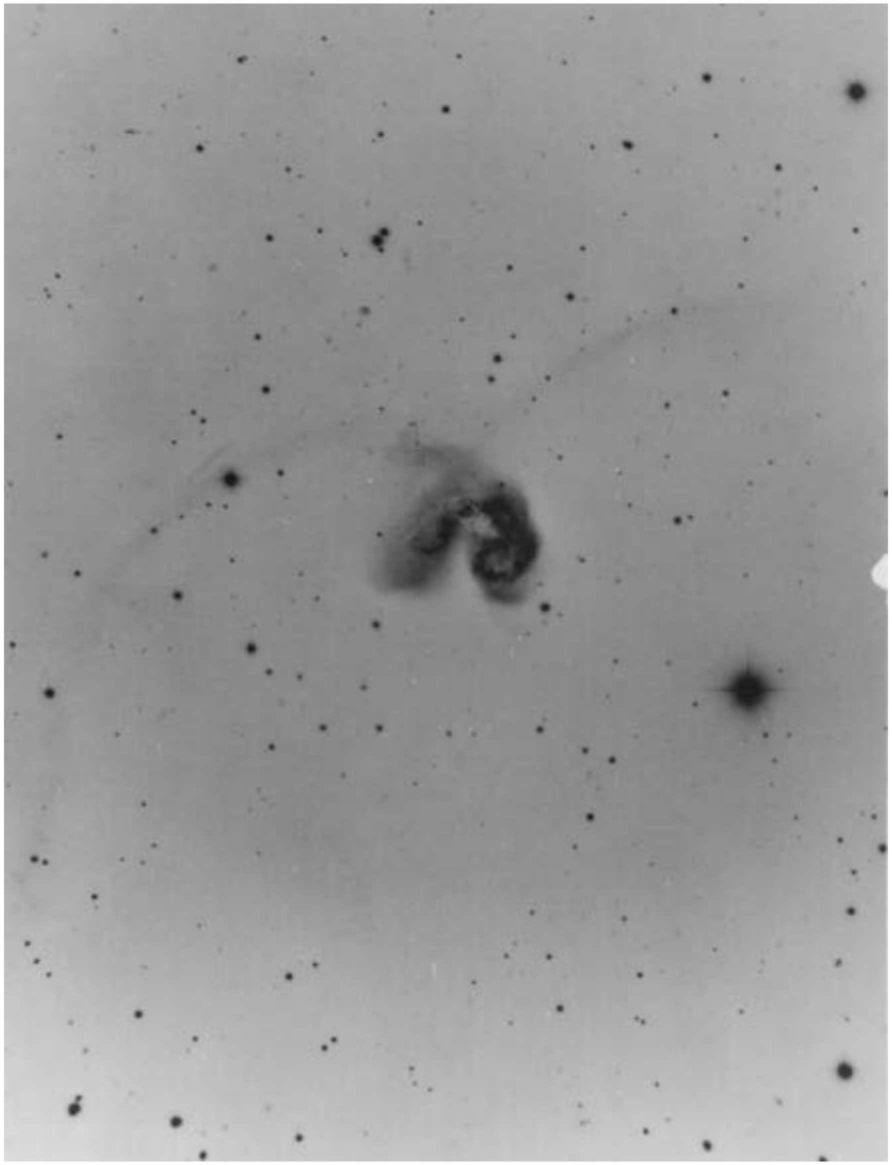

The Antennae

model from Toomre & Toomre (1972)

been concerned whether in fact it was possible to obtain seemingly *crossed* tails from tidal interactions. Figure 23 says we need not have worried.

By using figure 18, it is quite easy in retrospect to grasp the geometric essentials of this construction. Imagine that every bare companion in that ω survey carries an $i = +60°$ tail of its own, each such tail having been chosen from among the present four possibilities simply after a 180° visual rotation about the axis normal to the orbit

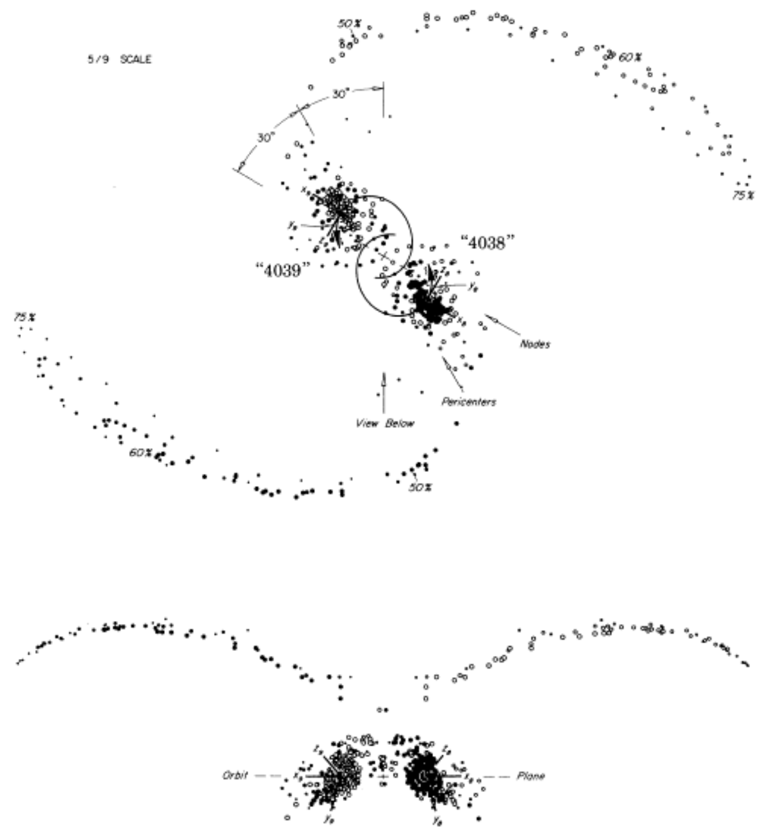

FIG. 23.—Symmetric model of NGC 4038/9. Here two identical disks of radius $0.75R_{min}$ suffered an $e \approx 0.5$ encounter with orbit angles $i_8 = i_9 = 60°$ and $\omega_8 = \omega_9 = -30°$ that appeared the same to both. The above all-inclusive views of the debris and remnants of these disks have been drawn exactly normal and edge-on to the orbit plane; the latter viewing direction is itself 30° from the line connecting the two pericenters. The viewing time is $t = 15$, or slightly past apocenter. The filled and open symbols again disclose the original loyalties of the various test particles.

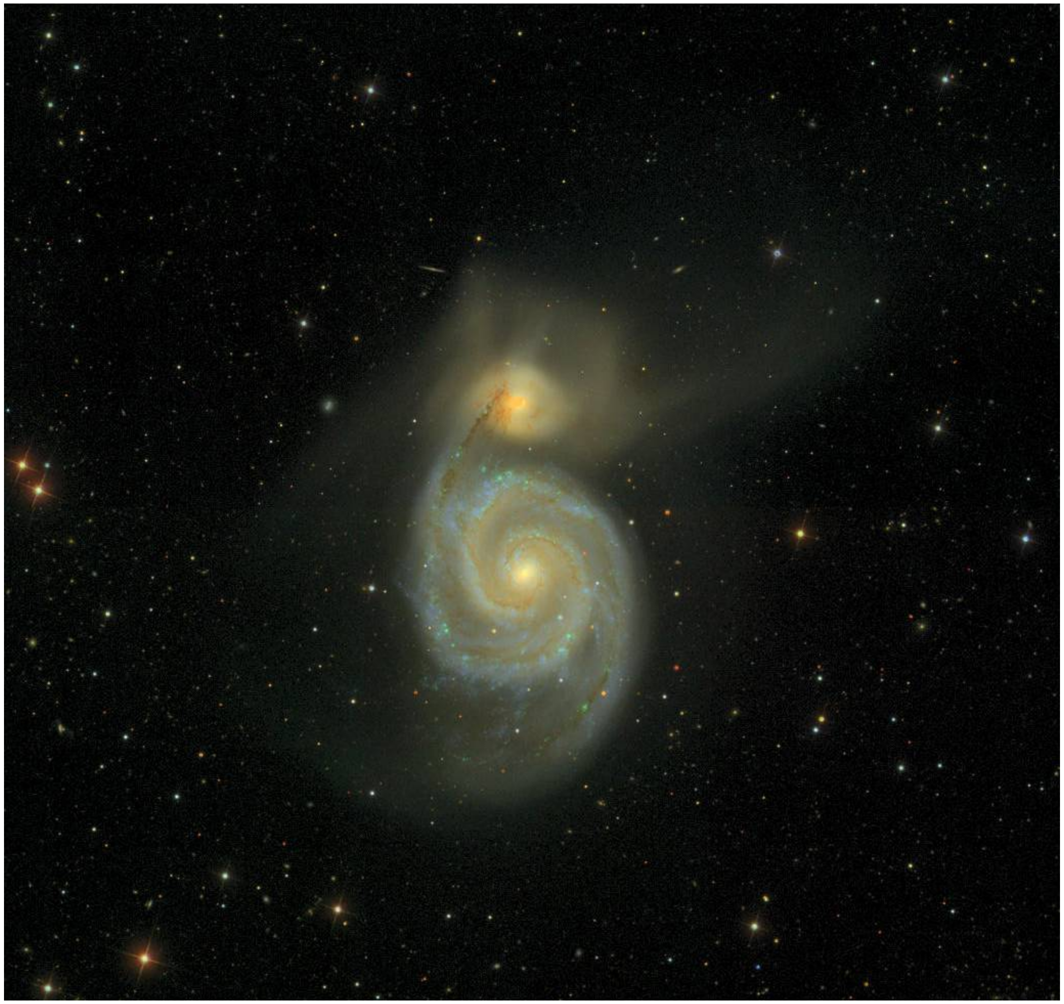

M51

model from Toomre & Toomre (1972)

at about that radius. It consists of two parts: One, of course, is the bridgelike northern arm which a number of observers (cf. Roberts and Warren 1970) have already felt partly obscures the companion. The other is the *broad*, curving, fainter counterarm to the south and southwest of the main disk. Though this second major clue is scarcely visible in the *Hubble Atlas* (Sandage 1961), it is very evident in the deeper *Sky Survey* and Arp 85 photographs and unmistakable in the IIIaJ exposure by van den Bergh (1969). Together with the projected position and excess line-of-sight velocity of the companion, it is these two features—and they alone—that comprised the prime goals of our reconstruction of the encounter shown in figures 20 and 21.

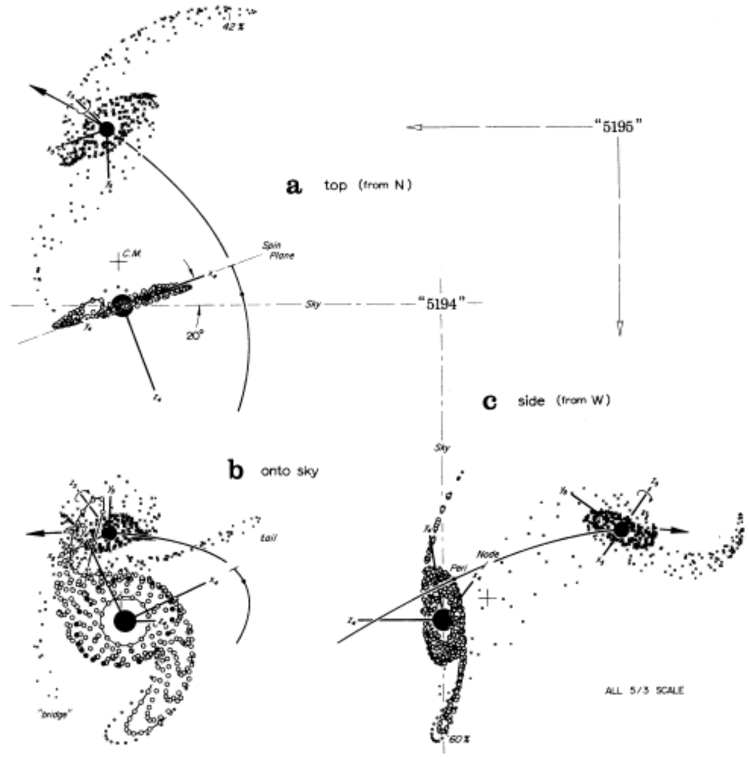

Fig. 21.—Model of the recent encounter between M51 and NGC 5195. Shown here at $t = 2.4$ are three mutually orthogonal views of the consequences of a highly elliptic $e = 0.8$ passage of a supposedly disklike "5195." This satellite was chosen to be one-third as massive, and of exactly 0.7 times the linear dimensions, of the "5194" primary—which itself contains particles from initial radii 0.2(0.05)0.4(0.033)0.633$R_{\min}$. The orbit plane differs by an angle $i_4 = -70°$ from the initial spin plane of the larger disk and by $i_5 = -60°$ from that of the smaller; however, the arguments $\omega_4 = \omega_5 = -15°$ of the pericenters were here kept identical, to make the above nodal axes x_4 and x_5 exactly antiparallel. The three views show the combined system as it would appear not only (*b*) to us ($\lambda_4 = 65°$, $\beta_4 = -20°$), but also edge-on to our sky from (*a*) the "north" ($-25°$, 90°) and (*c*) the "west" (65°, 70°) directions.

[redacted]

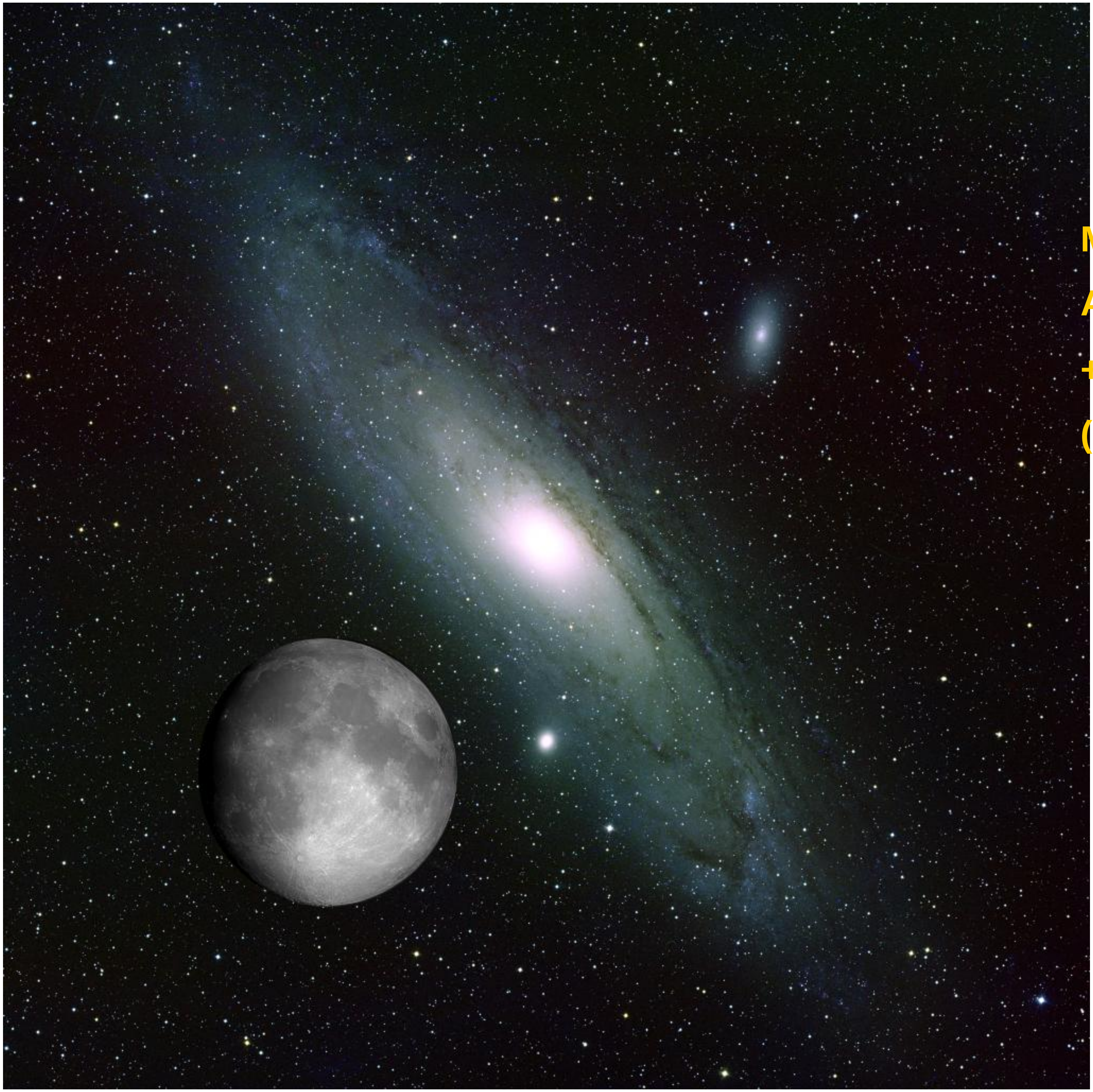

M31 =

Andromeda galaxy

+ NGC 205 + M32

(+ Moon, for scale)

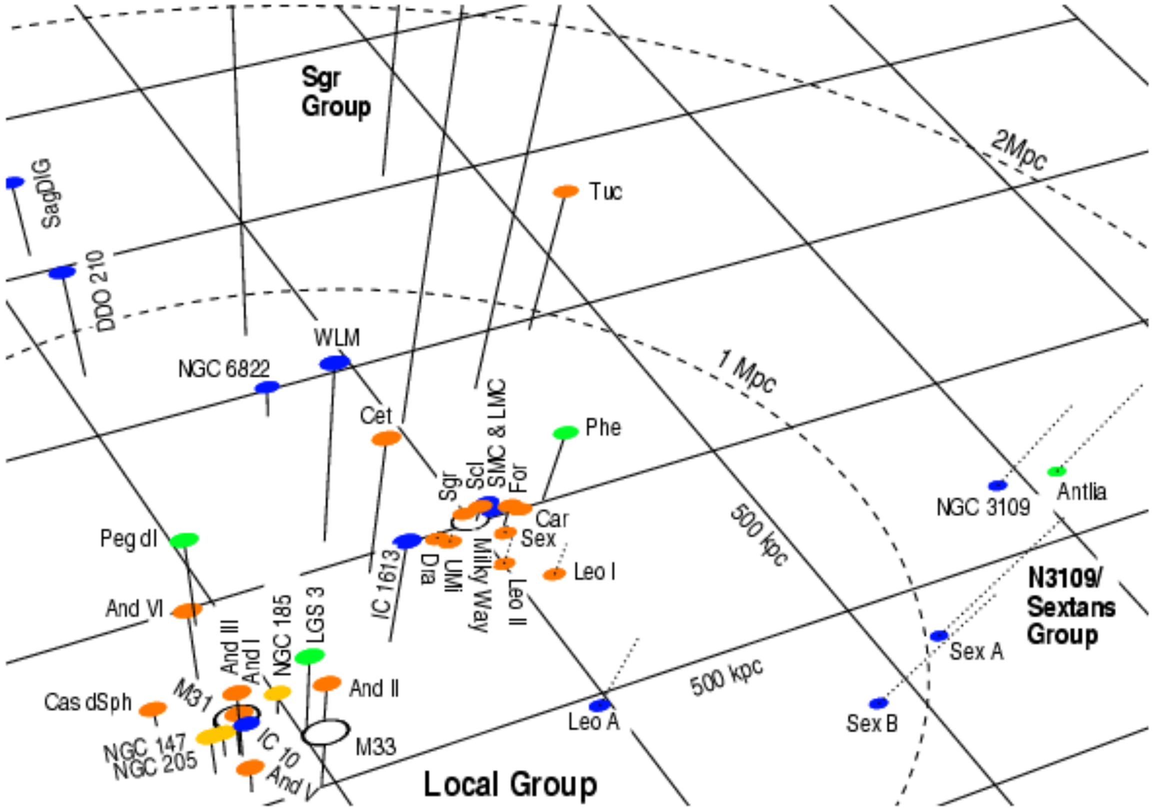

Figure 1. A scaled 3-D representation of the Local Group (LG). The dashed ellipsoid marks a radius of 1 Mpc around the LG barycenter (assumed to be at 462 kpc toward l = 121.7 and b = −21.3 following Courteau & van den Bergh 1999). Distances of galaxies from the the arbitrarily chosen plane through the Milky Way are indicated by solid lines (above the plane) and dotted lines (below). Morphological segregation is evident: The dEs and gas-deficient dSphs (light symbols) are closely concentrated around the large spirals (open symbols). DSph/dIrr transition types (e.g., Pegasus, LGS 3, Phoenix) tend to be somewhat more distant. Most dIrrs (dark symbols) are fairly isolated and located at larger distances. Also indicated are the locations of two nearby groups.

Grebel (2000)

Magellanic
clouds

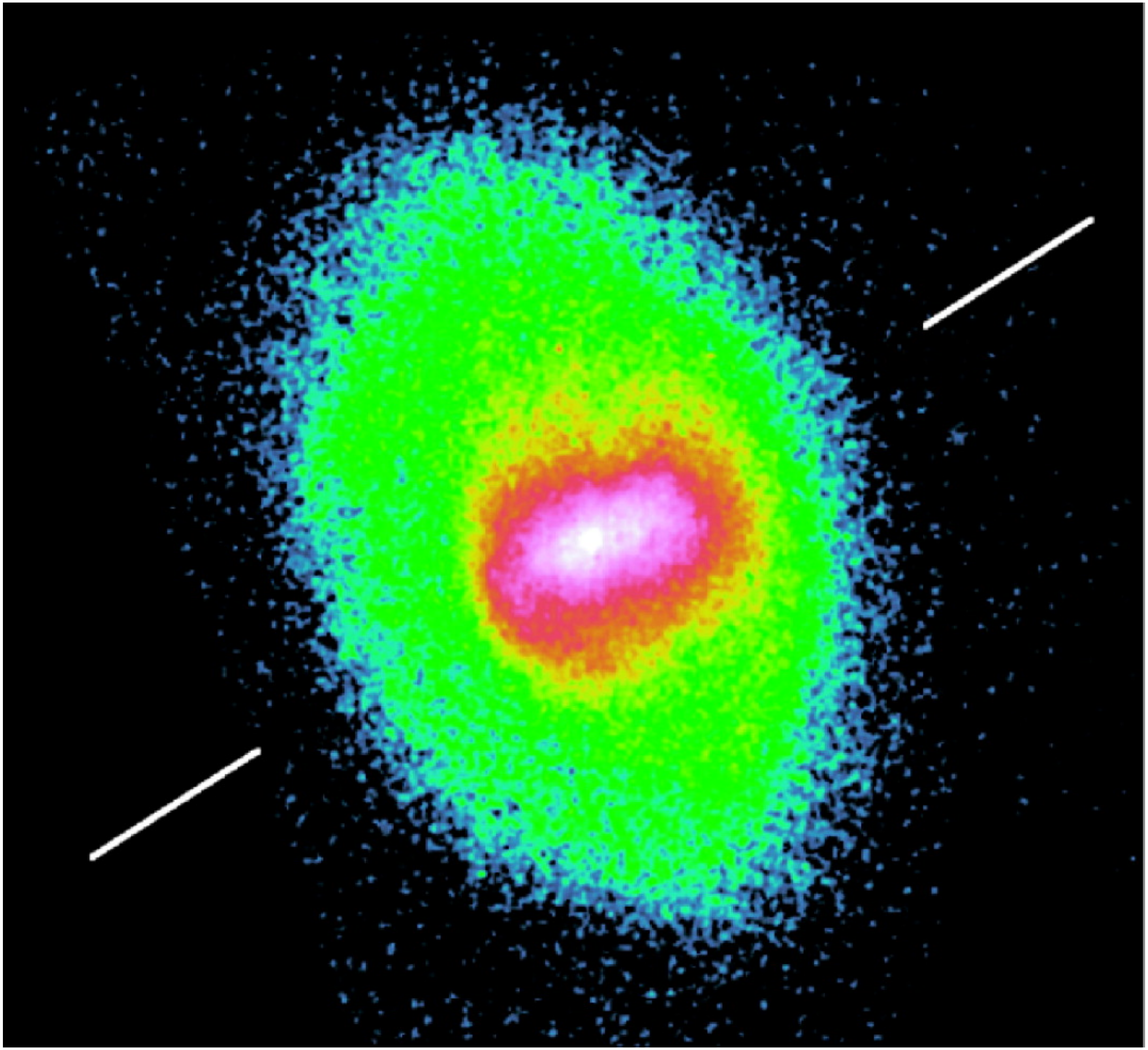

van der
Marel (2002)

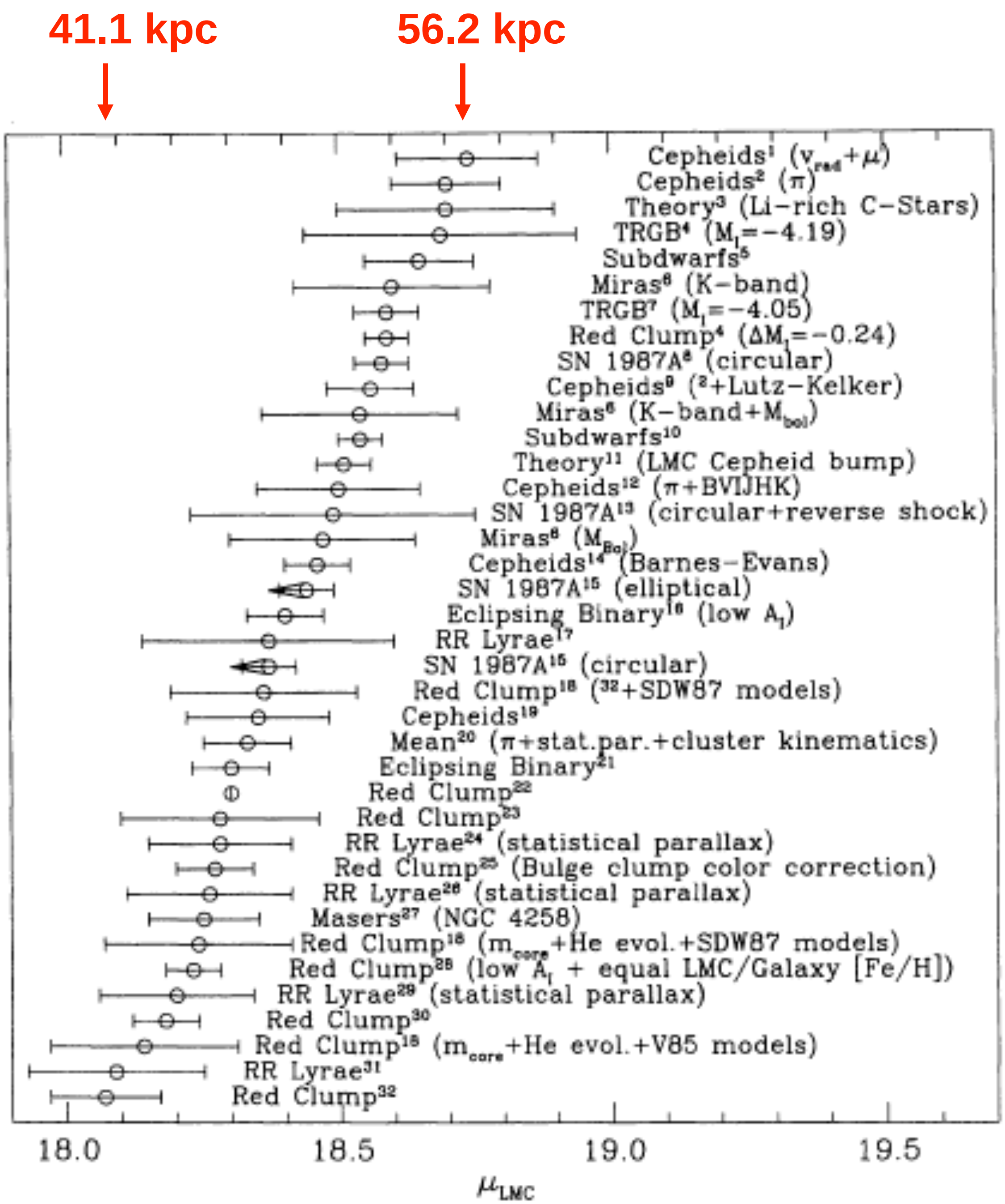
41.1 kpc
56.2 kpc
Cepheids[1] ($v_{rad}+\mu$)
Cepheids[2] (π)
Theory[3] (Li-rich C-Stars)
TRGB[4] ($M_I=-4.19$)
Subdwarfs[5]
Miras[6] (K-band)
TRGB[7] ($M_I=-4.05$)
Red Clump[4] ($\Delta M_I=-0.24$)
SN 1987A[8] (circular)
Cepheids[9] ([2]+Lutz-Kelker)
Miras[6] (K-band+M_{bol})
Subdwarfs[10]
Theory[11] (LMC Cepheid bump)
Cepheids[12] (π+BVIJHK)
SN 1987A[13] (circular+reverse shock)
Miras[6] (M_{Bol})
Cepheids[14] (Barnes-Evans)
SN 1987A[15] (elliptical)
Eclipsing Binary[16] (low A_I)
RR Lyrae[17]
SN 1987A[15] (circular)
Red Clump[18] ([32]+SDW87 models)
Cepheids[19]
Mean[20] (π+stat.par.+cluster kinematics)
Eclipsing Binary[21]
Red Clump[22]
Red Clump[23]
RR Lyrae[24] (statistical parallax)
Red Clump[25] (Bulge clump color correction)
RR Lyrae[26] (statistical parallax)
Masers[27] (NGC 4258)
Red Clump[18] (m_{core}+He evol.+SDW87 models)
Red Clump[28] (low A_I + equal LMC/Galaxy [Fe/H])
RR Lyrae[29] (statistical parallax)
Red Clump[30]
Red Clump[18] (m_{core}+He evol.+V85 models)
RR Lyrae[31]
Red Clump[32]
18.0
18.5
19.0
19.5
μ_{LMC}

Gibson (1999)

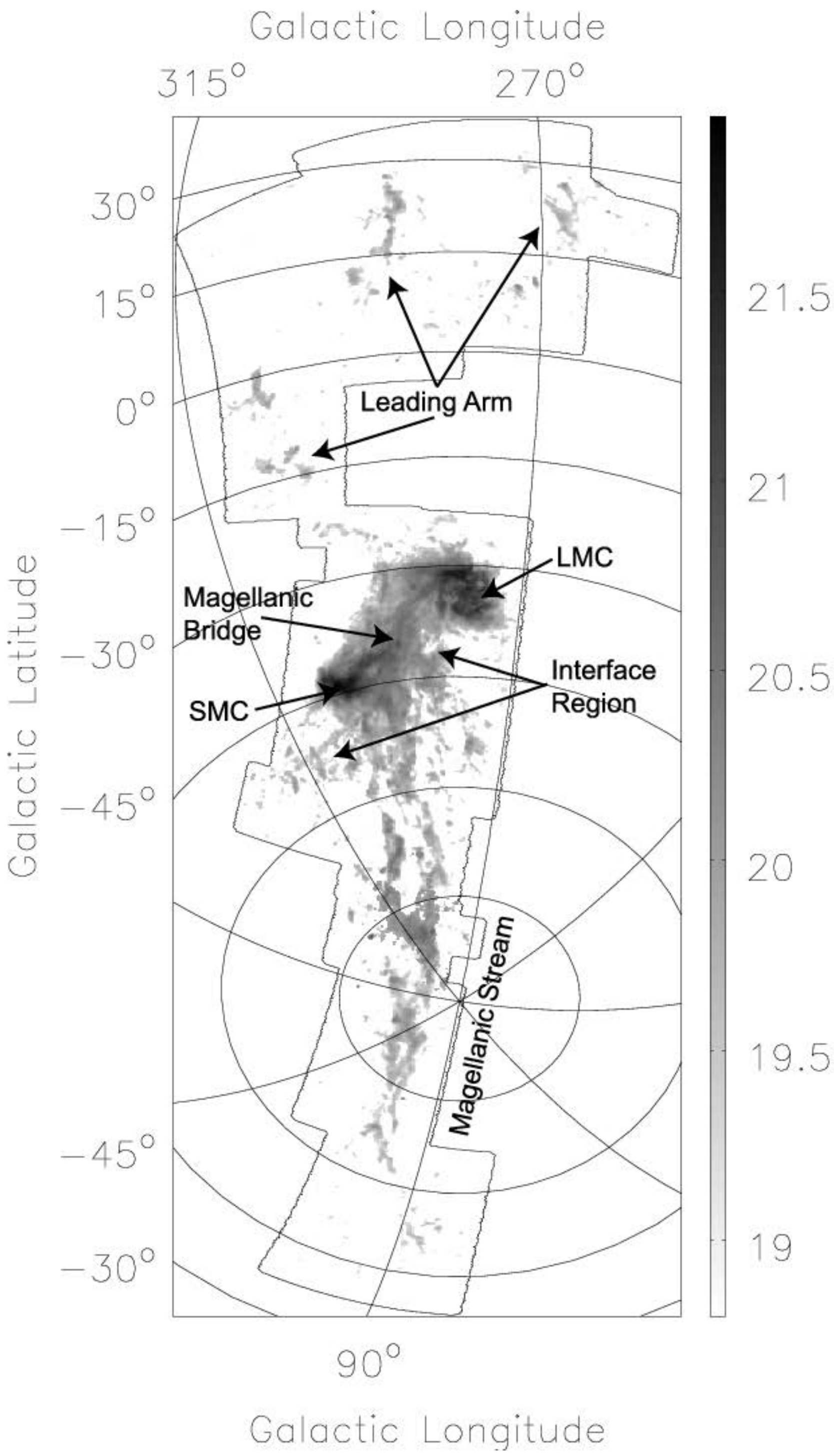

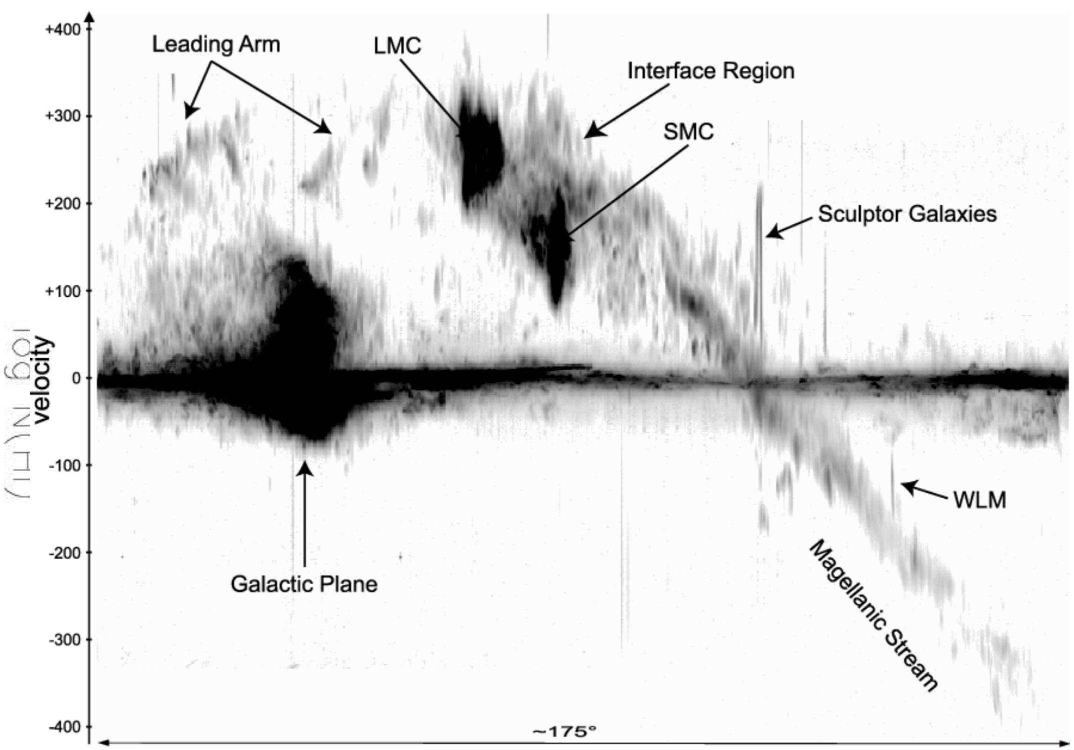

Bruns et al. (2005)

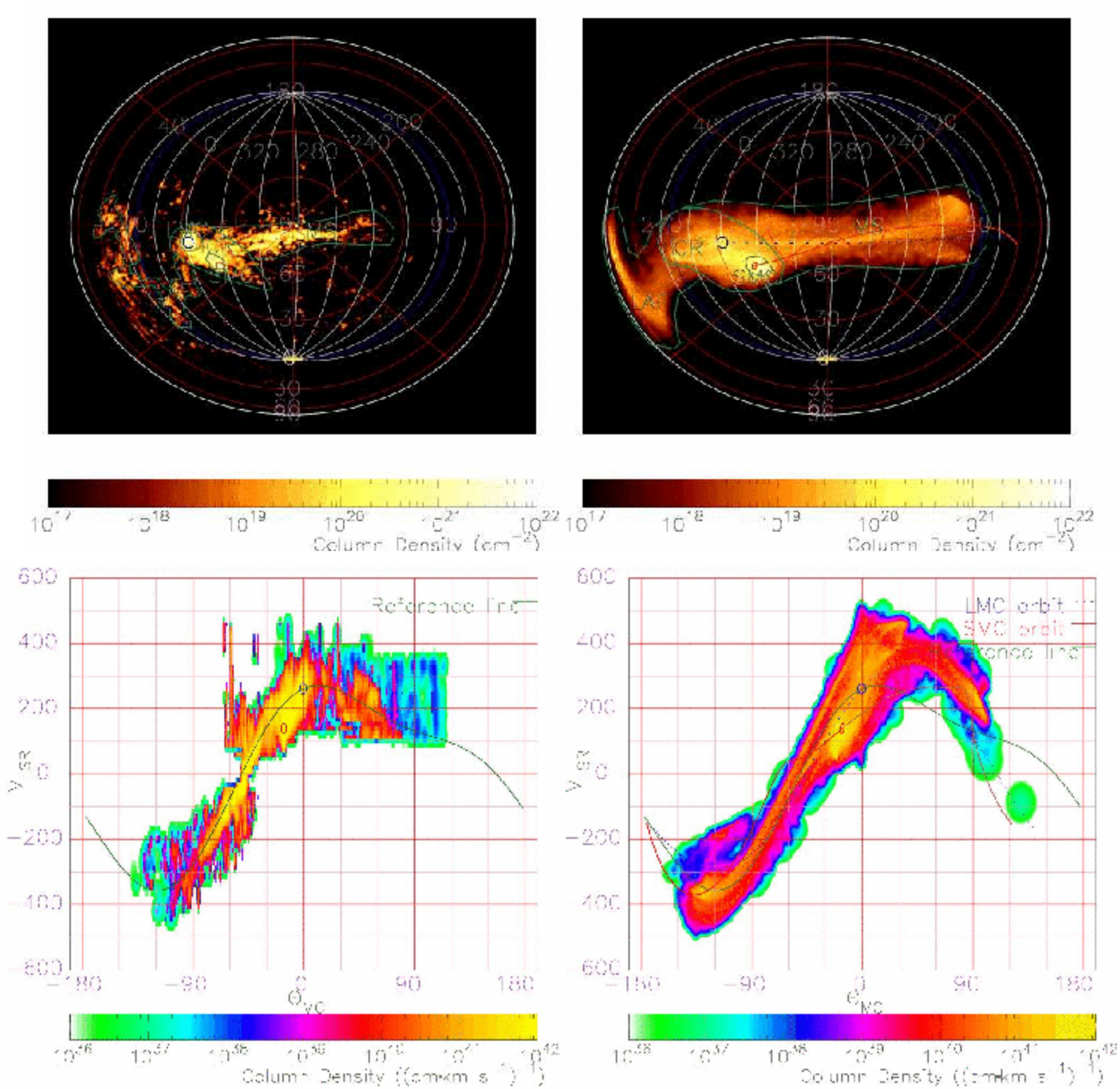

Connors et al. (2005)

Fornax dwarf galaxy

Leo I dwarf galaxy

Pegasus dwarf spheroidal galaxy

1,000 light years

Keck 10 meter telescope / Grebel & Guhathakurta

Ursa Minor dwarf galaxy (dSph)

Draco dwarf galaxy (dSph)

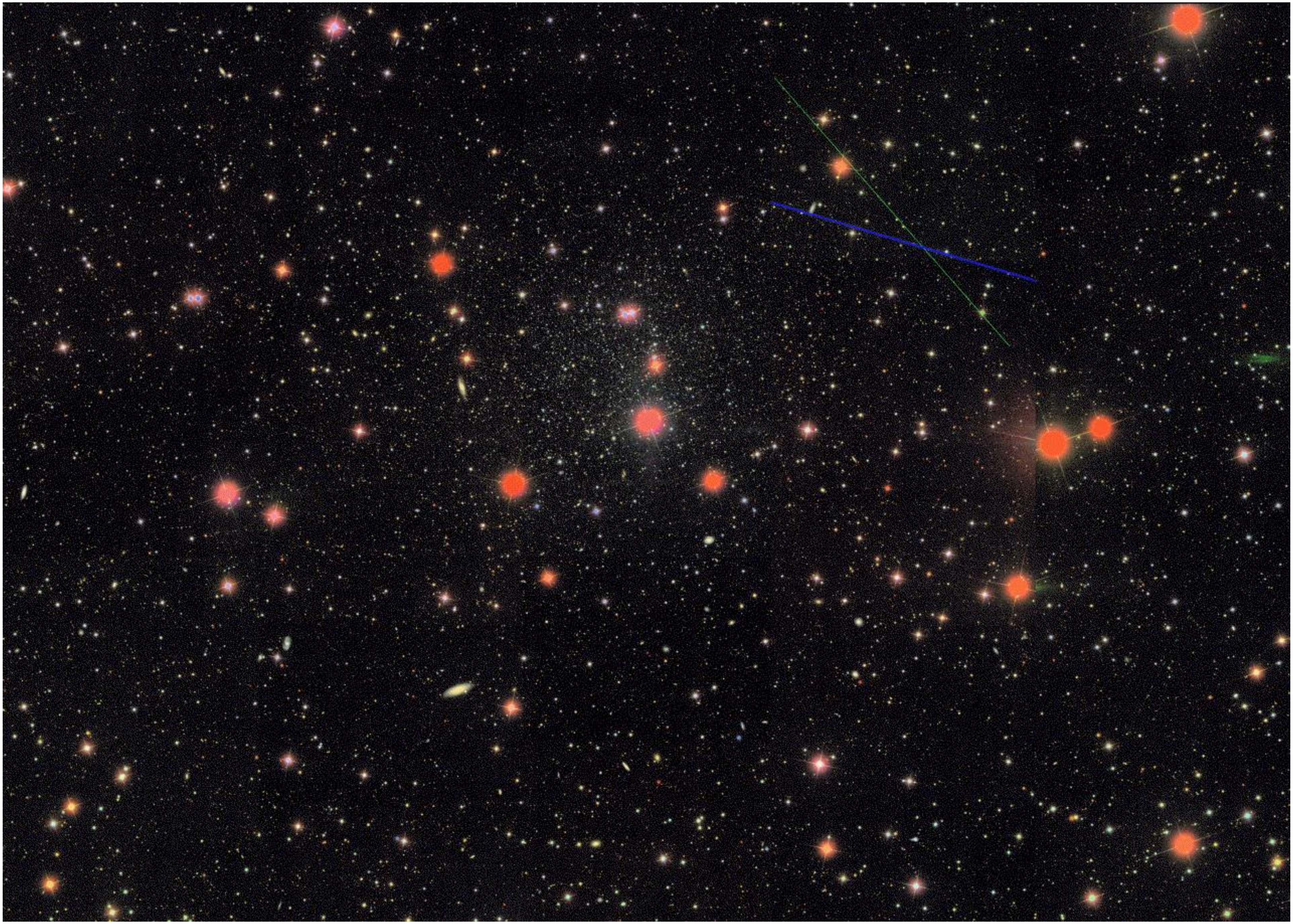

Draco dwarf galaxy

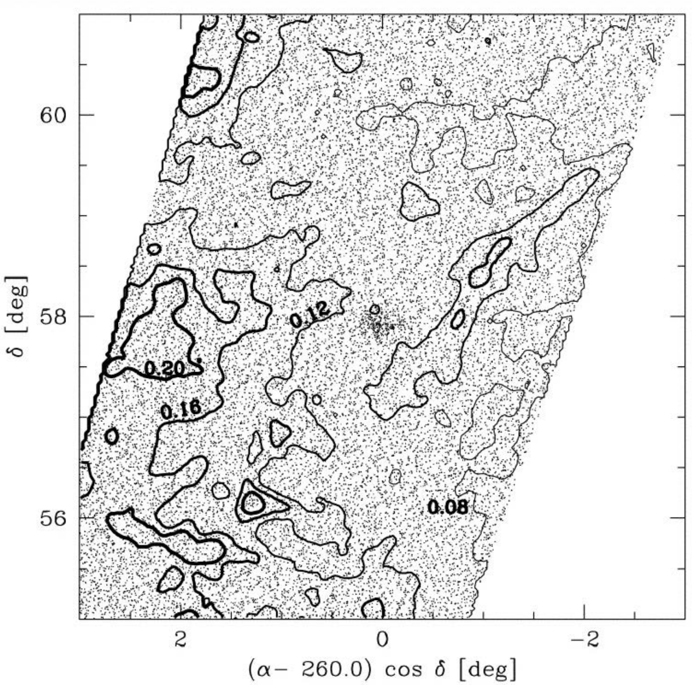

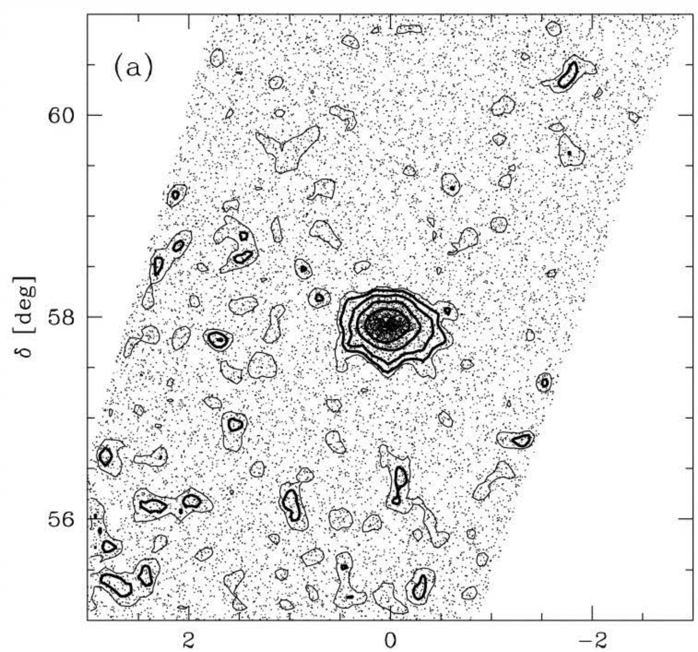

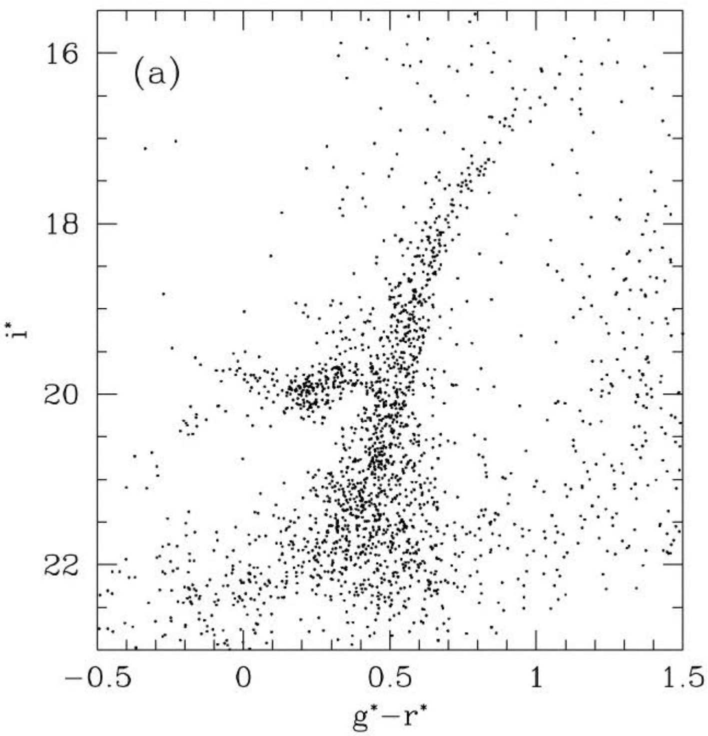

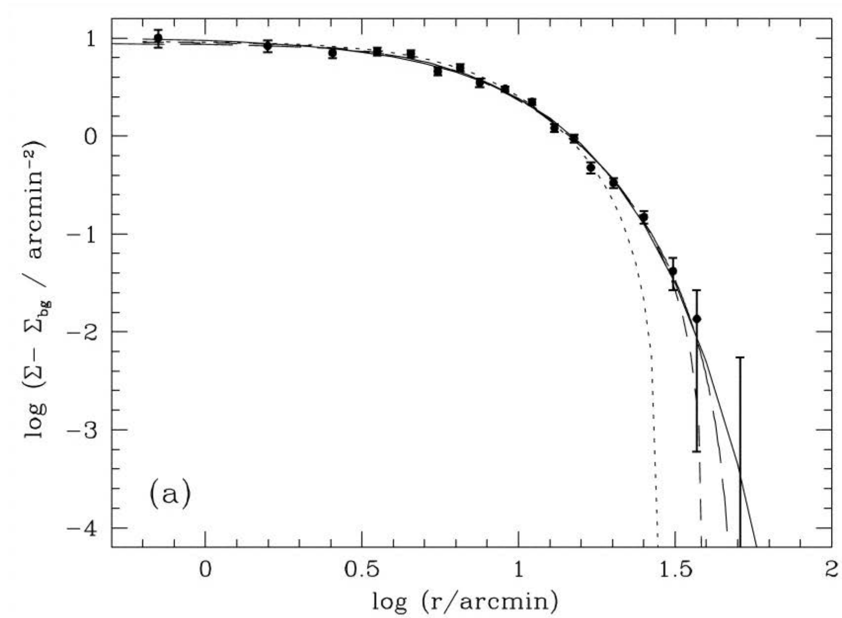

Odenkirchen et al. (2001)

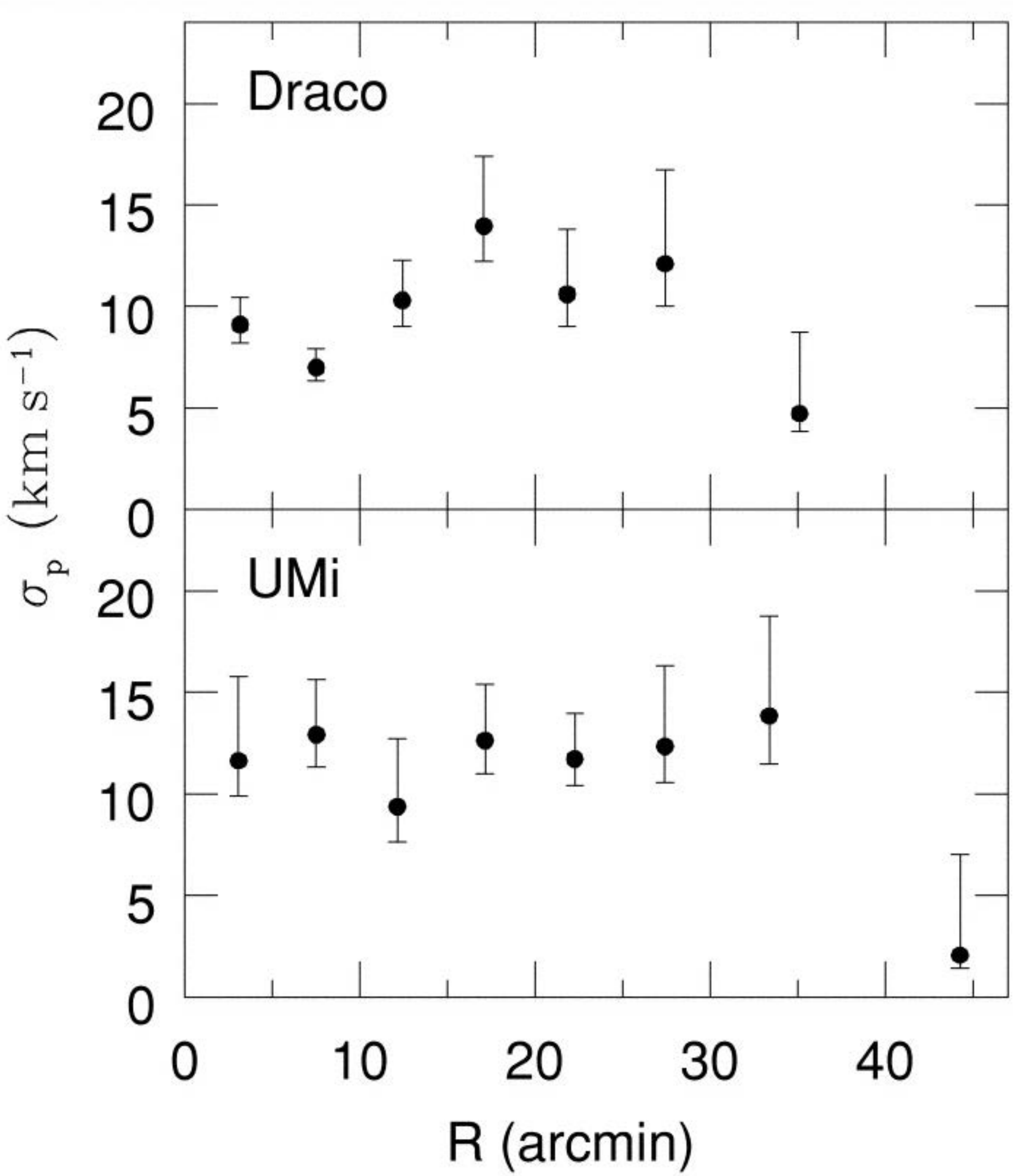

Wilkinson et al. (2004)

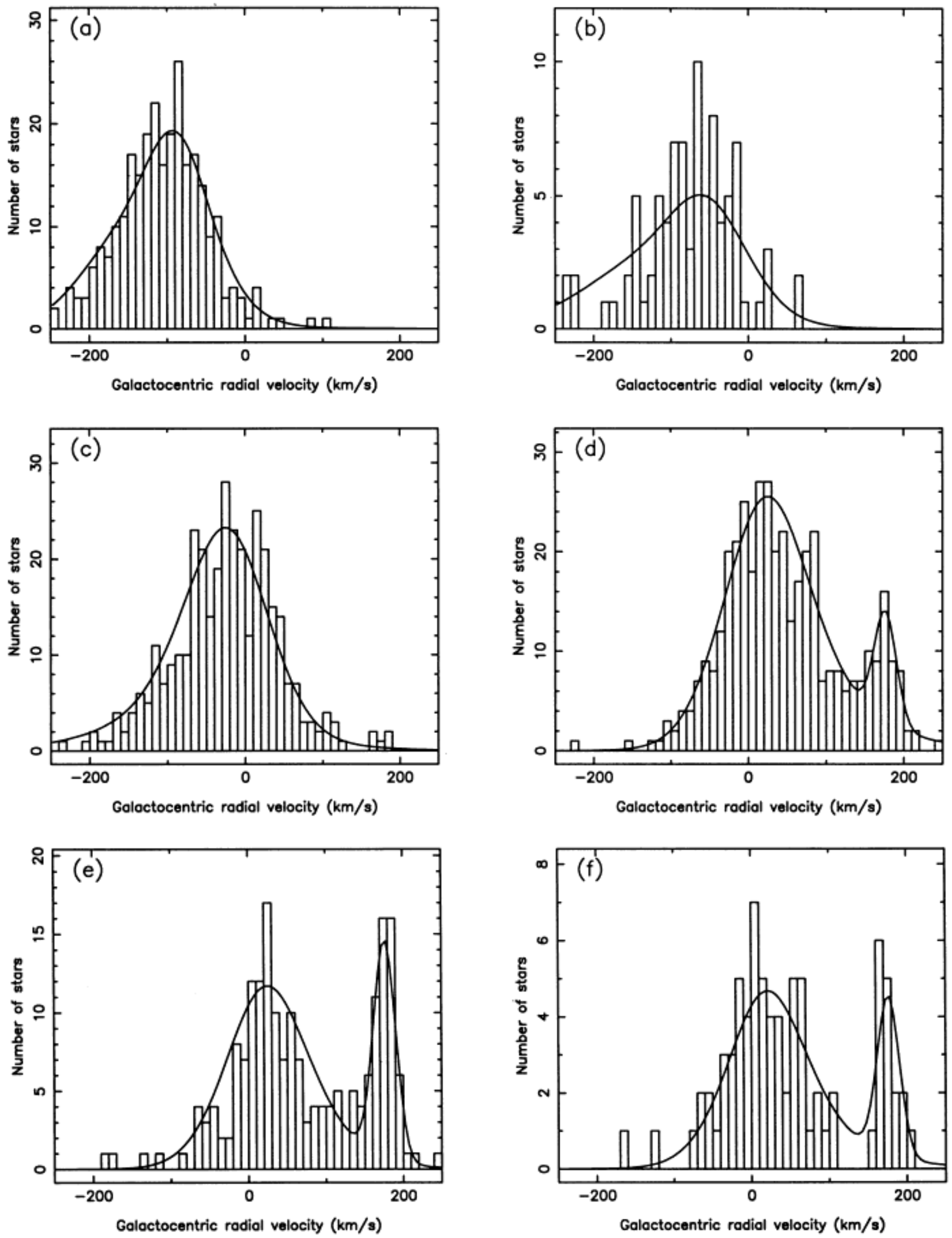

Figure 3. Comparison between the observed velocity distribution and that expected from the standard Galaxy model plus a Gaussian component of variable mean, dispersion and normalization which is included so as to account for the feature near 172 km s^{-1}. The lines of sight are the same as in Fig. 1.

Ibata & Gilmore (1995)

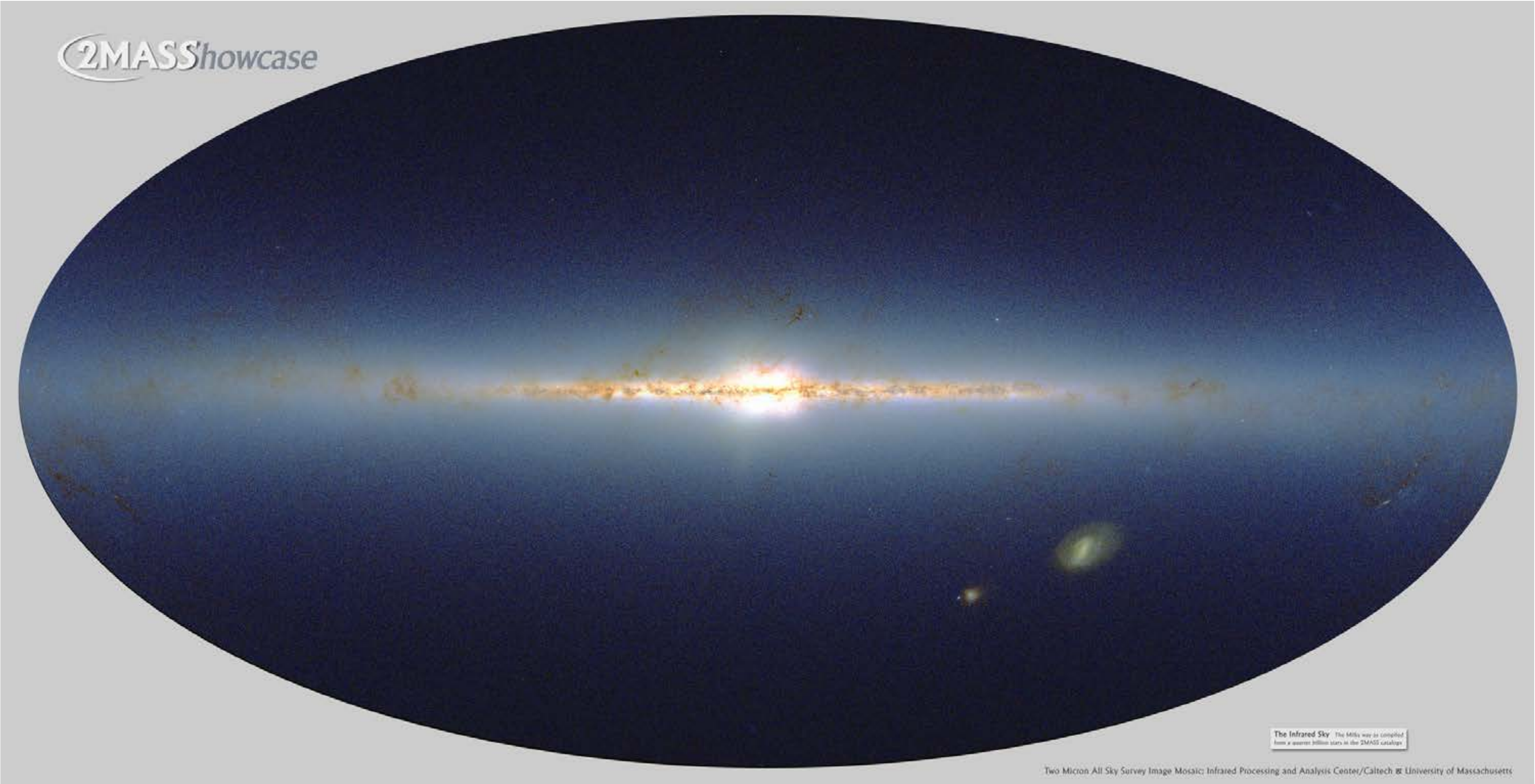
2MASSShowcase
Two Micron All Sky Survey Image Mosaic: Infrared Processing and Analysis Center/Caltech & University of Massachusetts

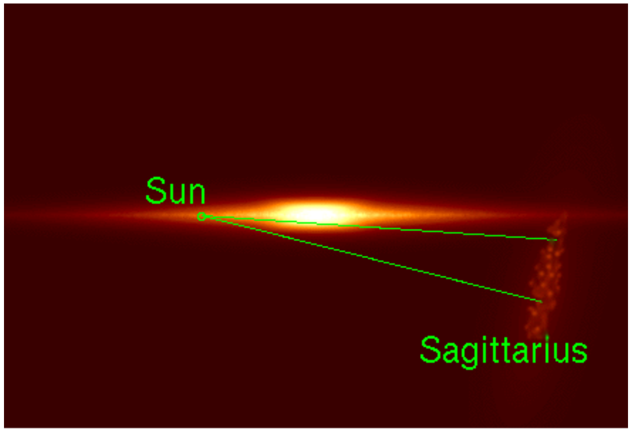
Sun
Sagittarius

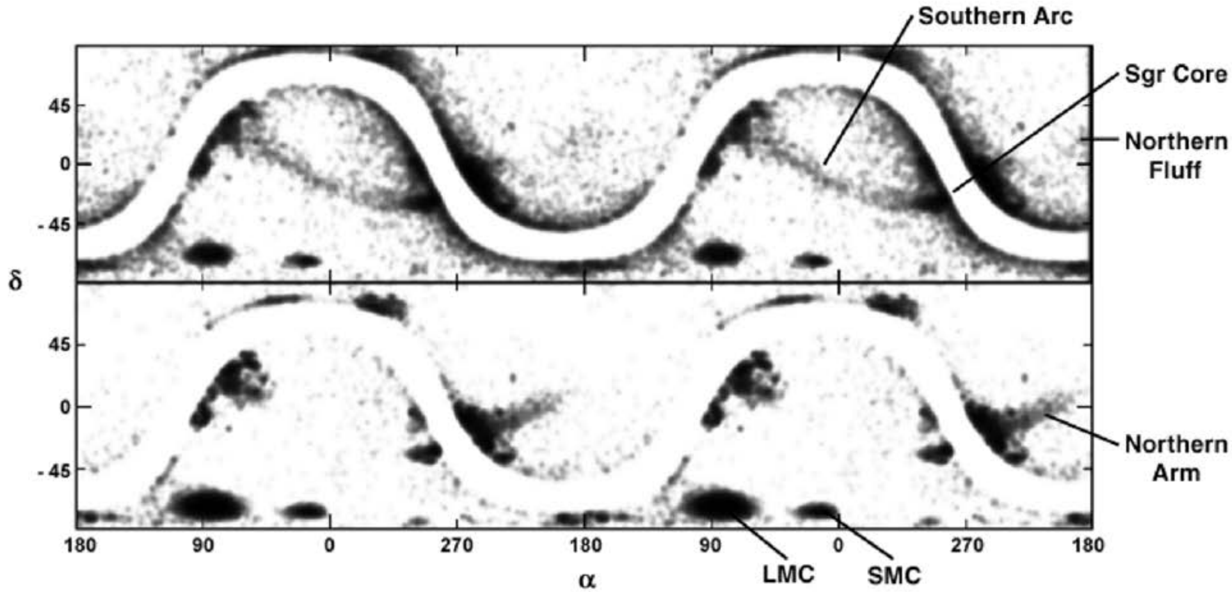

Majewski et al. (2003)

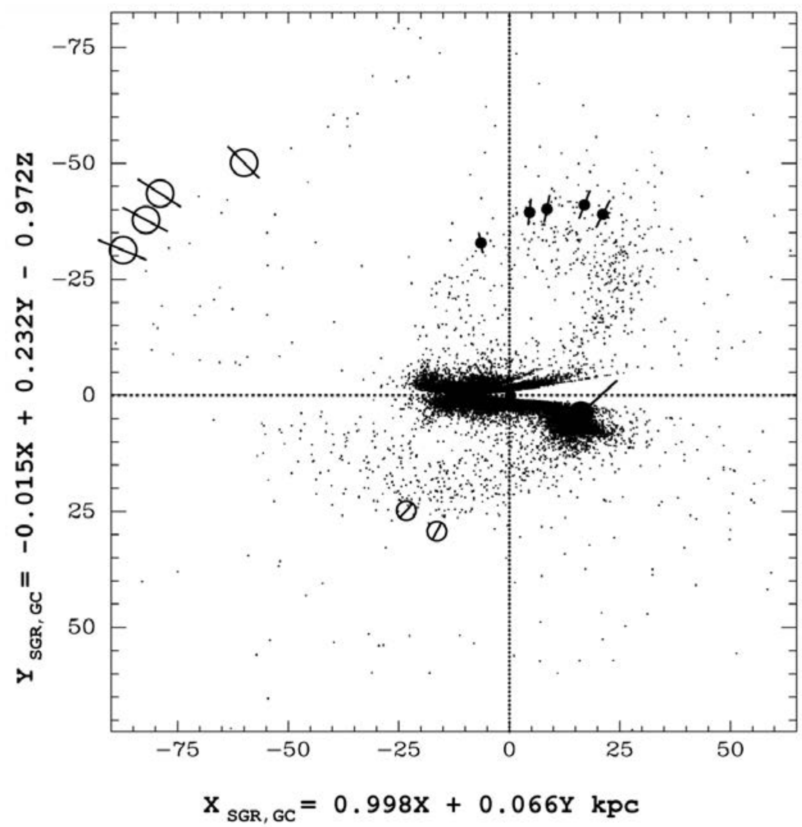

Newberg et al. (2003)

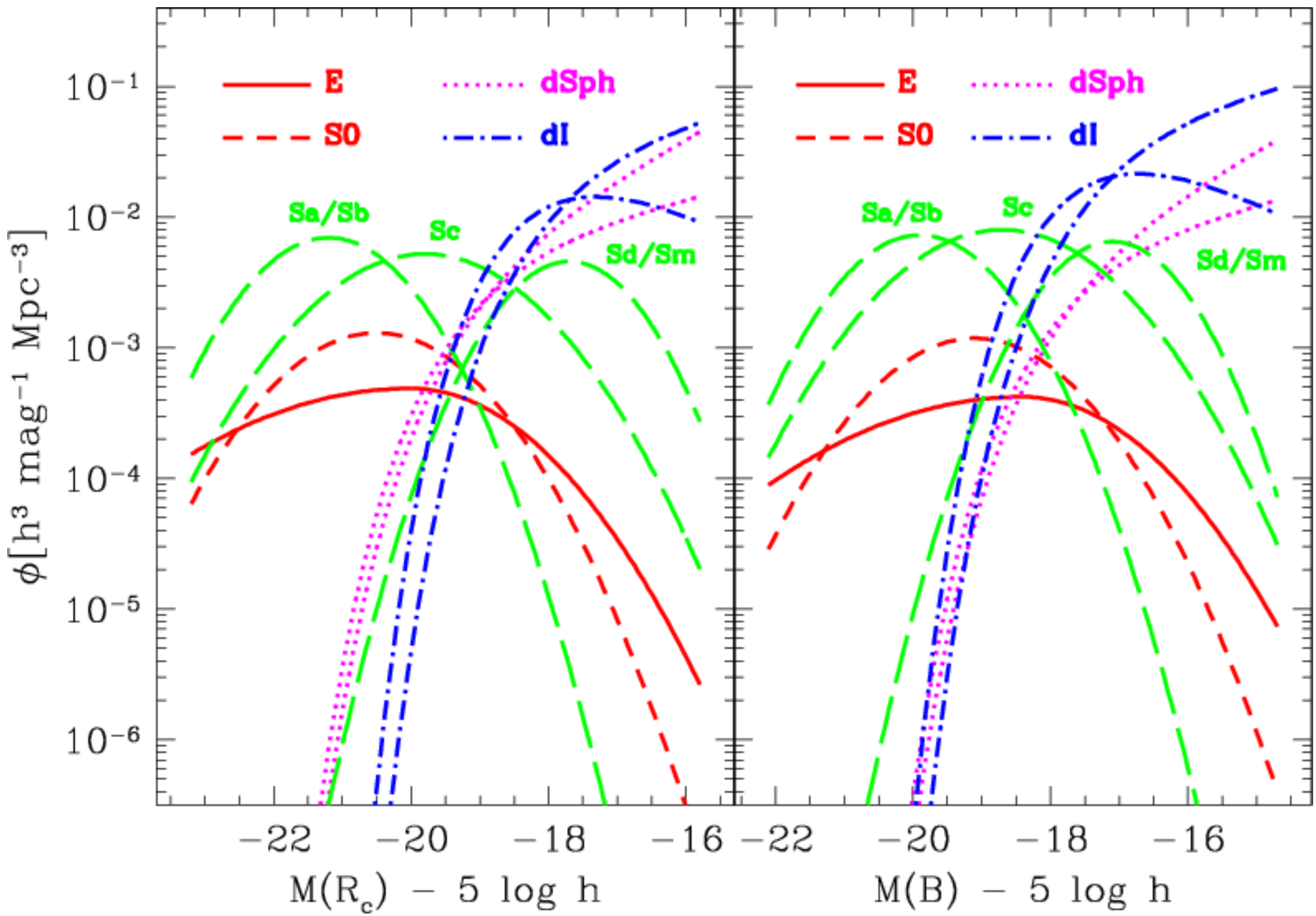

de Lapparent (2003)